



CMS-B2G-20-007

CERN-EP-2021-226
2024/07/05

Search for heavy resonances decaying to a pair of Lorentz-boosted Higgs bosons in final states with leptons and a bottom quark pair at $\sqrt{s} = 13$ TeV

The CMS Collaboration*

Abstract

A search for new heavy resonances decaying to a pair of Higgs bosons (HH) in proton-proton collisions at a center-of-mass energy of 13 TeV is presented. Data were collected with the CMS detector at the LHC in 2016–2018, corresponding to an integrated luminosity of 138 fb^{-1} . Resonances with a mass between 0.8 and 4.5 TeV are considered using events in which one Higgs boson decays into a bottom quark pair and the other into final states with either one or two charged leptons. Specifically, the single-lepton decay channel $\text{HH} \rightarrow b\bar{b}WW^* \rightarrow b\bar{b}\ell\nu q\bar{q}'$ and the dilepton decay channels $\text{HH} \rightarrow b\bar{b}WW^* \rightarrow b\bar{b}\ell\nu\ell\nu$ and $\text{HH} \rightarrow b\bar{b}\tau\tau \rightarrow b\bar{b}\ell\nu\ell\nu$ are examined, where ℓ in the final state corresponds to an electron or muon. The signal is extracted using a two-dimensional maximum likelihood fit of the $H \rightarrow b\bar{b}$ jet mass and HH invariant mass distributions. No significant excess above the standard model expectation is observed in data. Model-independent exclusion limits are placed on the product of the cross section and branching fraction for narrow spin-0 and spin-2 massive bosons decaying to HH. The results are also interpreted in the context of radion and bulk graviton production in models with a warped extra spatial dimension. The results provide the most stringent limits to date for $X \rightarrow \text{HH}$ signatures with final-state leptons and at some masses provide the most sensitive limits of all $X \rightarrow \text{HH}$ searches.

Submitted to the Journal of High Energy Physics

1 Introduction

The discovery of a Higgs boson (H) at the CERN LHC [1–3] validated the proposed mass generation mechanism within the standard model (SM) [4, 5], the so-called “Brout-Englert-Higgs mechanism.” A number of theoretical difficulties found in the simple model are ameliorated by an extended Higgs sector [6]. Supersymmetry [7–14] requires such an extended Higgs sector, with additional spin-0 particles. Models with warped extra dimensions, proposed by Randall and Sundrum [15], postulate the existence of a compact fourth spatial dimension with a warped metric. Such compactification creates heavy resonances arising as a tower of Kaluza-Klein excitations, leading to possible spin-0 radions [16–19] or spin-2 bulk gravitons [20–22]. The ATLAS [23–46] and CMS [47–71] Collaborations have conducted a number of searches for these particles, where the new bosons decay into vector bosons and/or SM Higgs bosons (WW , ZZ , WZ , HH , ZH , or WH).

In this paper, we present an expansion of a previous search [72] for heavy resonances (X) decaying to HH . The previous study considered a smaller data set of proton-proton (pp) collisions and searched for a signal in which one Higgs boson decayed to a bottom quark pair ($b\bar{b}$) and the second decayed to a W boson pair that decays as $WW^* \rightarrow \ell\nu q\bar{q}'$. The data set analyzed in Ref. [72] corresponded to collisions at $\sqrt{s} = 13$ TeV recorded in 2016 with an integrated luminosity of 36 fb^{-1} . In this new search, in addition to the $HH \rightarrow b\bar{b}\ell\nu q\bar{q}'$ decay channel from Ref. [72], two other signal decay channels are included by considering dilepton decays of the Higgs boson that does not decay to $b\bar{b}$: the $H \rightarrow WW^* \rightarrow \ell\nu\ell\nu$ and the $H \rightarrow \tau\tau \rightarrow \ell\nu\ell\nu$ decays. In all three cases, the ℓ denotes an electron or a muon; the analysis is also sensitive to leptonically decaying τ leptons in the $b\bar{b}WW^*$ decays. Events from $b\bar{b}\tau\tau$ comprise 30–35% of the total expected dilepton signal yield. The analysis is optimized for the three $X \rightarrow HH$ channels just mentioned, but signal events from $HH \rightarrow b\bar{b}ZZ^*$ are also included in our acceptance and constitute 1–3% of the total expected signal yield.

This search is performed on a data set of pp collisions at a center-of-mass energy of 13 TeV, collected in 2016–2018 at the CERN LHC, corresponding to an integrated luminosity of 138 fb^{-1} , and considers narrow resonances in the mass range $0.8 < m_X < 4.5$ TeV. The Higgs bosons have a high Lorentz boost because of the large values of m_X considered, so the decay products of each one are contained in a collimated cone. The degree of collimation is enough such that hadronically decaying bosons are each reconstructed as a single jet that has substructure consistent with a decay to two energetic quarks. The distinguishing characteristic of the signal is a peak in the two-dimensional (2D) plane of the $H \rightarrow b\bar{b}$ jet mass $m_{b\bar{b}}$ and the reconstructed HH invariant mass m_{HH} .

In the single-lepton (SL) channel, the quarks in the $H \rightarrow WW^* \rightarrow \ell\nu q\bar{q}'$ decay are reconstructed as a single large jet (the $q\bar{q}'$ jet) with a nearby lepton (e or μ). This jet is required to have substructure consistent with a decay to two energetic quarks. This Higgs boson decay chain is reconstructed as the $q\bar{q}'$ jet, the lepton, and the missing transverse momentum \vec{p}_T^{miss} . In the dilepton (DL) channel, two leptons are reconstructed in close proximity to each other, with \vec{p}_T^{miss} nearby, consistent with the expected neutrinos. In all channels considered, the $H \rightarrow b\bar{b}$ decay is reconstructed as a single large jet (the $b\bar{b}$ jet) with substructure and high transverse momentum p_T .

The main SM background in this search arises from top quark pair ($t\bar{t}$) production. This analysis is most sensitive to top quarks that have collimated decay products because of large Lorentz boosts. In the SL channel, the largest background comes from $t\bar{t}$ decays in which one top quark decays with a charged lepton and a neutrino ($t \rightarrow Wb \rightarrow \ell\nu b$), and the other decays exclu-

sively to quarks ($t \rightarrow Wb \rightarrow q\bar{q}'b$), which can be mistakenly reconstructed as the $b\bar{b}$ jet candidate. Other significant backgrounds in this channel are the production of W bosons in association with jets with $W \rightarrow \ell\nu$ (hereafter referred to as $W+\text{jets}$), and multijet events from quantum chromodynamic processes (QCD multijets), with either a lepton originating from heavy flavor decay or a hadron misidentified as a lepton. In the DL channel, the background yield is smaller than that of the SL channel by a factor of ≈ 60 . Top quark pair production is the dominant background here too, with approximately equal contributions from $t\bar{t}$ events with a single lepton in the final state and events in which both top quarks decay leptonically. Single-lepton $t\bar{t}$ events can fall into the DL channel when some part of the hadronic top quark decay is misidentified as a lepton. The other significant background in this channel is production of Z/γ^* bosons in association with jets ($Z/\gamma^*+\text{jets}$). These backgrounds are distinguished in data using the $m_{b\bar{b}}$ spectrum. Contributions from backgrounds with an SM Higgs boson (e.g., $t\bar{t}H$) are considered but found to be negligible in both channels.

The CMS detector and the simulated samples used to build the analysis are described in Sections 2 and 3, respectively. Relative to Ref. [72], this analysis incorporates new DL signal modes and employs new particle reconstruction and identification techniques in the SL channel. These include more efficient algorithms for identifying electrons and jets with b hadrons (b tagging) as well as an improved reconstruction procedure for the $H \rightarrow WW^* \rightarrow \ell\nu q\bar{q}'$ decay. The developments are discussed in Section 4, which details the event reconstruction and identification, including the final-state particles and the intermediate-state bosons. Section 5 discusses the selection criteria used to discriminate signal from background and the division of all events into 12 exclusive categories by the number of leptons, the lepton flavor, the quality of jet flavor tagging, and the $H \rightarrow WW^*$ decay kinematics. Section 6 details the model-building process for the signal and the background. The signal and SM background yields are estimated using a simultaneous maximum likelihood fit to the 2D $m_{b\bar{b}}$ and m_{HH} mass distributions in all 12 categories. All systematic uncertainties are discussed in Section 7, and the post-fit results are presented in Section 8. The analysis is summarized in Section 9.

Tabulated results are provided in the HEPData record for this analysis [73].

2 The CMS detector and global event reconstruction

The central feature of the CMS apparatus is a superconducting solenoid of 6 m internal diameter, providing a magnetic field of 3.8 T. Within the solenoid volume are a silicon pixel and strip tracker, a lead tungstate crystal electromagnetic calorimeter (ECAL), and a brass and scintillator hadron calorimeter (HCAL), each composed of a barrel and two endcap sections. Forward calorimeters extend the pseudorapidity (η) coverage provided by the barrel and endcap detectors. Muons are measured in gaseous detectors embedded in the steel flux-return yoke outside the solenoid. A more detailed description of the CMS detector, together with a definition of the coordinate system used and the relevant kinematic variables, can be found in Ref. [74].

Events of interest are selected using a two-tiered trigger system. The first level, composed of custom hardware processors, uses information from the calorimeters and muon detectors to select events at a rate of around 100 kHz within a fixed latency of about $4\ \mu\text{s}$ [75]. The second level, known as the high-level trigger, consists of a farm of processors running a version of the full event reconstruction software optimized for fast processing and reduces the event rate to around 1 kHz before data storage [76].

Event reconstruction relies on a particle-flow (PF) algorithm [77], which aims to identify each individual particle in an event with an optimized combination of information from the various

elements of the CMS detector. The vector \vec{p}_T^{miss} is computed as the negative vector p_T sum of all the PF candidates in an event, and its magnitude is denoted as p_T^{miss} [78]. The \vec{p}_T^{miss} is modified to account for corrections to the energy scale of the reconstructed jets in the event. In each event, jets are clustered from these PF candidates using the anti- k_T algorithm [79, 80] with a distance parameter of 0.4 (AK4 jets) and of 0.8 (AK8 jets).

The jet momentum is determined as the vectorial sum of all particle momenta in the jet, and is found from simulation to be, on average, within 5–10% of the true momentum over the entire p_T spectrum and detector acceptance. Additional pp interactions within the same or nearby bunch crossings (pileup) can contribute extra tracks and calorimetric energy depositions, increasing the apparent jet momentum. To mitigate this effect for AK4 jets, tracks identified as originating from pileup vertices are discarded, and an offset correction is applied to correct for residual contributions [77, 80]. For AK8 jets, a different pileup per particle identification algorithm [81, 82] reduces the effect of pileup by considering local shape variables [82] to rescale the momentum of each jet constituent according to its probability to originate from the primary vertex. Jet energy corrections are derived from simulation studies so that the average measured energy of jets becomes identical to that of particle-level jets. In situ measurements of the momentum balance in dijet, photon+jet, Z+jet, and multijet events are used to determine any residual differences between the jet energy scale in data and in simulation, and appropriate corrections are made [83].

3 Simulated samples

Signal and background yields are extracted from a fit to the data in the 2D $m_{b\bar{b}}$ and m_{HH} mass distribution using templates obtained from samples generated by Monte Carlo (MC) simulation.

The signal processes $\text{pp} \rightarrow X \rightarrow \text{HH} \rightarrow b\bar{b}VV^*$ (where $V = W$ or Z) and $\text{pp} \rightarrow X \rightarrow \text{HH} \rightarrow b\bar{b}\tau\tau$ are simulated for spin-0 radions and spin-2 gravitons in the bulk scenario of Randall–Sundrum models with warped extra dimensions. Only the $b\bar{b}WW^*$ events are used to optimize the analysis, but any $b\bar{b}ZZ^*$ events that pass the full selection are used in the signal acceptance. The simulated X bosons are produced via gluon fusion and with a narrow width (1 MeV) that is small compared to the experimental resolution of roughly 5%. The branching fractions used to normalize the signal correspond to those expected for SM Higgs boson decays. The signal is generated at leading order (LO) using the MADGRAPH5_aMC@NLO V5 2.4.2 generator [84] with the MLM merging scheme [85] for m_X of 0.8–4.5 TeV.

The MADGRAPH5_aMC@NLO generator is also used to produce the W+jets, $Z/\gamma^* \rightarrow \ell\ell$, and QCD multijet background samples at LO. The W+jets and $Z/\gamma^* \rightarrow \ell\ell$ samples are normalized using next-to-next-to-LO (NNLO) cross sections, calculated with FEWZ v3.1 [86]. Samples of WZ diboson production and of the associated production of $t\bar{t}$ with either a W or Z boson are also generated with MADGRAPH5_aMC@NLO but at next-to-LO (NLO) with the FxFx jet merging scheme [87]. The POWHEG v2 generator is used to produce samples for $t\bar{t}$, WW, ZZ, $t\bar{t}H$, and single top quark production at NLO [88–95]. Furthermore, the $t\bar{t}$ process is normalized to the NNLO cross section, computed with TOP++ v2.0 [96].

Parton showering and hadronization are simulated in the 2016 samples with PYTHIA v8.226 [97] using the CUETP8M1 [98] tune, except for the $t\bar{t}$, $t\bar{t}H$, and $X \rightarrow \text{HH} \rightarrow b\bar{b}VV^*$ signal samples, which are simulated using the CP5 tune. For 2017–2018, PYTHIA v8.230 and the CP5 tune [99] are used to produce the samples. The parton distribution functions (PDFs) used to produce the samples are the NNPDF 3.0 [100] set for the 2016 data set and the NNPDF 3.1 [101]

set for the 2017–2018 data sets. The simulation of the CMS detector is performed with the GEANT4 [102] toolkit. The simulated samples are weighted to have the same multiplicity distribution of pileup interactions as observed in data.

4 Decay chain reconstruction

All signal events, regardless of lepton multiplicity, feature a high- p_{T} jet that has substructure consistent with two b quark decays. This jet is opposite in the transverse plane to a collection of other particles from a boosted Higgs boson decay. In the SL channel, signal events feature a lepton originating from a boosted W boson decay and a nearby jet that has substructure consistent with a $W \rightarrow q\bar{q}'$ decay. Even at the lowest considered m_X of 0.8 TeV, the median angular distance $\Delta R = \sqrt{(\Delta\eta)^2 + (\Delta\phi)^2}$ (where ϕ is the azimuthal angle) between the $W \rightarrow q\bar{q}'$ decay and the lepton is approximately $\Delta R = 0.5$. In the DL channel, there are two high- p_{T} leptons originating from the decay of either a boosted W boson pair or a boosted τ lepton pair, but there is no jet in the vicinity of the leptons, resulting in a cleaner experimental signature.

Events are first selected by the trigger system with small year-to-year differences in the criteria. Events are triggered if they contain one of the following: an isolated muon with $p_{\mathrm{T}} > 24$ GeV (27 GeV in 2017), an isolated electron with $p_{\mathrm{T}} > 32$ GeV (27 GeV in 2016), or $H_{\mathrm{T}} > 1050$ GeV (900 GeV in 2016), where H_{T} is the scalar sum of jet p_{T} for all trigger-level AK4 jets with $p_{\mathrm{T}} > 30$ GeV. An inclusive-OR combination of lepton and H_{T} triggers is used because the high- m_X SL signal does not have leptons that are sufficiently isolated to pass the online lepton isolation selection, as the decay products $WW^* \rightarrow \ell\nu q\bar{q}'$ are highly collimated. Additional multiobject triggers that select events with at least one lepton and considerable jet energy supplement these triggers, helping to maintain high trigger efficiency for signal over the entire range of m_X . In particular, these multiobject triggers fire for events with $H_{\mathrm{T}} > 450$ GeV (400 GeV in 2016) and a lepton that has $p_{\mathrm{T}} > 15$ GeV and looser isolation requirements than for the previously mentioned isolated single-lepton triggers. These multiobject triggers are particularly helpful for the SL signal topology with the lepton close to the jet. The trigger efficiency is measured for $e\mu$ $t\bar{t}$ events in data for events passing offline selection criteria for H_{T} in the SL channel and both H_{T} and lepton p_{T} in the DL channel. We use $t\bar{t}$ events because the lepton and jet multiplicities resemble those in signal events. Simulation is corrected such that the trigger efficiency matches that in the data. In the SL channel, the trigger efficiency for signal events is over 96% at $m_X = 0.8$ TeV and increases to >99% above $m_X = 1.0$ TeV. In the DL channel, the trigger efficiency is >99% over the full range of m_X .

4.1 Electron and muon identification

Different selection criteria are required for the SL and DL channels to identify signal-like leptons because of the different decay topologies. First, however, an event in either channel must contain either a muon with $p_{\mathrm{T}} > 27$ GeV or an electron with $p_{\mathrm{T}} > 30$ GeV. In the DL channel, the other lepton must have $p_{\mathrm{T}} > 10$ GeV. All muons are required to have $|\eta| < 2.4$. Electrons in the DL channel are required to have $|\eta| < 2.5$, but those in the SL channel are restricted to the ECAL barrel region ($|\eta| < 1.479$) to suppress a significant contribution from the QCD multijet background with a small loss in signal acceptance. Leptons must satisfy reconstruction quality and identification requirements that are optimized to maintain large efficiency and low probability for misidentifying hadrons as leptons [103, 104]. Additionally, the impact parameters of lepton tracks with respect to the primary vertex are required to be consistent with those originating from this vertex. Looser constraints on the impact parameter are used in the DL channel because some of the leptons originate from $H \rightarrow \tau\tau$ decays, since tau leptons have a

longer lifetime than that of muons and electrons but shorter than that of b quarks. Leptons are required to be isolated with an isolation cone size designed for leptons from boosted decays, in which the cone size becomes smaller with larger p_T [105]. Because less hadronic energy is expected near the leptons in the DL channel than in the SL channel, the allowed extra transverse energy in the isolation cone is smaller.

In the SL channel, the electron selection efficiency has a maximum of 70% at $m_X = 0.8 \text{ TeV}$ and then degrades to 7.5% at $m_X = 4.5 \text{ TeV}$. This is caused by a selection imposed at a low-level reconstruction step on the ratio of the energy deposited in the HCAL to that deposited in the ECAL. Electrons in the $H \rightarrow WW^* \rightarrow e\nu q\bar{q}'$ decay often fail this selection because of nearby energy deposits from the $q\bar{q}'$ jet, which grow with larger boosts. However, the reconstruction of muons does not rely on such HCAL measurements and so is much more efficient than for electrons, but the isolation of muons is still sensitive to the $q\bar{q}'$ jet. As a result, the overall selection efficiency for signal muons is better than for electrons but still degrades for larger m_X ; the muon efficiency ranges from approximately 90% at $m_X = 0.8 \text{ TeV}$ down to 60% at $m_X = 4.5 \text{ TeV}$.

In the DL channel, where there is no $q\bar{q}'$ jet, the lepton selection efficiency is larger for all m_X than in the SL channel. Because of the increased boost of the system, the efficiency still drops toward high m_X , though not as severely as in the SL channel. For electrons, the reconstruction efficiency is much larger than in the SL channel because there is no jet near the leptons. The electron efficiency ranges from approximately 82% at $m_X = 0.8 \text{ TeV}$ down to 71% at $m_X = 4.5 \text{ TeV}$. The muon efficiency is also larger, ranging from approximately 96% at $m_X = 0.8 \text{ TeV}$ down to 91% at $m_X = 4.5 \text{ TeV}$. The lepton efficiencies are measured in simulation and data in a $Z \rightarrow \ell\ell$ sample, and the simulation is corrected to match the efficiency in data. The systematic uncertainties in these measurements are applied to the normalization of the signal.

4.2 Reconstruction and flavor identification of jets

Because of the boost imparted to the Higgs bosons by the decay of the much more massive X boson, the $H \rightarrow b\bar{b}$ and $W \rightarrow q\bar{q}'$ decays are each reconstructed as a single, merged AK8 jet with two-prong substructure. In order to prevent the $q\bar{q}'$ jet from containing the lepton's momentum in the SL channel, the PF candidates associated with the lepton are not included in the clustering of the set of jets from which the $q\bar{q}'$ jet is selected. Jets of both types are required to have $|\eta| < 2.4$ so that most of the jet particles are within the acceptance of the tracker.

The Higgs bosons have collimated decays and typically are produced back-to-back in the transverse plane, i.e., $\Delta\phi(H, H) \approx \pi$. The $b\bar{b}$ jet candidate is required to have $p_T > 200 \text{ GeV}$. In the SL channel, it is required to have a $\Delta\phi > 2.0$ separation from the lepton and a $\Delta R > 1.6$ separation from the $q\bar{q}'$ jet, while in the DL channel, it is required to have a $\Delta\phi > 2.0$ separation from the dilepton momentum and to not contain either lepton within the jet cone. The $q\bar{q}'$ jet in the SL channel is chosen as the closest AK8 jet in ΔR to the lepton, provided that it is found within $\Delta R < 1.2$ from the lepton and has $p_T > 50 \text{ GeV}$. Within both the $b\bar{b}$ and $q\bar{q}'$ jets, two subjets are reconstructed that must each have $p_T > 20 \text{ GeV}$. Constituents of the AK8 jets are first reclustered using the Cambridge–Aachen algorithm [106, 107]. The “modified mass drop tagger” algorithm [108, 109], also known as the “soft drop” (SD) algorithm, with angular exponent $\beta = 0$, soft cutoff threshold $z_{\text{cut}} < 0.1$, and characteristic radius $R_0 = 0.8$ [110], is applied to remove soft, wide-angle radiation from the jet. The subjets used are those remaining after the algorithm has removed all recognized soft radiation. The jet mass is the invariant mass of these two subjets. The SD mass of the $b\bar{b}$ jet is used to obtain the search variable $m_{b\bar{b}}$, after applying p_T -dependent corrections, so that $m_{b\bar{b}}$ in simulation is on average equal to the Higgs

boson mass of 125 GeV.

Identifying the $H \rightarrow b\bar{b}$ decay in signal events and discriminating against background events relies on tagging jets as likely to have originated from b hadron decays. The AK8 jets are identified as consistent with a $b\bar{b}$ decay using the DEEPAK8 mass-decorrelated $Z/H \rightarrow b\bar{b}$ tagger [111], with a discriminator denoted as $D_{Z/H \rightarrow b\bar{b}}$. This is a deep neural network based tagger, designed to discriminate high- p_T jets consistent with a $b\bar{b}$ substructure against light-flavor quark (u, d, s) or gluon jets. Furthermore, by design the tagger does not sculpt the jet mass distributions, thereby enabling the use of the jet mass in the background estimation. The b tagging efficiencies are measured in data, and the simulation is corrected for any discrepancies. In $t\bar{t}$ events, the most common events misreconstructed as signal, the $b\bar{b}$ jet candidate is typically reconstructed around the decay of one of the b quarks, while the other b quark decays into the opposite direction in the transverse plane. Identifying a b -tagged AK4 jet that is separated from the $b\bar{b}$ jet is an effective method of discriminating between such $t\bar{t}$ events and signal events, in which the $b\bar{b}$ jet is reconstructed from the two $H \rightarrow b\bar{b}$ quarks. To be considered a candidate b jet, an AK4 jet must have $p_T > 30$ GeV and be identified using the DEEPJET tagger [112–114] at a working point that has an efficiency of $\approx 80\%$ for selecting b jets and a misidentification probability of $\approx 1\%$ for light-flavor quark and gluon jets.

4.3 Reconstructing the HH system mass

Depending on whether the final state has one or two leptons, different strategies are employed to reconstruct the four-momentum of the Higgs boson that does not decay to $b\bar{b}$. The mass m_{HH} is then the invariant mass of this four-momentum and the $b\bar{b}$ jet four-momentum. The mass of the $b\bar{b}$ jet used in this calculation is not the SD mass $m_{b\bar{b}}$ but is rather the ungroomed jet mass. In Sections 4.3.1 and 4.3.2, respectively, the reconstruction strategies are described for the SL and DL channels.

4.3.1 Single-lepton channel

To reconstruct the Higgs boson four-momentum in the $H \rightarrow WW^* \rightarrow \ell\nu q\bar{q}'$ decay chain from the visible and invisible decay products, a likelihood-based technique that takes the reconstructed lepton, the \vec{p}_T^{miss} , and the $q\bar{q}'$ jet as input is employed. For each event, values for the following five parameters are extracted by maximizing a likelihood function:

- \vec{p}_ν : the three components of the neutrino momentum.
- $R_{q\bar{q}'}$: the jet response correction, a multiplicative scale factor applied to the p_T of the $q\bar{q}'$ jet. The jet p_T is allowed to vary because the uncertainty associated with the estimated p_T of this jet is large.
- $V_{q\bar{q}'}$: a boolean indicator of whether the $q\bar{q}'$ jet favors a larger or smaller mass than the leptonic W boson decay. This is largely a bookkeeping device for the W and W^* hypotheses.

With these parameters, the $H \rightarrow WW^*$ four-momentum can be fully determined. This four-momentum is then the sum of the neutrino four-momentum p_ν , the $q\bar{q}'$ jet four-momentum (with p_T modified by $R_{q\bar{q}'}$), and the four-momentum of the lepton.

The likelihood function is constructed with six probability density functions (pdfs) $P(x|\vec{y})$ estimated from signal simulation, where x is the corresponding observable in the pdf. The symbol \vec{y} represents the set of free parameters associated with that pdf, such as $V_{q\bar{q}'}$. These pdfs are

represented as one-dimensional (1D) histograms. The full likelihood function is:

$$\mathcal{L} = P(m_{\text{jet}}|V_{q\bar{q}'})P(p_T^{\text{jet}}|R_{q\bar{q}'}, V_{q\bar{q}'})P(m_{\ell\nu q\bar{q}'}|\vec{p}_\nu, R_{q\bar{q}'}, V_{q\bar{q}'})P(m_{\ell\nu}|\vec{p}_\nu, V_{q\bar{q}'})P(\vec{p}_T^{\text{miss}}|\vec{p}_\nu, V_{q\bar{q}'}). \quad (1)$$

The observable m_{jet} is the SD mass of the $q\bar{q}'$ jet, and its corresponding pdf is coarsely binned to remain insensitive to the precise modeling of the SD algorithm. The observable p_T^{jet} is the unmodified $q\bar{q}'$ jet p_T , and the pdf $P(p_T^{\text{jet}}|R_{q\bar{q}'}, V_{q\bar{q}'})$ is the jet p_T response. Two other observables, $m_{\ell\nu}$ and $m_{\ell\nu q\bar{q}'}$, are masses of the lepton-neutrino pair and the lepton-neutrino- $q\bar{q}'$ jet system.

The last factor in Eq. (1) represents the product of two pdfs, each corresponding to a single component of \vec{p}_T^{miss} :

$$P(\vec{p}_T^{\text{miss}}|\vec{p}_\nu, V_{q\bar{q}'}) = P(p_{T,\parallel}^{\text{miss}}|\vec{p}_\nu, V_{q\bar{q}'})P(p_{T,\perp}^{\text{miss}}|\vec{p}_\nu, V_{q\bar{q}'}). \quad (2)$$

The two observables $p_{T,\parallel}^{\text{miss}}$ and $p_{T,\perp}^{\text{miss}}$ are defined with respect to the reference frame of the $H \rightarrow WW^*$ decay, along the direction of \vec{p}_T^{reco} :

$$\vec{p}_T^{\text{reco}} = \vec{p}_T^{\text{miss}} + (\vec{p}_\ell + \vec{p}_{q\bar{q}' \text{ jet}})_T. \quad (3)$$

The two \vec{p}_T^{miss} pdf factors are parameterized as the components of the extra p_T^{miss} (relative to the neutrino momentum) that are parallel and perpendicular to this vector \vec{p}_T^{reco} . The extra p_T^{miss} along this direction arises primarily from mismeasurement of the $b\bar{b}$ jet, while the orthogonal component arises mostly from pileup and the underlying event.

The pdfs P of the observables are generally independent of m_X , but there is still some residual dependence. We account for this by producing two sets of pdfs, one at low p_T^{reco} ($< 600 \text{ GeV}$) and one at high p_T^{reco} ($> 1400 \text{ GeV}$). Then, event-by-event, the histogram of the pdf is obtained by interpolating between the two histograms at the two regimes of p_T^{reco} . This interpolation is performed linearly as a function of the event p_T^{reco} . The P are all dependent on whether the hadronically decaying W boson is heavier than the leptonically decaying W, so each factor is dependent on the free parameter $V_{q\bar{q}'}$. Correlations among the observables in the likelihood were studied and found not to affect the results significantly.

This method gives an m_{HH} resolution for signal events that is very similar to that from a direct calculation using the Higgs boson mass as a constraint (as in [72]), but for background events it typically returns lower values of m_{HH} than in the direct calculation. We take advantage of this fact using an alternative likelihood \mathcal{L}_{alt} , which is less constrained by the intermediate masses. Instead of fitting for the neutrino p_z , the masses $m_{\ell\nu}$ and $m_{\ell\nu q\bar{q}'}$ are included as free parameters. Both likelihoods are used to construct a discriminating variable between signal and background:

$$D_{\ell\nu q\bar{q}'} = -2 \log \mathcal{L} / \mathcal{L}_{\text{alt}}, \quad (4)$$

where \mathcal{L} is the likelihood described in Eq. (1). We discuss how $D_{\ell\nu q\bar{q}'}$ is used in Section 5.

4.3.2 Dilepton channel

Because of the absence of a $q\bar{q}'$ jet, the presence of larger p_T^{miss} , and much smaller backgrounds, there is no need for a likelihood-based technique to separate signal and background in the DL channel. Instead, we make simple assumptions regarding the decay kinematic distributions in order to reconstruct the full invisible four-momentum p_{inv} due to neutrinos. First, the transverse components of p_{inv} are taken directly from the \vec{p}_T^{miss} . Second, because the decay products of the boosted Higgs boson are collimated, we assume the polar angle θ of p_{inv} is equal to that of

the dilepton momentum: $\theta_{\text{inv}} = \theta_{\ell\ell}$. With this constraint, the z-component of p_{inv} is obtained. Lastly, the invisible invariant mass m_{inv} due to neutrinos is assumed to be 55 GeV, the mean of the distribution from signal simulation. The corresponding Higgs boson four-momentum is the summed four-momentum of p_{inv} and the dilepton four-momentum $p_{\ell\ell}$.

5 Event selection and categorization

Events are selected in this search if they pass the following criteria indicating that they could include the production and decay of an X boson. They are then divided into 12 distinct categories (eight SL and four DL). A separate set of criteria is applied to define control regions that are used to validate the modeling of background processes.

Offline, all events are required to have $H_T > 400$ GeV, either one electron with $p_T > 30$ GeV or one muon with $p_T > 27$ GeV, and a selected bb jet. Background from t̄t production is reduced by vetoing all events with an AK4 jet that is $\Delta R > 1.2$ from the bb jet and is identified as a b jet, as described in Section 4.2.

We ensure that the sets of events belonging to the SL and DL channels are disjoint. To accomplish this, we first impose that any event with exactly two oppositely charged lepton candidates passing the DL channel lepton selection be assigned as a DL event. Otherwise, if the event has at least one lepton candidate passing the SL channel lepton selection and also has fewer than two lepton candidates passing the DL channel lepton selection, it is classified as an SL event. In this case, the highest- p_T lepton candidate that passes the SL channel lepton selection is selected for Higgs boson reconstruction. If these two criteria cannot be fulfilled by the set of lepton candidates, the event is not used in the analysis.

The following sections review the event selection and categorization of events into the 12 exclusive search regions. Selections that are used only to discriminate signal from background and not to categorize events are detailed in Sections 5.1 and 5.2 for the SL and DL channels, respectively. Section 5.3 discusses the discriminating selections that are also used to categorize events.

5.1 Single-lepton channel event selection

In the SL channel, the q̄q' jet is chosen as the closest AK8 jet to the lepton, and it is required to have $p_T > 50$ GeV and be located within $\Delta R < 1.2$ of the lepton. Jets in background events tend to be produced at higher $|\eta|$ than those produced in signal events, which contain jets from the decay of a heavy particle. To exploit this property, the ratio of the p_T of $H \rightarrow WW^*$ divided by m_{HH} , denoted as p_T/m , is required to be >0.3 . The distribution of p_T/m is shown in Fig. 1 (upper right) for the data, expected pre-fit background, and two signal mass hypotheses with a normalization corresponding to a product of the cross section and branching fraction ($\sigma\mathcal{B}$) of 1.0 pb.

5.2 Dilepton channel event selection

Events in the DL channel must pass additional criteria. In signal events, the invariant mass of the two leptons is kinematically constrained by the mass of the boosted Higgs boson from which they originate, peaking near 30 GeV. Background in the $m_{\ell\ell}$ spectrum from Z/ γ^* + jets populates predominantly lower masses from the continuum and higher masses from the Z boson. Background from t̄t also populates higher masses since the leptons are typically opposite each other in the transverse plane. Requiring the dilepton invariant mass to satisfy $6 < m_{\ell\ell} < 75$ GeV reduces these backgrounds while preserving the signal. Requiring that

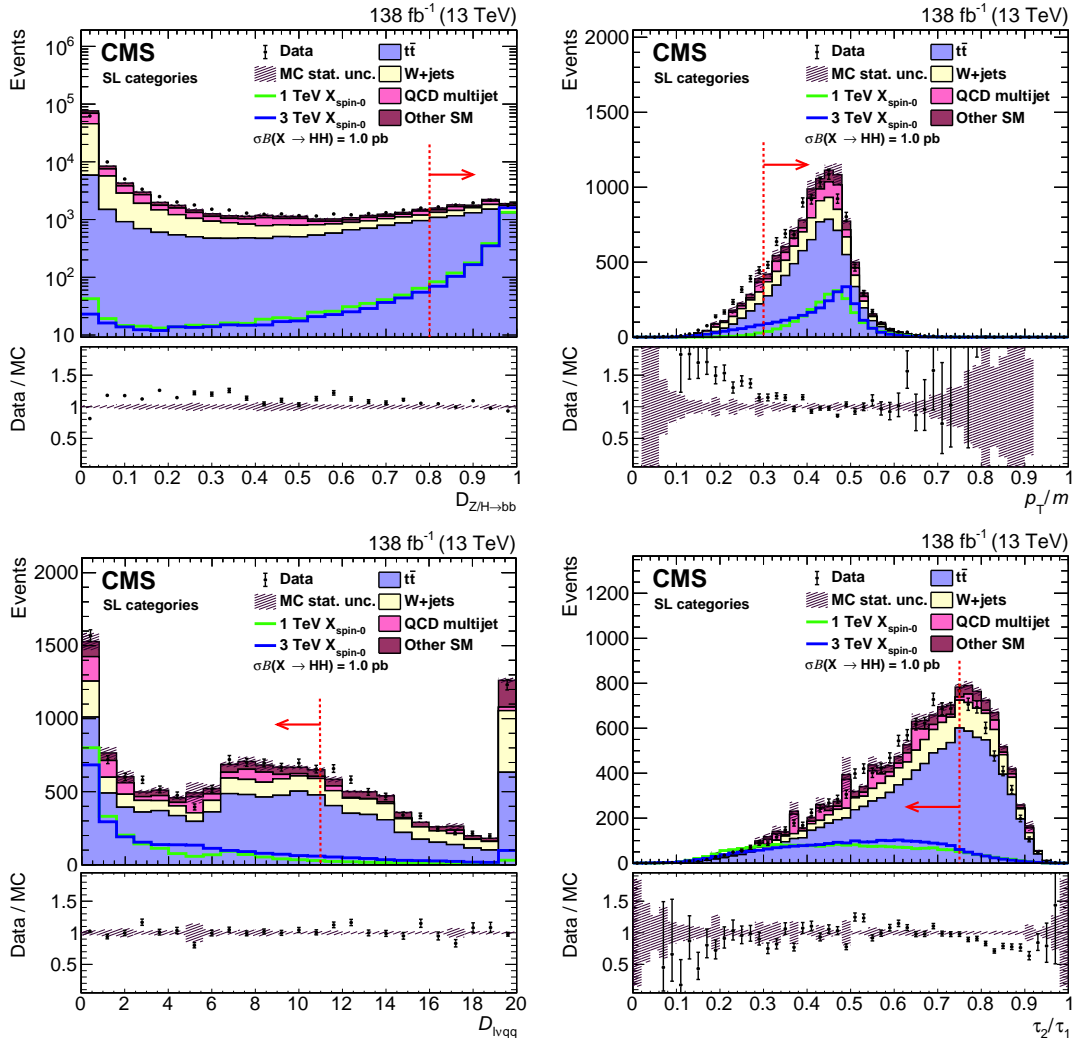


Figure 1: Single-lepton channel observables: distributions are shown for data (points), pre-fit simulated SM processes (filled histograms), and simulated signal (solid lines). The statistical uncertainty in the simulated sample is shown as the hatched band. Spin-0 signals for m_X of 1.0 and 3.0 TeV are displayed. The rightmost bin in the $D_{l\nu q\bar{q}'}$ plot contains the overflow events. For both signal models, $\sigma\mathcal{B}(X \rightarrow HH) = 1.0$ pb. The lower panels of each plot show the ratio of the data to the sum of all background processes. The red dashed line and arrow indicate the selected region of the variable of interest.

the leptons be close together in η - ϕ space with $\Delta R_{\ell\ell} < 1.0$ further helps to suppress the $t\bar{t}$ background. In $Z/\gamma^* + \text{jets}$ the \vec{p}_T^{miss} can be in the direction of the $b\bar{b}$ jet, away from the leptons, due to jet mismeasurements, while in signal the \vec{p}_T^{miss} is close to the leptons because of the boosted Higgs boson decay. Thus, we also require that $|\Delta\phi(\vec{p}_T^{\text{miss}}, \vec{p}_{\ell\ell})| < \pi/2$ to discriminate against $Z/\gamma^* + \text{jets}$. Background is further separated from signal by requiring $p_T^{\text{miss}} > 85 \text{ GeV}$. Figure 2 shows the distributions of the discriminating variables $m_{\ell\ell}$ (upper right), $\Delta R_{\ell\ell}$ (middle left), p_T^{miss} (middle right), and $\Delta\phi(\vec{p}_T^{\text{miss}}, \vec{p}_{\ell\ell})$ (lower).

5.3 Event categorization

Events are categorized by event properties that reflect the signal purity, and the categorization is the same over the full range of m_X . In the SL channel, electron and muon events are separated because their reconstruction efficiencies for background and signal are different, resulting in different signal purities. The electron and muon categories are labeled “e” and “ μ ,” respectively, in the figures. Likewise, in the DL channel, events with leptons of the same flavor and of the opposite (different) flavor are separated because the background composition is different between these two cases. These are labeled “SF” and “OF,” respectively, in the figures. We do not separate ee from $\mu\mu$ in the DL channel because these events have similar ratios of signal to background. For all events, there are two categories for $b\bar{b}$ jet tagging, constructed from different subsets of the distribution of the DEEPAK8 mass-decorrelated $Z/H \rightarrow b\bar{b}$ discriminator $D_{Z/H \rightarrow b\bar{b}}$, introduced in Section 4.2. The distribution of $D_{Z/H \rightarrow b\bar{b}}$ is shown in the upper left plot of Figs. 1 and 2 for the SL and DL channels, respectively. The discriminator value ranges from 0 to 1, with larger values indicating that the jet is more consistent with $b\bar{b}$ substructure. We use two working points that yield a loose category defined by $0.8 < D_{Z/H \rightarrow b\bar{b}} < 0.97$ (labelled “bL”) and a tight category defined by $D_{Z/H \rightarrow b\bar{b}} \geq 0.97$ (labelled “bT”). One more criterion for categorization, related to the $H \rightarrow WW^* \rightarrow \ell\nu q\bar{q}'$ decay, is implemented for the SL channel but not the DL channel. This categorization relies on both the τ_2/τ_1 N -subjettiness ratio [115] of the $q\bar{q}'$ jet (denoted now as τ_2/τ_1) and the $H \rightarrow WW^*$ likelihood discriminator $D_{\ell\nu q\bar{q}'}$ that was first introduced in Eq. (4). The ratio τ_2/τ_1 measures how consistent the jet substructure is with a two-prong decay versus a single-prong decay, with lower values more strongly indicating a two-prong decay. Figure 1 shows the distributions of $D_{\ell\nu q\bar{q}'}$ (lower left) and τ_2/τ_1 (lower right). All events in the SL but not in the DL search region are required to satisfy both $\tau_2/\tau_1 < 0.75$ and $D_{\ell\nu q\bar{q}'} < 11.0$. We construct a low-purity category (labeled “LP”) with events that satisfy either $0.45 < \tau_2/\tau_1 < 0.75$ or $2.5 < D_{\ell\nu q\bar{q}'} < 11.0$ and a high-purity category (labeled “HP”) with events that satisfy both $\tau_2/\tau_1 < 0.45$ and $D_{\ell\nu q\bar{q}'} < 2.5$. In 2016 data, the lower working point for τ_2/τ_1 is 0.55 instead of 0.45.

The selections just described are combined to produce 12 distinct search categories (eight SL and four DL). When describing a single category, the label is a combination of those listed above. For example, in the SL channel the tightest $b\bar{b}$ jet tagging category with a low-purity selection on the $H \rightarrow WW^*$ decay in the electron channel is: “e, bT, LP.” The categories and their corresponding labels are summarized in Tables 1 and 2.

The search is performed for $30 < m_{b\bar{b}} < 210 \text{ GeV}$ and $700 < m_{HH} < 5050 \text{ GeV}$. Extending the $m_{b\bar{b}}$ mass window down to 30 GeV helps to capture the background in the fit, but events below 30 GeV would be relatively difficult to model since these are events for which the SD algorithm removes nearly all of the jet energy. The m_{HH} lower bound is chosen such that the m_{HH} distribution is monotonically decreasing for the full background. The upper bound is several hundred GeV above the highest mass event observed in data.

For spin-0 scenarios, the combined selection efficiency for SL channel events to pass the criteria

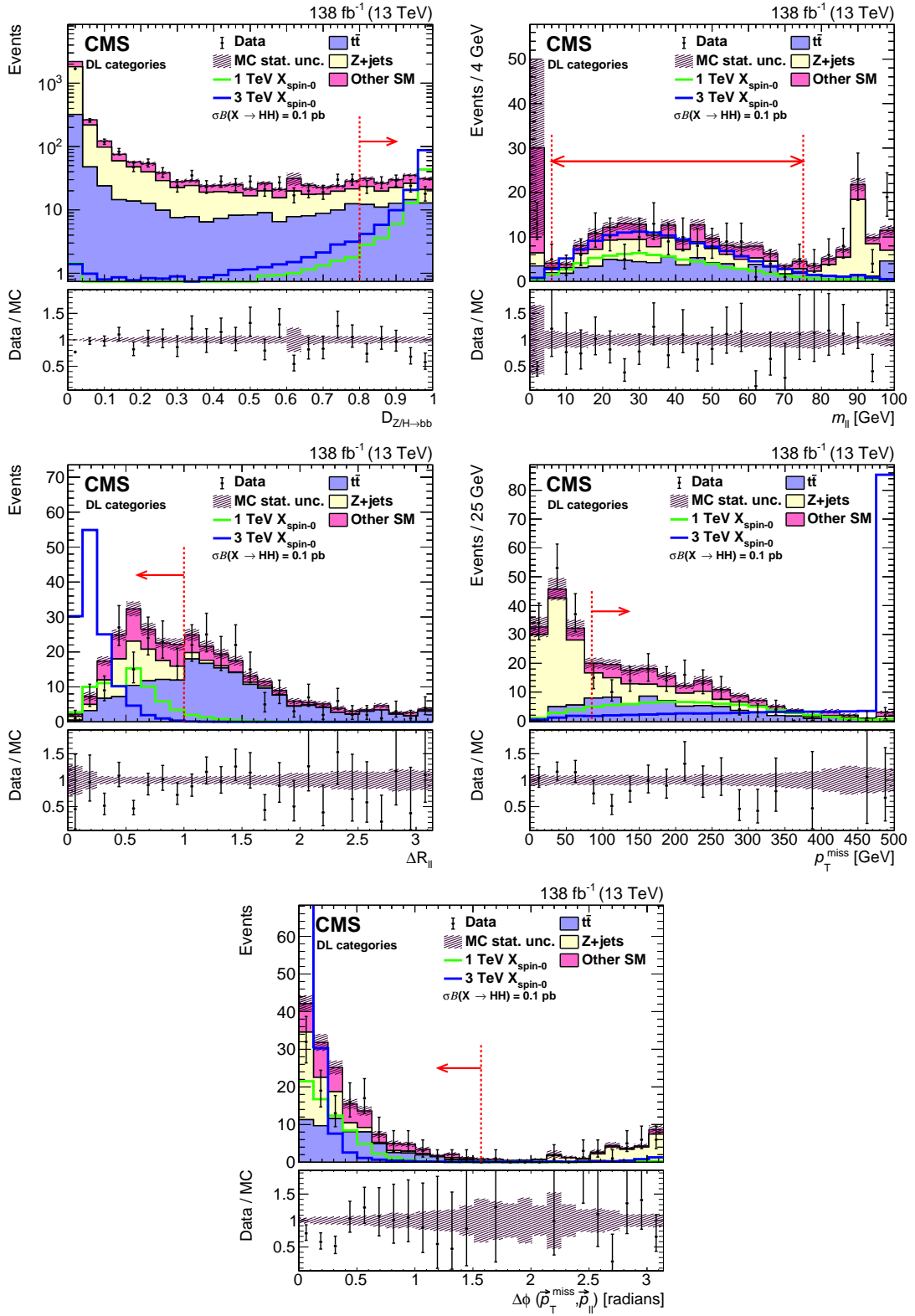


Figure 2: Dilepton channel observables: distributions are shown for data (points), pre-fit simulated SM processes (filled histograms), and simulated signal (solid lines). The statistical uncertainty in the simulated sample is shown as the hatched band. Spin-0 signals for m_X of 1.0 and 3.0 TeV are displayed. The rightmost bin in the m_{ll} , ΔR_{ll} , and p_T^{miss} plots contains the overflow events. For both signal models, $\sigma\mathcal{B}(X \rightarrow HH)$ is set to 0.1 pb. The lower panels of each plot show the ratio of the data to the sum of all background processes. The red dashed line and arrow indicate the selected region of the variable of interest.

Table 1: The SL channel event categorization and corresponding category labels. All combinations of the two lepton flavors, two $b\bar{b}$ jet tagging, and two $H \rightarrow WW^*$ decay purity selections are used to form eight independent event categories. The lower τ_2/τ_1 working point is 0.55 (0.45) in 2016 (2017–2018).

Categorization type	Selection	Label
Lepton flavor	Electron	e
	Muon	μ
$b\bar{b}$ jet tagging	$0.8 < D_{Z/H \rightarrow b\bar{b}} < 0.97$	bL
	$D_{Z/H \rightarrow b\bar{b}} > 0.97$	bT
$H \rightarrow WW^*$ purity	$0.45(0.55) < \tau_2/\tau_1 < 0.75$ or $2.5 < D_{\ell\nu q\bar{q}'} < 11.0$	LP
	$\tau_2/\tau_1 < 0.45(0.55)$ and $D_{\ell\nu q\bar{q}'} < 2.5$	HP

Table 2: The DL channel event categorization and corresponding category labels. All combinations of the two lepton flavors and two $b\bar{b}$ jet tagging selections are used to form four independent event categories.

Categorization type	Selection	Label
Lepton flavor	Two electrons or two muons	SF
	One electron and one muon	OF
$b\bar{b}$ jet tagging	$0.8 < D_{Z/H \rightarrow b\bar{b}} < 0.97$	bL
	$D_{Z/H \rightarrow b\bar{b}} > 0.97$	bT

of any event category is 9% at $m_X = 0.8$ TeV. The efficiency increases with m_X up to 23% at $m_X = 1.5$ TeV because the Higgs boson decays become more collimated. Above 1.5 TeV, the selection efficiency decreases to a minimum of 14% at $m_X = 4.5$ TeV for two main reasons: the b tagging efficiency degrades for high- p_T jets and the lepton isolation worsens for extremely collimated Higgs boson decays. For DL channel events, the combined selection efficiency to pass the criteria of any event category is 9% at $m_X = 0.8$ TeV, increases sharply with m_X to 30% at $m_X = 1.5$ TeV, and then increases more slowly to 36% at $m_X = 4.5$ TeV. The efficiency grows over the full range of m_X because in the absence of a nearby jet, the leptons become easier to select at high p_T . Tables 3 and 4 show the efficiencies for each individual selection requirement with the full selection otherwise applied.

Table 3: Efficiencies of each selection criterion in the SL channel with the rest of the full selection applied. The efficiencies for the total expected SM background and signals at 1.0 and 3.0 TeV are shown.

SL channel selection	Background	Signal	
		1 TeV	3 TeV
b jet veto	0.31	0.87	0.82
$D_{Z/H \rightarrow b\bar{b}} > 0.8$	0.07	0.81	0.84
$\tau_2/\tau_1 < 0.75$	0.69	0.91	0.92
$D_{\ell\nu q\bar{q}'} < 11.0$	0.63	0.87	0.83
$p_T/m > 0.3$	0.87	0.97	0.86

The Higgs bosons in signal events from a spin-2 X boson are produced at lower values of $|\eta|$ than those from a spin-0 X, resulting in larger selection efficiencies for spin-2 events. The relative increase in efficiency for spin-2 signal is larger at low mass ($\approx 40\%$) than at high mass ($\approx 15\%$).

Table 4: Efficiencies of each selection criterion in the DL channel with the rest of the full selection applied. The efficiencies for the total expected SM background and signals at 1.0 and 3.0 TeV are shown.

DL channel selection	Background	Signal	
		1 TeV	3 TeV
b jet veto	0.45	0.86	0.84
$D_{Z/H \rightarrow b\bar{b}} > 0.8$	0.05	0.81	0.83
$p_T^{\text{miss}} > 85 \text{ GeV}$	0.55	0.88	0.97
$6 < m_{\ell\ell} < 75 \text{ GeV}$	0.62	0.95	0.94
$\Delta R_{\ell\ell} < 1.0$	0.51	0.93	0.998
$ \Delta\phi(\vec{p}_T^{\text{miss}}, \vec{p}_{\ell\ell}) < \pi/2$	0.83	0.98	0.97

5.4 Control regions

Two control regions (CRs) are used to validate the SM background estimation and systematic uncertainties. These regions are depleted of signal by construction, and the events within them are not used to search for signal. The first, labeled “top CR,” targets background events with top quarks, particularly $t\bar{t}$. Such events are selected by inverting the AK4 jet b tag veto. To increase the statistical power of the sample, the p_T/m selection is removed for SL channel events, and the $\Delta R_{\ell\ell}$ selection is altered to $\Delta R_{\ell\ell} > 0.4$ for DL channel events. Events in this CR are then divided into the 12 categories previously described in Section 5.3. The $m_{b\bar{b}}$ and m_{HH} distributions in this CR are similar to the distributions in the signal region for backgrounds with top quarks. The top quark p_T spectrum in $t\bar{t}$ events has been shown to be mismodeled in simulation [116, 117]. A small p_T -dependent correction, on the order of a few percent, is measured in an expanded version of this CR and applied to the $t\bar{t}$ simulation.

While the top CR is an adequate probe of processes that involve top quarks, it is not sensitive to background from $Z/\gamma^* + \text{jets}$, $W + \text{jets}$, or QCD multijet processes. Instead, a second CR, labeled “non-top CR,” is used to study the modeling of these processes. The selection of events in this CR is the same as for the signal region, except that the $b\bar{b}$ jet is required to be inconsistent with having $b\bar{b}$ substructure, i.e., $0.01 < D_{Z/H \rightarrow b\bar{b}} < 0.04$. We exclude events with $D_{Z/H \rightarrow b\bar{b}} < 0.01$ because of substantial mismodeling in that region. As a result, events in this CR are not categorized by $b\bar{b}$ jet tagging, yielding half as many (six) categories here as in the top CR. Because it has fewer categories, the non-top CR cannot in principle test the modeling of the b tagging of light-flavor quark or gluon jets. Instead, we rely on the top CR to verify that this modeling is well-behaved.

Ultimately, the final values of the normalization and shape of each background component and their corresponding uncertainties are determined in the 2D fit to the data in the search region.

6 Background and signal modeling

The search is performed by simultaneously estimating the signal and background yields with a 2D maximum likelihood fit of the data in the 12 event categories. The data are binned in two dimensions, $m_{b\bar{b}}$ and m_{HH} , within the ranges $30 < m_{b\bar{b}} < 210 \text{ GeV}$ and $700 < m_{HH} < 5050 \text{ GeV}$. The $m_{b\bar{b}}$ bin width is 6 GeV, and the m_{HH} bin width is variable: 25 GeV width at the low end of the mass range, 50 GeV width in the middle of the mass range, and 75 GeV at high mass. These bin widths are smaller than the mass resolutions of the signal in the relevant parts of m_{HH} space. Signal and background mass distributions are modeled using a number of 2D templates that are created using only simulation, which is smoothed using different strategies described

in the rest of this section before the templates are fit to data. Independent templates are used for each event category. Shape and normalization uncertainties that account for possible differences between data and simulation are included while executing the fit. This fitting method was previously presented in Ref. [59].

6.1 Background component classification

To perform the fit to data, we split the background into components and then generate 2D templates in the $m_{b\bar{b}}$ and m_{HH} mass plane for each component independently. The normalization and shape of each component is then allowed to vary in the fit to the data in each search category.

Instead of splitting by SM process, we distinguish four components by particle-level information, such that they each have distinct $m_{b\bar{b}}$ distribution shapes. The background is divided by counting in simulation the number of generator-level quarks from the immediate decay of a top quark or vector boson within $\Delta R < 0.8$ of the $b\bar{b}$ jet axis. The first component is the “ m_t background,” in which all three quarks from a single top quark decay fulfill this criterion. The second component is the “ m_W background,” identified as the events that do not fulfill the m_t background criterion but in which both quarks from either a Z or W boson fall within the jet cone. Both of these backgrounds contain resonant peaks in the $m_{b\bar{b}}$ shape corresponding to either the top quark or W boson mass. The “lost-t/W background” contains events in which at least one quark is contained within the $b\bar{b}$ jet cone, but not the full set needed to satisfy one of the previous two requirements. Finally, all other events are designated by the “q/g background”. The first three categories are primarily composed of $t\bar{t}$ events, while the q/g background is composed mostly of W+jets and QCD multijet processes in the SL channel and of Z/ γ^* +jets in the DL channel. The background classification is summarized in Table 5. Figure 3 shows the pre-fit $m_{b\bar{b}}$ spectrum separately for the SL and DL channels. The background components are shown either as SM processes or with the background classification just described.

Table 5: The four background components with their kinematical properties and defining number of generator-level quarks within $\Delta R < 0.8$ of the $b\bar{b}$ jet axis.

Bkg. category	Dominant SM processes	Resonant in $m_{b\bar{b}}$	Num. of particle-level quarks
m_t	$t\bar{t}$	top quark mass	3 from top quark
m_W	$t\bar{t}$	W boson mass	2 from W boson
lost-t/W	$t\bar{t}$	No	1 or 2
q/g	V+jets and QCD multijet	No	0

6.2 Template construction strategy

For each of the four background components, a unique template in the $m_{b\bar{b}}$ and m_{HH} mass plane is produced for each of the 12 event categories. First, we produce a small set of inclusive templates that have more statistical power than the set of events in each individual search category. These inclusive templates are made by combining events in multiple categories and by relaxing selections, provided that the inclusive shape remains consistent with the shape for the full selection. Then, for each of the 12 event categories, the inclusive templates are fit to the simulated mass distributions to produce a unique template. This fit is performed in a similar manner and with a similar parameterization of the template shape as is done for the fit to data. The background templates and associated systematic uncertainties are ultimately validated by fitting to data in dedicated CRs, a procedure described in Section 6.5.

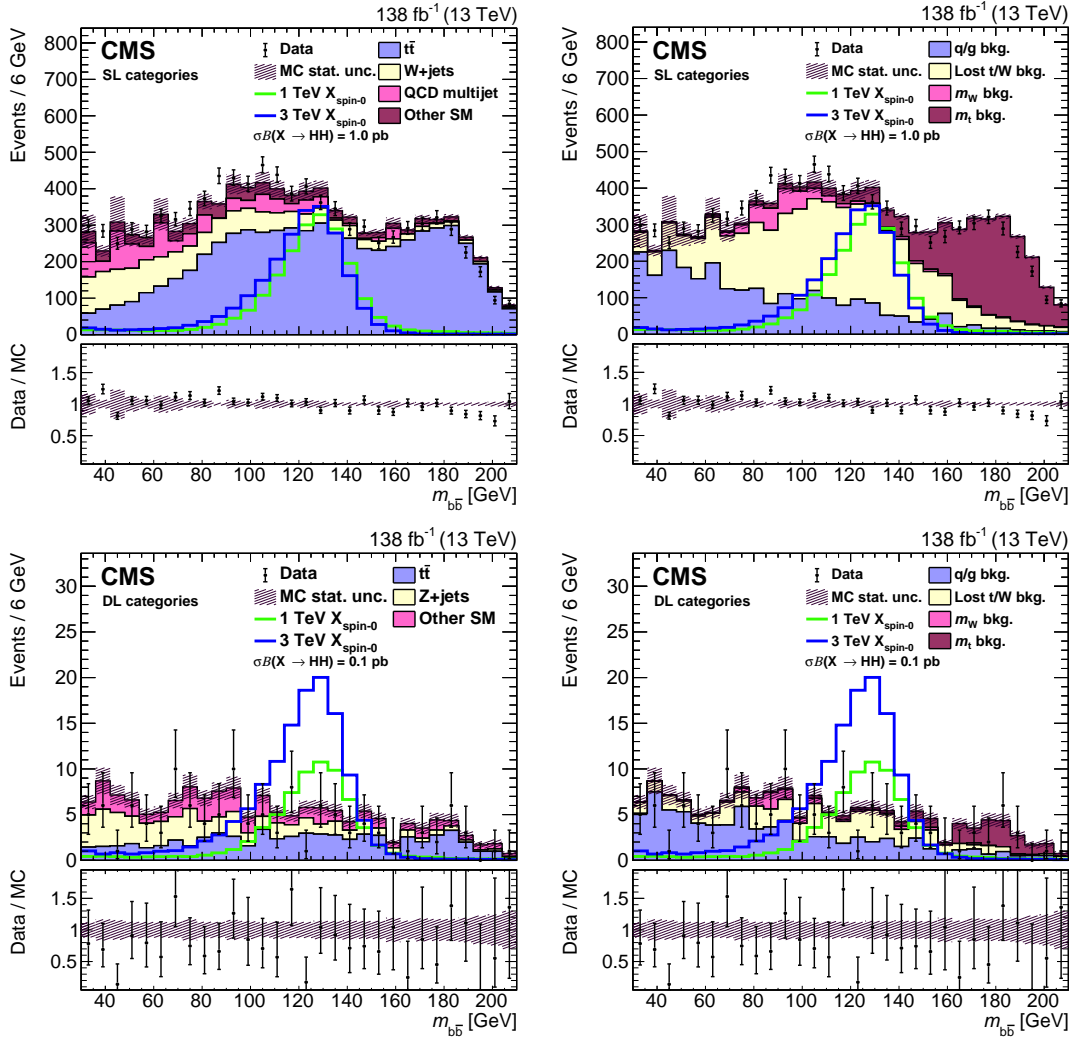


Figure 3: The pre-fit m_{bb} distributions for the SL (upper row) and DL (lower row) channels. The data are shown as the points with error bars. In each plot, the pre-fit background (filled histograms) is shown broken down either according to the SM process (left) or according to the background classification of Section 6.1 (right). The total simulated background is the same in each case. The statistical uncertainty in the simulated sample is shown as the hatched band. Spin-0 signals for m_X of 1.0 and 3.0 TeV are also shown (solid lines). The product $\sigma\mathcal{B}(X \rightarrow HH)$ is set to 1.0 pb for the SL channel and 0.1 pb for the DL channel. The lower panels of each plot show the ratio of the data to the sum of all background processes.

In the SL channel, a modified approach is used when building templates that reduces fluctuations due to the limited size of the QCD multijet simulated event sample. The bb jet reconstruction in the QCD multijet simulation is similar to that in $W+jets$, and the $W+jets$ simulation has much more statistical power. Both processes contribute significantly to the q/g background, with light-flavored quark or gluon AK8 jets that are misidentified as b jets, yielding very similar falling shapes in the m_{bb} spectrum and similar bb jet tagging distributions. Instead of using the QCD simulation directly in the q/g background modeling, a combined distribution is created by measuring the ratio of QCD to $W+jets$ event yields as a function of m_{HH} and then using these corrections to scale up the $W+jets$ simulation. Corrections and distributions are obtained for each lepton flavor and $H \rightarrow WW^*$ purity category, since the bb jet tagging between $W+jets$ and QCD is equivalent. This distribution is then used as input to the q/g background

modeling to account for both processes.

6.3 Background modeling

The background templates are modeled using conditional probabilities of $m_{b\bar{b}}$ as a function of m_{HH} so that the templates include the correlation of these two variables, fully described in Ref. [72]. The full 2D template is defined as:

$$P_{\text{bkg}}(m_{b\bar{b}}, m_{HH}) = P_{b\bar{b}}(m_{b\bar{b}} | m_{HH}, \theta_1) P_{HH}(m_{HH} | \theta_2), \quad (5)$$

where $P_{b\bar{b}}$ is a 2D conditional probability distribution, P_{HH} is a 1D probability distribution, and θ_1 and θ_2 are sets of nuisance parameters used to account for background shape uncertainties. The sets θ_1 and θ_2 do not share any common nuisance parameters.

The P_{HH} templates are produced by smoothing 1D m_{HH} histograms with kernel density estimation (KDE) [118–120]. To produce these templates, we use Gaussian kernels with adaptive bandwidths, which are parameters of the KDE that control the smoothing and are dependent on the local event density. We do this to apply less smoothing to regions of the distribution with many events and more smoothing to regions with few events. For $m_{HH} \gtrsim 2 \text{ TeV}$, where there are very few events in simulation or in data, the m_{HH} tail is further smoothed by fitting with an exponential function.

The 2D templates $P_{b\bar{b}}$ are obtained with different methods for the resonant and nonresonant background components. For each of the resonant backgrounds (m_t and m_W), we fit the $m_{b\bar{b}}$ distributions with a double Crystal Ball function [121, 122] centered around m_t and m_W , respectively. This function has a Gaussian core, which is used to model the bulk of the $m_{b\bar{b}}$ resonance, and power-law tails, which account for the effects of jet misreconstruction. The fits are performed for events binned in m_{HH} to capture the dependence of the $m_{b\bar{b}}$ shape on m_{HH} . For the nonresonant backgrounds (lost-t/W and q/g), the $P_{b\bar{b}}$ are estimated from 2D histograms using 2D KDE. Independent KDE parameters are used for each dimension and each background when building the $P_{b\bar{b}}$ templates. As done for the P_{HH} tail modeling, the high-mass m_{HH} distribution tail here is exponentially smoothed. The normalizations from simulation are used as the initial values for the background normalizations in the fit to data.

6.4 Signal modeling

The signal templates are also defined following Ref. [72] using conditional probabilities:

$$P_{\text{signal}}(m_{b\bar{b}}, m_{HH} | m_X) = P_{HH}(m_{HH} | m_{b\bar{b}}, m_X, \theta'_1) P_{b\bar{b}}(m_{b\bar{b}} | m_X, \theta'_2). \quad (6)$$

The sets θ'_1 and θ'_2 do not share any common nuisance parameters. However, θ'_2 and θ_1 from Eq. (5) do share two nuisance parameters corresponding to the mass scale and resolution uncertainties of SD jets in the $m_{b\bar{b}}$ dimension. This is discussed in more detail in Section 7.1.2.

The P_{signal} distributions are first obtained for discrete m_X values by fitting histograms of the signal mass distributions. The mass shapes for spin-0 and spin-2 signals are very similar, and so the modeling is performed on the combined set of events and applied to both spin hypotheses. Models continuous in m_X are then produced by interpolating the fit parameters. The 1D $P_{b\bar{b}}$ templates are created by fitting the $m_{b\bar{b}}$ spectra with a double Crystal Ball function, and the mass resolution is slightly larger than 10%, with the largest resolution at low mass. The modeling of events in the bL category also contains an exponential component to model the small fraction of signal events with no resonant peak in the distribution.

The 2D P_{HH} templates are designed to account for correlations between m_{HH} and $m_{b\bar{b}}$. These m_{HH} distributions are also modeled with a double Crystal Ball function, but with an additional linear dependence on $m_{b\bar{b}}$, parameterized by $\Delta_{b\bar{b}} = (m_{b\bar{b}} - \mu_{b\bar{b}})/\sigma_{b\bar{b}}$. Here, $\mu_{b\bar{b}}$ and $\sigma_{b\bar{b}}$ are the mean and width parameters, respectively, in the fit to the $m_{b\bar{b}}$ spectra. To accomplish this, the mean parameter μ_{HH} in the Crystal Ball function fit is then taken to be

$$\mu_{\text{HH}} = \mu_0(1 + \mu_1\Delta_{b\bar{b}}), \quad (7)$$

where μ_0 and μ_1 are fit parameters. With this approach, we can account for mismeasurements of the $b\bar{b}$ jet that result in mismeasurements of m_{HH} . The resolution of the m_{HH} resonance, denoted as σ_{HH} , is also dependent on $m_{b\bar{b}}$ such that

$$\sigma_{\text{HH}} = \begin{cases} \sigma_0(1 + \sigma_1\Delta_{b\bar{b}}), & \Delta_{b\bar{b}} < 0 \\ \sigma_0, & \Delta_{b\bar{b}} > 0 \end{cases} \quad (8)$$

where σ_0 and σ_1 are fit parameters. In the case that the SD algorithm produces an undermeasurement of $m_{b\bar{b}}$ by removing too much energy from the Higgs boson decay, the correlation increases, and the m_{HH} resolution grows wider. For $|\Delta_{b\bar{b}}| > 2.5$, we use the value at the boundary, since the correlation does not hold for severe mismeasurements. The m_{HH} resolution is $\approx 5\%$.

The product of the acceptance and efficiency for $X \rightarrow \text{HH}$ events to fall into any of the individual search categories is taken from simulation. As done for the signal shape parameters, the efficiency is interpolated along m_X . Uncertainties in the relative acceptances and in the integrated luminosity of the sample are included in the 2D maximum likelihood fit that is used to obtain confidence intervals for the $X \rightarrow \text{HH}$ process. The signal modeling is tested using toy experiments in which we fit the templates to pseudodata that contain a fixed amount of signal; no significant bias in the fitted signal yield is found.

6.5 Validation of background models with control region data

The background models are validated in the top CR and non-top CR data samples. For both CRs, background templates are constructed in the same way as for the search region, except using the CR selection. The background templates are then fit to the CR data with the same nuisance parameters that are used in the standard 2D maximum likelihood fit. In the non-top CR, the m_t background is negligible and not included in the modeling. The result of the simultaneous fit is shown in Fig. 4 for both CRs. To improve visualization, the displayed binning in these and subsequent histograms is coarser than the binning used in the maximum likelihood fit. The projections in both mass dimensions are shown for the combination of all event categories. The fit results model the data well, indicating that the shape uncertainties can account sufficiently for potential differences between data and simulation.

7 Systematic uncertainties

Systematic uncertainties that affect the normalization and shape of the signal and background are modeled with nuisance parameters in the 2D maximum likelihood fit to data. Nuisance parameters for shape uncertainties have Gaussian constraints, while normalization uncertainties have log-normal constraints. In certain cases a single nuisance parameter may affect both the normalization and the shape of a resonance, in which case the nuisance parameter constraint is Gaussian. Detailed methods of parameterizing the background and signal uncertainties are described in Sections 7.1 and 7.2, respectively.

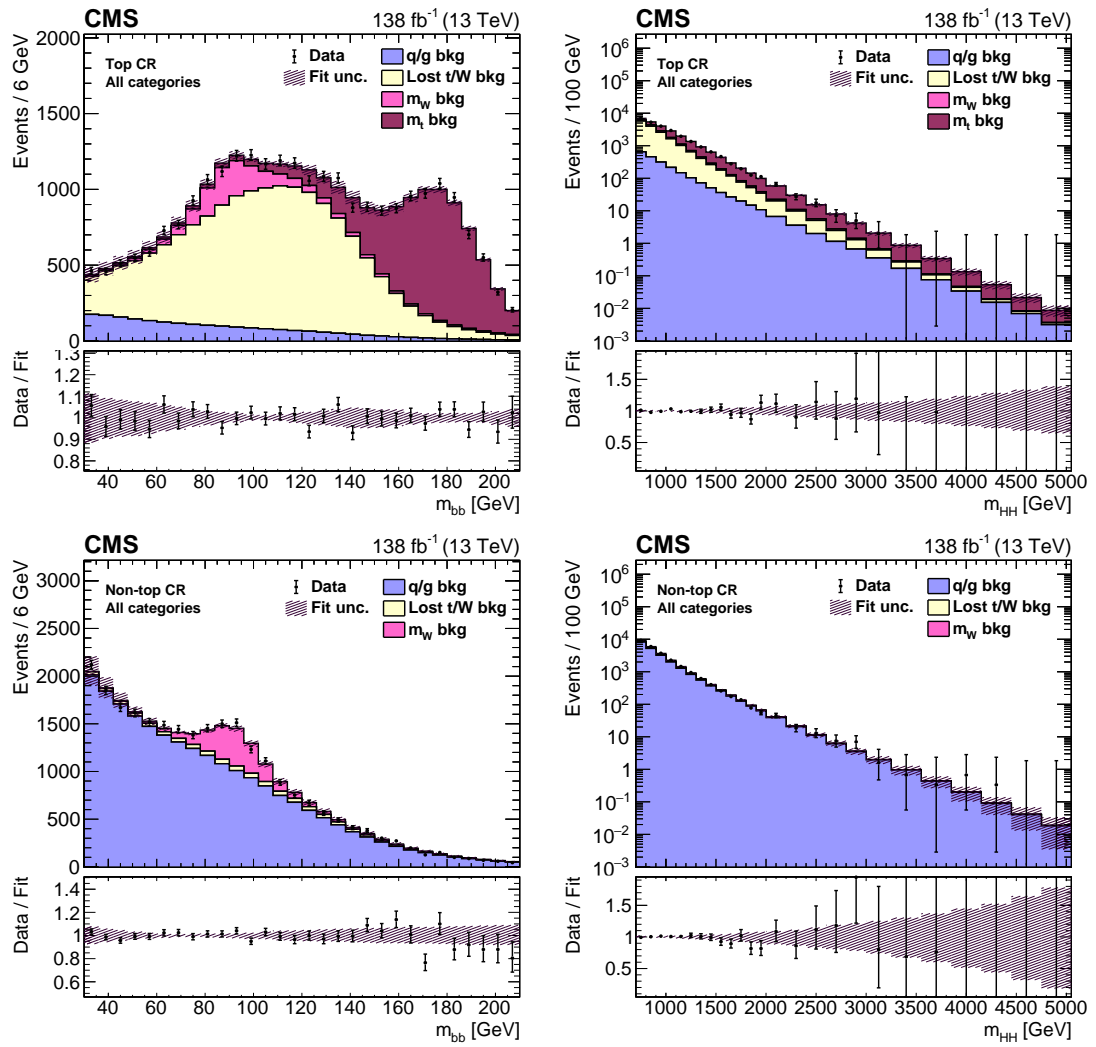


Figure 4: The post-fit model compared to data in the top CR (upper plots) and non-top CR (lower plots), projected into $m_{b\bar{b}}$ (left) and m_{HH} (right). Events from all categories are combined. The fit result is the filled histogram, with the different colors indicating different background components. The background shape uncertainty is shown as the hatched band. The lower panels of each plot show the ratio of the data to the fit result.

To implement nonresonant mass shape uncertainties, templates are first generated with modified event weights that include multiplicative parameters proportional to $m_{b\bar{b}}$, m_{HH} , $1/m_{b\bar{b}}$, and $1/m_{HH}$. Each of these four modifications produces two alternative templates that represent an upward and downward shift from the nominal model. The 2D fit then interpolates between these two alternative templates to constrain the magnitudes of these parameters. Resonant mass shape uncertainties are implemented as uncertainties in the mean and width parameters of a double Crystal Ball function. In most cases, different nuisance parameters are used for the background shape uncertainties from those used for the signal uncertainties.

All background and signal uncertainties are listed in Tables 6 and 7, respectively, with their initial sizes. A single uncertainty type can be applied to multiple event categories with independent nuisance parameters for each category. The background model contains 104 total nuisance parameters, while the signal model contains 27, with two parameters shared between signal and background. The descriptions of all uncertainties and their correlations are also

described in the rest of this section.

7.1 Background uncertainties

Background uncertainty parameters are chosen by considering possible discrepancies between data and simulation, such as in the relative background composition or in the jet energy scale. Studies of the two CRs are used to verify that the chosen uncertainties cover such differences. The fitted values do not depend strongly on the sizes of the pre-fit uncertainties because they serve as loose constraints on the fit. We verify this by inflating all pre-fit background uncertainties by a factor of two and observing that the final result does not change. Therefore, the pre-fit uncertainties are sufficiently large to account for discrepancies between data and simulation in the CRs. More complex background models, such as those with more nuisance parameters or higher-order shape distortions, were previously studied in Ref. [72] but were not found to be necessary.

Table 6: Background systematic uncertainties included in the maximum likelihood fit. The uncertainty types with “normalization” correspond to uncertainties in the background yield, while all others are uncertainties in the background shape. The N_p column indicates the number of nuisance parameters used to model the uncertainty. In the last two columns, σ_I refers to the initial estimate of the uncertainty, and σ_C refers to the constrained uncertainty obtained post-fit. For the q/g , $t\bar{t}$, and lost-t/W shape uncertainties, “scale” uncertainties are those implemented with alternative templates with multiplicative parameters proportional to mass m , and “inverse scale” uncertainties are those implemented with parameters proportional to $1/m$.

Uncertainty type	Processes	N_p	σ_I	σ_C/σ_I
SD jet $m_{b\bar{b}}$ scale	m_W, m_t , signal	2	0.54%, 2.0% (m_t)	98%, 19% (m_t)
SD jet $m_{b\bar{b}}$ resolution	m_W, m_t , signal	2	8.6%, 17.2% (m_t)	95%, 25% (m_t)
q/g normalization	q/g	12	50% (1 ℓ), 100% (2 ℓ)	37–78%
q/g m_{HH} scale	q/g	10	$\pm 0.5 m_{HH} / \text{TeV}$	78–99%
q/g m_{HH} inverse scale	q/g	10	$\pm 1.4 \text{TeV} / m_{HH}$	64–99%
q/g $m_{b\bar{b}}$ scale	q/g	4	$\pm 0.00375 m_{b\bar{b}} / \text{GeV}$	81–99%
q/g $m_{b\bar{b}}$ inverse scale	q/g	4	$\pm 15 \text{GeV} / m_{b\bar{b}}$	77–99%
Lost-t/W $m_{b\bar{b}}$ scale	lost-t/W	4	$\pm 0.003 m_{b\bar{b}} / \text{GeV}$	71–99%
Lost-t/W $m_{b\bar{b}}$ inverse scale	lost-t/W	4	$\pm 18 \text{GeV} / m_{b\bar{b}}$	88–99%
$t\bar{t}$ normalization	lost-t/W, m_W, m_t	12	35% (1 ℓ), 70% (2 ℓ)	19–68%
$t\bar{t}$ relative normalization	lost-t/W, m_W, m_t	8	35% (1 ℓ), 70% (2 ℓ)	9–96%
$t\bar{t}$ m_{HH} scale	lost-t/W, m_W, m_t	12	$\pm 0.25 m_{HH} / \text{TeV}$	84–99%
$t\bar{t}$ m_{HH} relative scale	lost-t/W, m_W, m_t	8	$\pm 0.25 m_{HH} / \text{TeV}$	74–99%
$t\bar{t}$ m_{HH} inverse scale	lost-t/W, m_W, m_t	12	$\pm 0.7 \text{TeV} / m_{HH}$	61–99%

In the following subsections, we detail the parameterization of the different uncertainties for the background.

7.1.1 Background normalization uncertainties

The m_W , m_t , and lost-t/W backgrounds all primarily arise from $t\bar{t}$ production. Consequently, some uncertainties are applied by treating these three backgrounds together, referred to collectively as the $t\bar{t}$ background in Table 6. We account for differences between data and simulation in the $t\bar{t}$ normalization by including independent nuisance parameters for each category that allow the normalizations of these backgrounds to vary in a correlated manner (“ $t\bar{t}$ normalization”). However, the three $t\bar{t}$ -dominated background components exhibit differences in the

b tagging efficiency and the $b\bar{b}$ jet p_T spectrum, so we include additional nuisance parameters (“ $t\bar{t}$ relative normalization”) that allow the relative normalizations of each of these to vary within the absolute normalization, which itself also varies. Separate nuisance parameters are used to control the q/g background normalization, as this is the only background component to arise primarily from non- $t\bar{t}$ processes.

7.1.2 Background shape uncertainties

The shape uncertainties for the backgrounds are modeled differently depending on whether or not the shape is resonant in the $m_{b\bar{b}}$ dimension. All backgrounds are nonresonant in the m_{HH} dimension, and mismodeling of the background p_T spectrum can manifest as an incorrect m_{HH} scale. To account for this, the m_{HH} shape uncertainties are implemented with alternative background templates built with parameters proportional to m_{HH} (“scale”) and $1/m_{HH}$ (“inverse scale”), as described in the beginning of Section 7. For the q/g background, a pair of these nuisance parameters is included for each category in the SL channel and for each b tagging category in the DL channel. For the $t\bar{t}$ -dominated backgrounds, we include a pair of these nuisance parameters for each search category. Furthermore, to allow the $t\bar{t}$ -dominated backgrounds to be anticorrelated, we include nuisance parameters for the relative m_{HH} scale (alternative templates built with factors proportional to m_{HH}) for each b tagging category, separately for the SL and DL channels.

The q/g and lost-t/W backgrounds are nonresonant in $m_{b\bar{b}}$, and thus alternative templates are also used to encode the shape uncertainties for the $m_{b\bar{b}}$ dimension with factors proportional to $m_{b\bar{b}}$ or $1/m_{b\bar{b}}$. The uncertainties account for mismodeling in the simulated jet energy scale and resolution. For both of these nonresonant backgrounds, the $m_{b\bar{b}}$ shape does not depend on the lepton flavor or the $H \rightarrow WW^*$ purity, and so there is a pair of nuisance parameters for each background and each $b\bar{b}$ jet tagging category, separately for the SL and DL channels.

For the m_W and m_t backgrounds in the $m_{b\bar{b}}$ dimension, where resonances are constructed using AK8 SD jets, the jet mass uncertainties are dependent on the jet substructure. Because of this, the jet mass uncertainties for the signal and the m_W background, respectively from the two-prong decays $H \rightarrow b\bar{b}$ and $W \rightarrow q\bar{q}'$, are correlated. This is the only such instance where signal and background are correlated, sharing nuisance parameters. Uncertainties that have been measured in data for W boson decays into merged jets in $t\bar{t}$ events are found to cover discrepancies between our simulation and data for the m_W background but not for the m_t background. We do not expect these uncertainties to cover discrepancies in the m_t background because the SD algorithm behaves differently for the three-prong top quark jets ($t \rightarrow b\bar{q}\bar{q}'$) in this background. Thus, these uncertainties are larger than for two-prong jets and are not correlated with the m_W jet mass shape uncertainties, as seen in the upper two rows of Table 6.

7.2 Signal uncertainties

As shown in Table 7, uncertainties are applied to the normalization of the signal to account for mismeasurements in the total integrated luminosity [123–125], the pileup profile, the trigger efficiency, the lepton selection efficiencies, and other detector effects. Signal acceptance uncertainties from the choices of the PDFs and also the factorization and renormalization scales are also applied. The scale uncertainties are obtained following Refs. [126, 127], and the PDF uncertainty is evaluated using the NNPDF 3.1 PDF set [101].

The signal acceptance and the m_{HH} resonance scale and resolution all have uncertainties due to the jet energy scale and resolution, the unclustered energy resolution, and other detector

Table 7: Signal systematic uncertainties included in the maximum likelihood fit. The N_p column indicates the number of nuisance parameters used to model the uncertainty. In the “Uncertainty values” column, some uncertainties are noted as affecting both the yield (Y) and m_{HH} shape (S for scale, R for resolution) of the signal. All other uncertainties, except the SD jet mass uncertainties, are uncertainties in the signal yield alone.

Uncertainty type	N_p	Uncertainty values
SD jet $m_{b\bar{b}}$ scale	1	0.54%
SD jet $m_{b\bar{b}}$ resolution	1	8.6%
Integrated luminosity	1	1.6%
PDFs+scales	1	spin-0: 2.0%, spin-2: 2.5%
Trigger	6	1ℓ : 2.0%, 2ℓ : 3.0%
Pileup	1	1ℓ : 1.0%, 2ℓ : 0.6%
Electron reconstruction	1	1ℓ : 0.5%, 2ℓ : <0.8%
Electron identification	2	1ℓ : 4.2%, 2ℓ : <2.6%
Muon identification	2	1ℓ : 2.3%, 2ℓ : <2.3%
Electron isolation	1	1ℓ : 6%, 2ℓ : 3% for each electron
Muon isolation	1	1ℓ : 6%, 2ℓ : 2% for each muon
Jet energy scale	1	Y : 2%, $S(m_{\text{HH}})$: 0.8%, $R(m_{\text{HH}})$: 3%
Jet energy resolution	1	Y : 0.5%. $S(m_{\text{HH}})$: 0.3%, $R(m_{\text{HH}})$: 4%
Unclustered energy	1	Y : 0.5%, $S(m_{\text{HH}})$: 0.1%, $R(m_{\text{HH}})$: 1.5%
Other detector effects	2	Y : 0.6%, $R(m_{\text{HH}})$: 1.0%
AK4 b tag efficiency	1	<4.0%
AK4 b tag misidentification rate	1	<2.5%
$b\bar{b}$ jet tagging	1	bL: 8.5%, bT: 11.5%
$q\bar{q}'$ jet τ_2/τ_1 efficiency	1	LP: 26% HP: 6.7%

effects. The same $m_{b\bar{b}}$ resonance scale and resolution uncertainties that are applied for the m_W background are applied to the signal because they are both SD jets with two-prong substructure.

The $q\bar{q}'$ jet τ_2/τ_1 selection efficiency is measured in a $t\bar{t}$ data sample enriched with hadronically decaying W bosons. The uncertainties in this measurement are included as normalization uncertainties in the $H \rightarrow WW^*$ decay purity categories, and the LP and HP uncertainties are anticorrelated. Normalization uncertainties are also applied to account for the efficiency and misidentification rate of AK4 jet b tagging used to identify and reject jets from $t\bar{t}$ production. The uncertainty in the $b\bar{b}$ jet tagging efficiency is included as a single nuisance parameter that varies the signal normalization and is dependent on both the $b\bar{b}$ jet tagging category and m_X . These $b\bar{b}$ jet tagging uncertainties are the dominant uncertainties associated with the signal normalization, followed by the uncertainties in the τ_2/τ_1 efficiencies.

8 Results

The data are interpreted by performing a maximum likelihood fit in the 2D ($m_{b\bar{b}}, m_{\text{HH}}$) mass plane using one model containing only background processes and using one containing both background and signal processes. We find that the background-only model fits the data well. We interpret the results as upper limits at 95% confidence level (CL) on $\sigma\mathcal{B}(X \rightarrow HH)$.

The quality of the fit is quantified with a likelihood ratio goodness-of-fit test using the saturated model [128]. The probability distribution function of the test statistic is obtained with toy

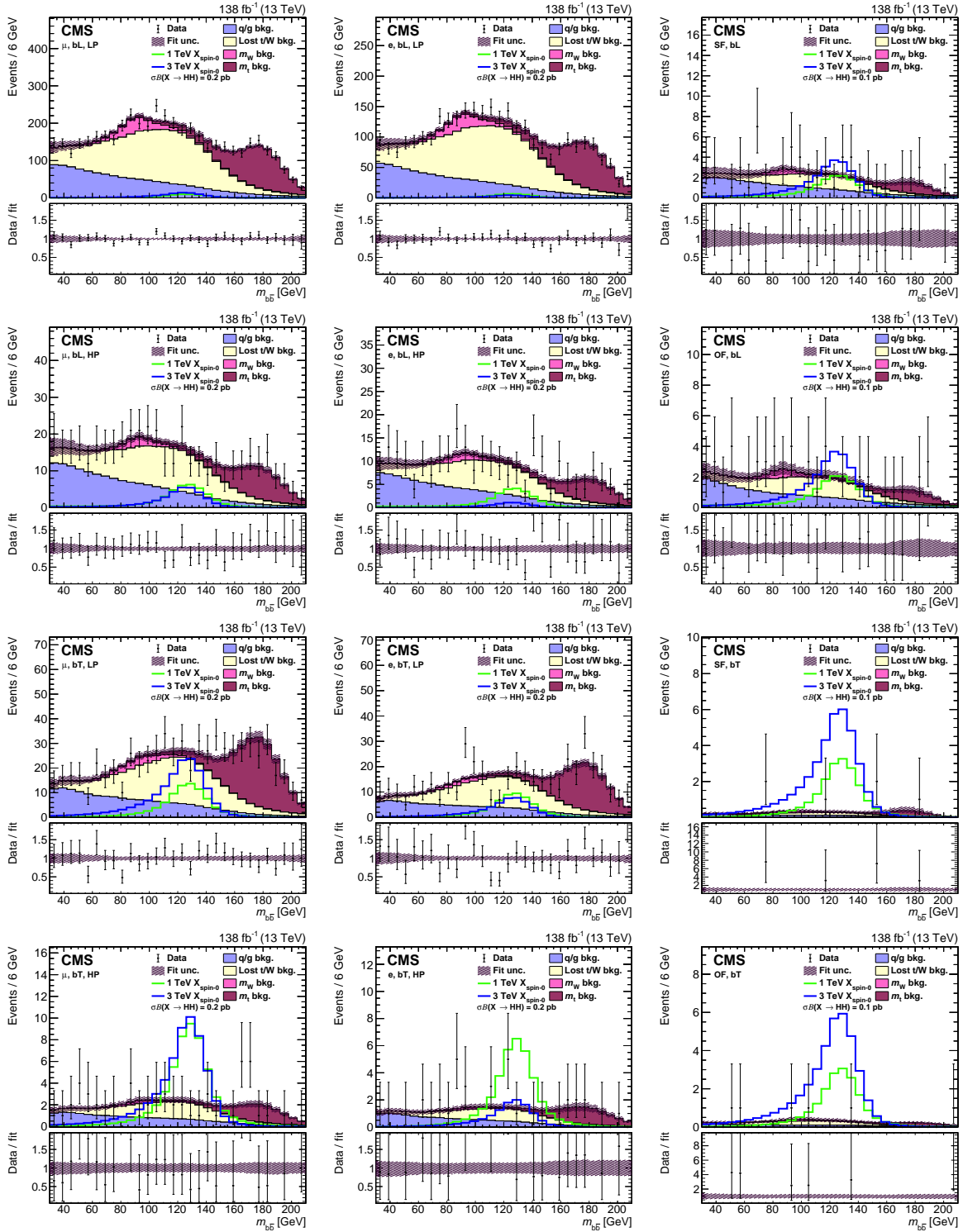


Figure 5: The background-only 2D fit result compared to data projected onto the $m_{b\bar{b}}$ axis for both the SL and DL channels. The label for each search category is in the upper left of each plot. The fit result is the filled histogram, with the different colors indicating different background components. The background shape uncertainty from the fit is shown as the hatched band. Example spin-0 signal distributions for $m_X = 1.0$ and 3.0 TeV are shown as solid lines, with $\sigma\mathcal{B}(X \rightarrow HH)$ set to 0.2 and 0.1 pb for the SL and DL channels, respectively. The lower panels show the ratio of the data to the fit result. Only nonzero data entries are shown in the interest of clarity.

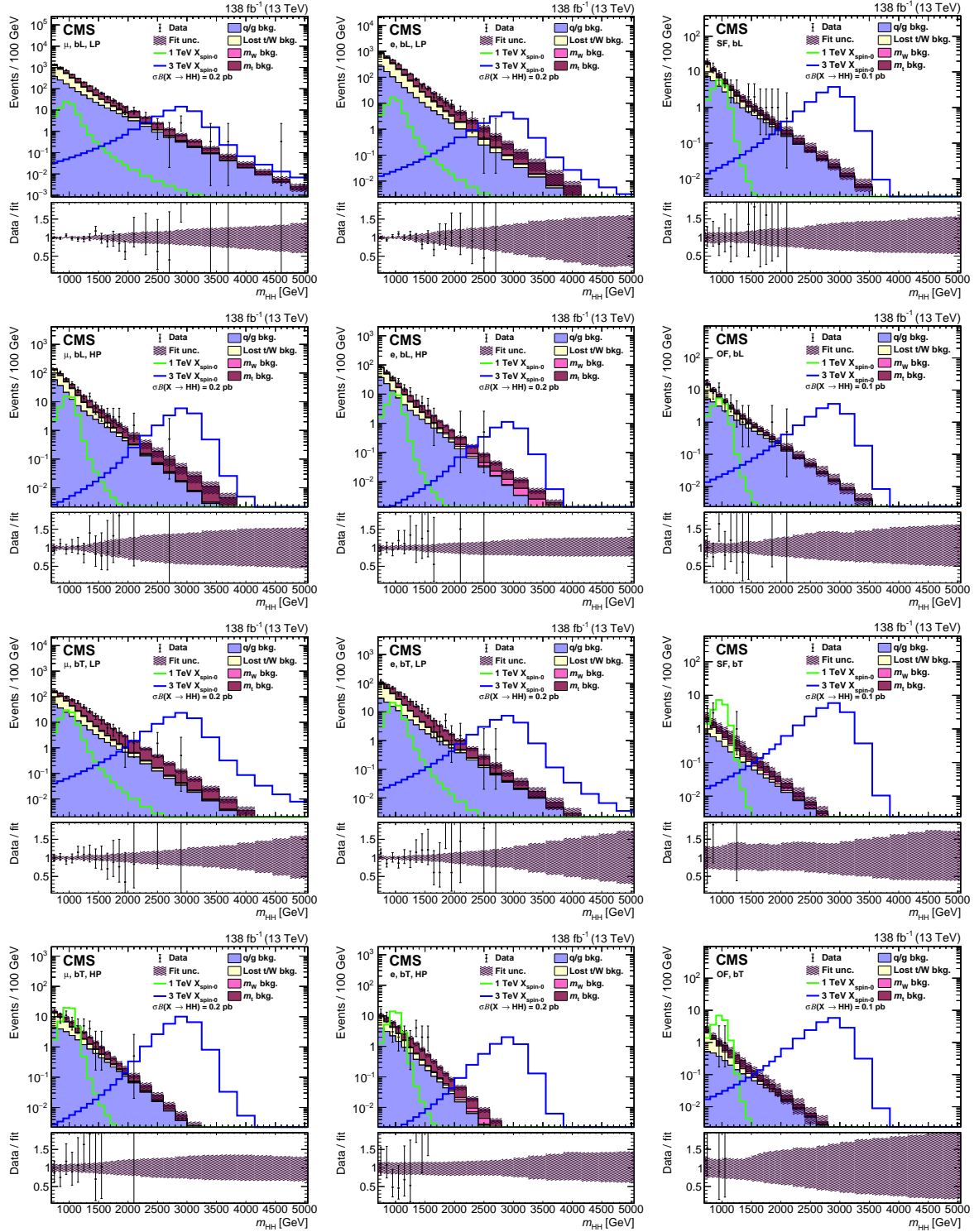


Figure 6: The background-only 2D fit result compared to data projected onto the m_{HH} axis for both the SL and DL channels. The label for each search category is in the upper left of each plot. The fit result is the filled histogram, with the different colors indicating different background components. The background shape uncertainty from the fit is shown as the hatched band. Example spin-0 signal distributions for $m_X = 1.0$ and 3.0 TeV are shown as solid lines, with $\sigma\mathcal{B}(X \rightarrow \text{HH})$ set to 0.2 and 0.1 pb for the SL and DL channels, respectively. The lower panels of each plot show the ratio of the data to the fit result. Only nonzero data entries are shown in the interest of clarity.

experiments, and the observed value is within the central 68% interval of expected results. The best-fit values of the nuisance parameters are consistent with the initial $\pm 1\sigma$ range of uncertainty.

The fit result and the data are projected in $m_{b\bar{b}}$ for each event category in Fig. 5. The $m_{b\bar{b}}$ shape is modeled well by the background-only model, and each background component is important in at least some subspace of the mass range. Particularly, the resonant peaks corresponding to the W boson and top quark are correctly modeled by the fit. Similarly, the m_{HH} projections of the fit are shown in Fig. 6. There is good agreement for the full m_{HH} mass range in these figures as well.

Upper limits are shown at 95% CL in Fig. 7 for both the spin-0 and spin-2 boson scenarios. The limits are evaluated using the asymptotic approximation [129] of the CL_s method [130, 131]. The observed exclusion limits are consistent with the expected limits. A spin-0 signal at $m_X = 0.8$ TeV is excluded for $\sigma\mathcal{B} > 24.5$ fb, and the exclusion limits strengthen over the full mass range to $\sigma\mathcal{B} > 0.78$ fb at $m_X = 4.5$ TeV. Spin-2 signals have larger acceptance, and so the exclusion limits on these signals are stronger: at $m_X = 0.8$ TeV, we exclude $\sigma\mathcal{B} > 16.7$ fb, and at $m_X = 4.5$ TeV we exclude $\sigma\mathcal{B} > 0.67$ fb.

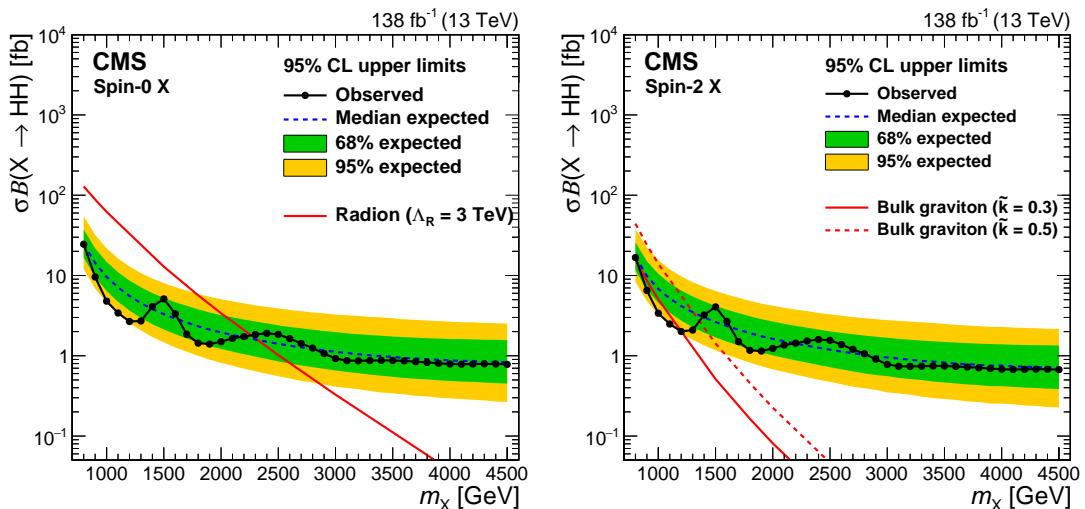


Figure 7: Observed and expected 95% CL upper limits on the product of the cross section and branching fraction to HH for a generic spin-0 (left) and spin-2 (right) boson X , as functions of mass. Example radion and bulk graviton predictions are also shown. The HH branching fraction is assumed to be 25% for radions and 10% for bulk gravitons.

Table 8 shows the event yields for each search category that are observed in data and are expected before and after a background-only fit, along with the associated post-fit uncertainty in the total background yield in each category. Figure 8 shows the expected exclusion limit at 95% CL for each search category alone. In general, the tight (bT) bb jet tagging categories are the most sensitive over the full range of m_X , since these contain the most signal and the least amount of background. The DL categories are generally more sensitive than most SL categories since the background yields are much lower in the DL channel. A notable exception to this trend is the μ bT LP category, which is the most sensitive above approximately 2.5 TeV. At high m_X , the electron categories in the SL channel are the least sensitive because the electron reconstruction efficiency is degraded.

Relative to the $X \rightarrow b\bar{b}\ell\nu q\bar{q}'$ search in Ref. [72], this analysis ranges from 6 times more sensitive at low m_X to 14 times more sensitive at high m_X . The improvements in sensitivity arise primar-

Table 8: Event yields broken down by search category. For each category, shown are the event yields observed in data, expected before and after a fit of the background-only model, and the corresponding relative uncertainty.

Search category	Observed	Expected (pre-fit)	Expected (post-fit)	Post-fit uncertainty
μ bL LP	4542	4362.2	4540.9	1.5%
μ bL HP	417	402.4	416.1	4.8%
μ bT LP	657	731.8	658.5	4.2%
μ bT HP	56	67.0	57.3	10.0%
e bL LP	2945	2973.7	2945.4	1.9%
e bL HP	248	246.1	247.7	5.7%
e bT LP	423	443.0	423.9	4.2%
e bT HP	37	41.0	37.7	14.6%
SF bL	59	70.2	59.6	14.2%
OF bL	50	61.1	50.8	13.5%
SF bT	6	11.3	7.9	31.6%
OF bT	6	11.6	8.1	25.8%

ily from three developments. First, an improvement in the expected upper limits by a factor of ≈ 3.5 is achieved because of the larger integrated luminosity alone. This level of improvement is expected because the number of background events is much smaller than the number of signal events under a typical signal peak, even at low m_X . Second, because of improved techniques in the SL channel alone, we achieve similar sensitivity at $m_X = 0.8$ TeV and up to a ≈ 2 times improvement at $m_X = 4.5$ TeV. Finally, the addition of the DL channel provides significant improvement in sensitivity. At low m_X , the DL channel is $\approx 70\%$ more sensitive than the SL channel, largely because the background level is over an order of magnitude smaller. At high m_X , where there is virtually no background in any channel, the DL channel has similar sensitivity to the SL channel. This occurs because the dilepton signal efficiency is largest at high mass, and in the SL channel, despite the larger branching fraction, the lepton efficiency (particularly for electrons) degrades at high mass because of the nearby $q\bar{q}'$ jet.

This search yields the most sensitive upper limits for $X \rightarrow HH$ production with leptons in the final state. The only $X \rightarrow HH$ searches that are more sensitive in any subspace of the considered m_X and for any spin hypothesis are those in the $b\bar{b}b\bar{b}$ final state from ATLAS and CMS, each of which extend only up to 3.0 TeV. From 0.8 to 3.0 TeV, the sensitivity of this search is mostly comparable to and in some places stronger than the $b\bar{b}b\bar{b}$ searches.

Predicted radion and bulk graviton cross sections [132] are also shown in Fig. 7 in the context of Randall–Sundrum models that allow the SM fields to propagate through an extra dimension. Typical model parameters are chosen as proposed in Ref. [133]. A branching fraction of 25% to HH and an ultraviolet cutoff $\Lambda_R = 3$ TeV are assumed for the radion, which is excluded for $m_X < 2.25$ TeV. A 10% branching fraction is assumed for the bulk graviton, which occurs in scenarios that include significant coupling between the bulk graviton and top quarks. Bulk graviton production cross sections depend on the dimensionless quantity $\tilde{k} = \sqrt{8\pi k/M_{Pl}}$, where k is the curvature of the extra dimension and M_{Pl} is the Planck mass. For this interpretation, we choose $\tilde{k} = 0.3$ and 0.5. The bulk gravitons with $\tilde{k} = 0.3$ and 0.5 are excluded for $m_X < 1.20$ and 1.35 TeV, respectively. For these particular signal parameters, the radion and bulk graviton decay widths are larger than the 1 MeV width chosen for signal sample generation but much smaller than the detector resolution.

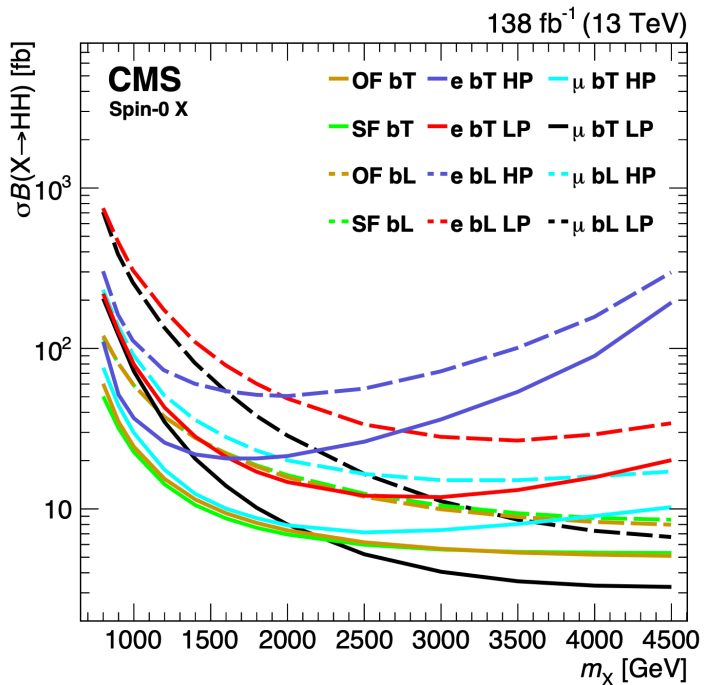


Figure 8: Median expected upper limits at 95% confidence level for each of the 12 search categories individually.

9 Summary

A search has been performed for new bosons (narrow resonances) decaying to a pair of Higgs bosons (HH) where one decays into a bottom quark pair ($b\bar{b}$) and the other via one of three different modes into final states with leptons. The large Lorentz boost of the Higgs bosons produces a distinct experimental signature with one jet that has substructure consistent with the decay $H \rightarrow b\bar{b}$. For the Higgs boson that does not decay to $b\bar{b}$, the single-lepton decay $H \rightarrow WW^* \rightarrow \ell\nu q\bar{q}'$ and the dilepton decays $H \rightarrow WW^* \rightarrow \ell\nu\ell\nu$ and $H \rightarrow \tau\tau \rightarrow \ell\nu\ell\nu$ are considered. In the single-lepton channel, the experimental signature is characterized by a second large jet with a nearby lepton, which is consistent with the decay of $H \rightarrow WW^*$. In the dilepton channel, the experimental signature contains two leptons and significant missing transverse momentum. This search uses a sample of proton-proton collisions at $\sqrt{s} = 13$ TeV, corresponding to an integrated luminosity of 138 fb^{-1} , collected by the CMS detector at the LHC. The primary standard model backgrounds—production of top quark pairs and of vector bosons in association with jets—are suppressed by reconstructing the HH decay chain and applying selections to discriminate signal from background. The signal and background yields are estimated by a two-dimensional template fit in the plane of the $b\bar{b}$ jet mass and the HH resonance mass. The templates are validated in a variety of data control regions and are shown to model the data well. The data are consistent with the expected standard model background. Upper limits are set on the product of the cross section and branching fraction for new bosons decaying to HH. The observed limit at 95% confidence level for a spin-0 (spin-2) boson ranges from 24.5 (16.7) fb at 0.8 TeV to 0.78 (0.67) fb at 4.5 TeV. The results of this search provide the most stringent exclusion limits to date for $X \rightarrow HH$ signatures with leptons in the final state and are among the most stringent of all $X \rightarrow HH$ searches, at certain mass points the most sensitive.

Acknowledgments

We congratulate our colleagues in the CERN accelerator departments for the excellent performance of the LHC and thank the technical and administrative staffs at CERN and at other CMS institutes for their contributions to the success of the CMS effort. In addition, we gratefully acknowledge the computing centers and personnel of the Worldwide LHC Computing Grid and other centers for delivering so effectively the computing infrastructure essential to our analyses. Finally, we acknowledge the enduring support for the construction and operation of the LHC, the CMS detector, and the supporting computing infrastructure provided by the following funding agencies: BMBWF and FWF (Austria); FNRS and FWO (Belgium); CNPq, CAPES, FAPERJ, FAPERGS, and FAPESP (Brazil); MES and BNSF (Bulgaria); CERN; CAS, MoST, and NSFC (China); MINCIENCIAS (Colombia); MSES and CSF (Croatia); RIF (Cyprus); SENESCYT (Ecuador); MoER, ERC PUT and ERDF (Estonia); Academy of Finland, MEC, and HIP (Finland); CEA and CNRS/IN2P3 (France); BMBF, DFG, and HGF (Germany); GSRI (Greece); NKFIH (Hungary); DAE and DST (India); IPM (Iran); SFI (Ireland); INFN (Italy); MSIP and NRF (Republic of Korea); MES (Latvia); LAS (Lithuania); MOE and UM (Malaysia); BUAP, CINVESTAV, CONACYT, LNS, SEP, and UASLP-FAI (Mexico); MOS (Montenegro); MBIE (New Zealand); PAEC (Pakistan); MSHE and NSC (Poland); FCT (Portugal); JINR (Dubna); MON, RosAtom, RAS, RFBR, and NRC KI (Russia); MESTD (Serbia); MCIN/AE and PCTI (Spain); MOSTR (Sri Lanka); Swiss Funding Agencies (Switzerland); MST (Taipei); ThEPCenter, IPST, STAR, and NSTDA (Thailand); TUBITAK and TAEK (Turkey); NASU (Ukraine); STFC (United Kingdom); DOE and NSF (USA).

Individuals have received support from the Marie-Curie program and the European Research Council and Horizon 2020 Grant, contract Nos. 675440, 724704, 752730, 758316, 765710, 824093, 884104, and COST Action CA16108 (European Union); the Leventis Foundation; the Alfred P. Sloan Foundation; the Alexander von Humboldt Foundation; the Belgian Federal Science Policy Office; the Fonds pour la Formation à la Recherche dans l'Industrie et dans l'Agriculture (FRIA-Belgium); the Agentschap voor Innovatie door Wetenschap en Technologie (IWT-Belgium); the F.R.S.-FNRS and FWO (Belgium) under the "Excellence of Science – EOS" – be.h project n. 30820817; the Beijing Municipal Science & Technology Commission, No. Z191100007219010; the Ministry of Education, Youth and Sports (MEYS) of the Czech Republic; the Deutsche Forschungsgemeinschaft (DFG), under Germany's Excellence Strategy – EXC 2121 "Quantum Universe" – 390833306, and under project number 400140256 - GRK2497; the Lendület ("Momentum") Program and the János Bolyai Research Scholarship of the Hungarian Academy of Sciences, the New National Excellence Program ÚNKP, the NKFIH research grants 123842, 123959, 124845, 124850, 125105, 128713, 128786, and 129058 (Hungary); the Council of Science and Industrial Research, India; the Latvian Council of Science; the Ministry of Science and Higher Education and the National Science Center, contracts Opus 2014/15/B/ST2/03998 and 2015/19/B/ST2/02861 (Poland); the Fundação para a Ciência e a Tecnologia, grant CEECIND/01334/2018 (Portugal); the National Priorities Research Program by Qatar National Research Fund; the Ministry of Science and Higher Education, projects no. 14.W03.31.0026 and no. FSWW-2020-0008, and the Russian Foundation for Basic Research, project No.19-42-703014 (Russia); MCIN/AEI/10.13039/501100011033, ERDF "a way of making Europe", and the Programa Estatal de Fomento de la Investigación Científica y Técnica de Excelencia María de Maeztu, grant MDM-2017-0765 and Programa Severo Ochoa del Principado de Asturias (Spain); the Stavros Niarchos Foundation (Greece); the Rachadapisek Sompot Fund for Postdoctoral Fellowship, Chulalongkorn University and the Chulalongkorn Academic into Its 2nd Century Project Advancement Project (Thailand); the Kavli Foundation; the Nvidia Corporation; the SuperMicro Corporation; the Welch Foundation, contract C-1845; and

the Weston Havens Foundation (USA).

References

- [1] ATLAS Collaboration, “Observation of a new particle in the search for the standard model Higgs boson with the ATLAS detector at the LHC”, *Phys. Lett. B* **716** (2012) 01, doi:[10.1016/j.physletb.2012.08.020](https://doi.org/10.1016/j.physletb.2012.08.020), arXiv:[1207.7214](https://arxiv.org/abs/1207.7214).
- [2] CMS Collaboration, “Observation of a new boson at a mass of 125 GeV with the CMS experiment at the LHC”, *Phys. Lett. B* **716** (2012) 30, doi:[10.1016/j.physletb.2012.08.021](https://doi.org/10.1016/j.physletb.2012.08.021), arXiv:[1207.7235](https://arxiv.org/abs/1207.7235).
- [3] CMS Collaboration, “Observation of a new boson with mass near 125 GeV in pp collisions at $\sqrt{s} = 7$ and 8 TeV”, *JHEP* **06** (2013) 081, doi:[10.1007/JHEP06\(2013\)081](https://doi.org/10.1007/JHEP06(2013)081), arXiv:[1303.4571](https://arxiv.org/abs/1303.4571).
- [4] F. Englert and R. Brout, “Broken symmetry and the mass of gauge vector mesons”, *Phys. Rev. Lett.* **13** (1964) 321, doi:[10.1103/PhysRevLett.13.321](https://doi.org/10.1103/PhysRevLett.13.321).
- [5] P. W. Higgs, “Broken symmetries and the masses of gauge bosons”, *Phys. Rev. Lett.* **13** (1964) 508, doi:[10.1103/PhysRevLett.13.508](https://doi.org/10.1103/PhysRevLett.13.508).
- [6] G. C. Branco et al., “Theory and phenomenology of two-Higgs-doublet models”, *Phys. Rept.* **516** (2012) 1, doi:[10.1016/j.physrep.2012.02.002](https://doi.org/10.1016/j.physrep.2012.02.002), arXiv:[1106.0034](https://arxiv.org/abs/1106.0034).
- [7] P. Ramond, “Dual theory for free fermions”, *Phys. Rev. D* **3** (1971) 2415, doi:[10.1103/PhysRevD.3.2415](https://doi.org/10.1103/PhysRevD.3.2415).
- [8] Y. A. Gol'fand and E. P. Likhtman, “Extension of the algebra of Poincaré group generators and violation of P invariance”, *JETP Lett.* **13** (1971) 323.
- [9] A. Neveu and J. H. Schwarz, “Factorizable dual model of pions”, *Nucl. Phys. B* **31** (1971) 86, doi:[10.1016/0550-3213\(71\)90448-2](https://doi.org/10.1016/0550-3213(71)90448-2).
- [10] D. V. Volkov and V. P. Akulov, “Possible universal neutrino interaction”, *JETP Lett.* **16** (1972) 438.
- [11] J. Wess and B. Zumino, “A Lagrangian model invariant under supergauge transformations”, *Phys. Lett. B* **49** (1974) 52, doi:[10.1016/0370-2693\(74\)90578-4](https://doi.org/10.1016/0370-2693(74)90578-4).
- [12] J. Wess and B. Zumino, “Supergauge transformations in four dimensions”, *Nucl. Phys. B* **70** (1974) 39, doi:[10.1016/0550-3213\(74\)90355-1](https://doi.org/10.1016/0550-3213(74)90355-1).
- [13] P. Fayet, “Supergauge invariant extension of the Higgs mechanism and a model for the electron and its neutrino”, *Nucl. Phys. B* **90** (1975) 104, doi:[10.1016/0550-3213\(75\)90636-7](https://doi.org/10.1016/0550-3213(75)90636-7).
- [14] H. P. Nilles, “Supersymmetry, supergravity and particle physics”, *Phys. Rep.* **110** (1984) 1, doi:[10.1016/0370-1573\(84\)90008-5](https://doi.org/10.1016/0370-1573(84)90008-5).
- [15] L. Randall and R. Sundrum, “A large mass hierarchy from a small extra dimension”, *Phys. Rev. Lett.* **83** (1999) 3370, doi:[10.1103/PhysRevLett.83.3370](https://doi.org/10.1103/PhysRevLett.83.3370), arXiv:[hep-ph/9905221](https://arxiv.org/abs/hep-ph/9905221).

- [16] W. D. Goldberger and M. B. Wise, “Modulus stabilization with bulk fields”, *Phys. Rev. Lett.* **83** (1999) 4922, doi:10.1103/PhysRevLett.83.4922, arXiv:hep-ph/9907447.
- [17] O. DeWolfe, D. Z. Freedman, S. S. Gubser, and A. Karch, “Modeling the fifth dimension with scalars and gravity”, *Phys. Rev. D* **62** (2000) 046008, doi:10.1103/PhysRevD.62.046008, arXiv:hep-th/9909134.
- [18] C. Csaki, M. Graesser, L. Randall, and J. Terning, “Cosmology of brane models with radion stabilization”, *Phys. Rev. D* **62** (2000) 045015, doi:10.1103/PhysRevD.62.045015, arXiv:hep-ph/9911406.
- [19] C. Csaki, M. L. Graesser, and G. D. Kribs, “Radion dynamics and electroweak physics”, *Phys. Rev. D* **63** (2001) 065002, doi:10.1103/PhysRevD.63.065002, arXiv:hep-th/0008151.
- [20] H. Davoudiasl, J. L. Hewett, and T. G. Rizzo, “Phenomenology of the Randall-Sundrum gauge hierarchy model”, *Phys. Rev. Lett.* **84** (2000) 2080, doi:10.1103/PhysRevLett.84.2080, arXiv:hep-ph/9909255.
- [21] K. Agashe, H. Davoudiasl, G. Perez, and A. Soni, “Warped gravitons at the LHC and beyond”, *Phys. Rev. D* **76** (2007) 036006, doi:10.1103/PhysRevD.76.036006, arXiv:hep-ph/0701186.
- [22] A. L. Fitzpatrick, J. Kaplan, L. Randall, and L.-T. Wang, “Searching for the Kaluza-Klein graviton in bulk RS models”, *JHEP* **09** (2007) 013, doi:10.1088/1126-6708/2007/09/013, arXiv:hep-ph/0701150.
- [23] ATLAS Collaboration, “Searches for Higgs boson pair production in the $hh \rightarrow b\bar{b}\tau\tau, \gamma\gamma WW^*, \gamma\gamma bb, bbbb$ channels with the ATLAS detector”, *Phys. Rev. D* **92** (2015) 092004, doi:10.1103/PhysRevD.92.092004, arXiv:1509.04670.
- [24] ATLAS Collaboration, “Search for a new resonance decaying to a W or Z boson and a Higgs boson in the $\ell\ell/\ell\nu/\nu\nu + b\bar{b}$ final states with the ATLAS detector”, *Eur. Phys. J. C* **75** (2015) 263, doi:10.1140/epjc/s10052-015-3474-x, arXiv:1503.08089.
- [25] ATLAS Collaboration, “Search for Higgs boson pair production in the $b\bar{b}b\bar{b}$ final state from pp collisions at $\sqrt{s} = 8$ TeV with the ATLAS detector”, *Eur. Phys. J. C* **75** (2015) 412, doi:10.1140/epjc/s10052-015-3628-x, arXiv:1506.00285.
- [26] ATLAS Collaboration, “Search for Higgs boson pair production in the $\gamma\gamma b\bar{b}$ final state using pp collision data at $\sqrt{s} = 8$ TeV from the ATLAS detector”, *Phys. Rev. Lett.* **114** (2015) 081802, doi:10.1103/PhysRevLett.114.081802, arXiv:1406.5053.
- [27] ATLAS Collaboration, “Search for WZ resonances in the fully leptonic channel using pp collisions at $\sqrt{s} = 8$ TeV with the ATLAS detector”, *Phys. Lett. B* **737** (2014) 223, doi:10.1016/j.physletb.2014.08.039, arXiv:1406.4456.
- [28] ATLAS Collaboration, “Search for heavy resonances decaying to a W or Z boson and a Higgs boson in the $q\bar{q}^{(\prime)}b\bar{b}$ final state in pp collisions at $\sqrt{s} = 13$ TeV with the ATLAS detector”, *Phys. Lett. B* **774** (2017) 494, doi:10.1016/j.physletb.2017.09.066, arXiv:1707.06958.

- [29] ATLAS Collaboration, “Search for WW/WZ resonance production in $\ell\nu qq$ final states in pp collisions at $\sqrt{s} = 13$ TeV with the ATLAS detector”, *JHEP* **03** (2018) 042, doi:[10.1007/JHEP03\(2018\)042](https://doi.org/10.1007/JHEP03(2018)042), arXiv:[1710.07235](https://arxiv.org/abs/1710.07235).
- [30] ATLAS Collaboration, “Search for resonant WZ production in the fully leptonic final state in proton-proton collisions at $\sqrt{s} = 13$ TeV with the ATLAS detector”, *Phys. Lett. B* **787** (2018) 68, doi:[10.1016/j.physletb.2018.10.021](https://doi.org/10.1016/j.physletb.2018.10.021), arXiv:[1806.01532](https://arxiv.org/abs/1806.01532).
- [31] ATLAS Collaboration, “Search for heavy resonances decaying into WW in the $e\nu\mu\nu$ final state in pp collisions at $\sqrt{s} = 13$ TeV with the ATLAS detector”, *Eur. Phys. J. C* **78** (2018) 24, doi:[10.1140/epjc/s10052-017-5491-4](https://doi.org/10.1140/epjc/s10052-017-5491-4), arXiv:[1710.01123](https://arxiv.org/abs/1710.01123).
- [32] ATLAS Collaboration, “Searches for heavy ZZ and ZW resonances in the $\ell\ell qq$ and $\nu\nu qq$ final states in pp collisions at $\sqrt{s} = 13$ TeV with the ATLAS detector”, *JHEP* **03** (2018) 009, doi:[10.1007/JHEP03\(2018\)009](https://doi.org/10.1007/JHEP03(2018)009), arXiv:[1708.09638](https://arxiv.org/abs/1708.09638).
- [33] ATLAS Collaboration, “Search for heavy ZZ resonances in the $\ell^+\ell^-\ell^+\ell^-$ and $\ell^+\ell^-\nu\bar{\nu}$ final states using proton-proton collisions at $\sqrt{s} = 13$ TeV with the ATLAS detector”, *Eur. Phys. J. C* **78** (2018) 293, doi:[10.1140/epjc/s10052-018-5686-3](https://doi.org/10.1140/epjc/s10052-018-5686-3), arXiv:[1712.06386](https://arxiv.org/abs/1712.06386).
- [34] ATLAS Collaboration, “Search for heavy resonances decaying into a W or Z boson and a Higgs boson in final states with leptons and b-jets in 36 fb^{-1} of $\sqrt{s} = 13$ TeV pp collisions with the ATLAS detector”, *JHEP* **03** (2018) 174, doi:[10.1007/JHEP03\(2018\)174](https://doi.org/10.1007/JHEP03(2018)174), arXiv:[1712.06518](https://arxiv.org/abs/1712.06518).
- [35] ATLAS Collaboration, “Search for diboson resonances with boson-tagged jets in pp collisions at $\sqrt{s} = 13$ TeV with the ATLAS detector”, *Phys. Lett. B* **777** (2018) 91, doi:[10.1016/j.physletb.2017.12.011](https://doi.org/10.1016/j.physletb.2017.12.011), arXiv:[1708.04445](https://arxiv.org/abs/1708.04445).
- [36] ATLAS Collaboration, “Search for Higgs boson pair production in the $b\bar{b}WW^*$ decay mode at $\sqrt{s} = 13$ TeV with the ATLAS detector”, *JHEP* **04** (2019) 092, doi:[10.1007/JHEP04\(2019\)092](https://doi.org/10.1007/JHEP04(2019)092), arXiv:[1811.04671](https://arxiv.org/abs/1811.04671).
- [37] ATLAS Collaboration, “Search for pair production of Higgs bosons in the $b\bar{b}b\bar{b}$ final state using proton-proton collisions at $\sqrt{s} = 13$ TeV with the ATLAS detector”, *JHEP* **01** (2019) 030, doi:[10.1007/JHEP01\(2019\)030](https://doi.org/10.1007/JHEP01(2019)030), arXiv:[1804.06174](https://arxiv.org/abs/1804.06174).
- [38] ATLAS Collaboration, “Search for resonant and non-resonant Higgs boson pair production in the $b\bar{b}\tau^+\tau^-$ decay channel in pp collisions at $\sqrt{s} = 13$ TeV with the ATLAS detector”, *Phys. Rev. Lett.* **121** (2018) 191801, doi:[10.1103/PhysRevLett.121.191801](https://doi.org/10.1103/PhysRevLett.121.191801), arXiv:[1808.00336](https://arxiv.org/abs/1808.00336). [Erratum: doi:[10.1103/PhysRevLett.122.089901](https://doi.org/10.1103/PhysRevLett.122.089901)].
- [39] ATLAS Collaboration, “Combination of searches for non-resonant and resonant Higgs boson pair production in the $b\bar{b}\gamma\gamma$, $b\bar{b}\tau^+\tau^-$ and $b\bar{b}b\bar{b}$ decay channels using pp collisions at $\sqrt{s} = 13$ TeV with the ATLAS detector”, Technical Report ATLAS-CONF-2021-052, 2021.
- [40] ATLAS Collaboration, “Combination of searches for Higgs boson pairs in pp collisions at $\sqrt{s} = 13$ TeV with the ATLAS detector”, *Phys. Lett. B* **800** (2020) 135103, doi:[10.1016/j.physletb.2019.135103](https://doi.org/10.1016/j.physletb.2019.135103), arXiv:[1906.02025](https://arxiv.org/abs/1906.02025).

- [41] ATLAS Collaboration, “Search for diboson resonances in hadronic final states in 139 fb^{-1} of pp collisions at $\sqrt{s} = 13 \text{ TeV}$ with the ATLAS detector”, *JHEP* **09** (2019) 091, doi:[10.1007/JHEP09\(2019\)091](https://doi.org/10.1007/JHEP09(2019)091), arXiv:[1906.08589](https://arxiv.org/abs/1906.08589). [Erratum: doi:[10.1007/JHEP06\(2020\)042](https://doi.org/10.1007/JHEP06(2020)042)].
- [42] ATLAS Collaboration, “Search for the $HH \rightarrow b\bar{b}b\bar{b}$ process via vector-boson fusion production using proton-proton collisions at $\sqrt{s} = 13 \text{ TeV}$ with the ATLAS detector”, *JHEP* **07** (2020) 108, doi:[10.1007/JHEP07\(2020\)108](https://doi.org/10.1007/JHEP07(2020)108), arXiv:[2001.05178](https://arxiv.org/abs/2001.05178). [Errata: doi:[10.1007/JHEP01\(2021\)145](https://doi.org/10.1007/JHEP01(2021)145), doi:[10.1007/JHEP05\(2021\)207](https://doi.org/10.1007/JHEP05(2021)207)].
- [43] ATLAS Collaboration, “Search for heavy diboson resonances in semileptonic final states in pp collisions at $\sqrt{s} = 13 \text{ TeV}$ with the ATLAS detector”, *Eur. Phys. J. C* **80** (2020) 1165, doi:[10.1140/epjc/s10052-020-08554-y](https://doi.org/10.1140/epjc/s10052-020-08554-y), arXiv:[2004.14636](https://arxiv.org/abs/2004.14636).
- [44] ATLAS Collaboration, “Search for resonances decaying into a weak vector boson and a Higgs boson in the fully hadronic final state produced in proton–proton collisions at $\sqrt{s} = 13 \text{ TeV}$ with the ATLAS detector”, *Phys. Rev. D* **102** (2020) 112008, doi:[10.1103/PhysRevD.102.112008](https://doi.org/10.1103/PhysRevD.102.112008), arXiv:[2007.05293](https://arxiv.org/abs/2007.05293).
- [45] ATLAS Collaboration, “Reconstruction and identification of boosted di- τ systems in a search for Higgs boson pairs using 13 TeV proton-proton collision data in ATLAS”, *JHEP* **11** (2020) 163, doi:[10.1007/JHEP11\(2020\)163](https://doi.org/10.1007/JHEP11(2020)163), arXiv:[2007.14811](https://arxiv.org/abs/2007.14811).
- [46] ATLAS Collaboration, “Search for resonant pair production of Higgs bosons in the $b\bar{b}b\bar{b}$ final state using pp collisions at $\sqrt{s} = 13 \text{ TeV}$ with the ATLAS detector”, ATLAS Conference Note ATLAS-CONF-2021-035, 2021.
- [47] CMS Collaboration, “Combination of searches for heavy resonances decaying to WW, WZ, ZZ, WH, and ZH boson pairs in proton-proton collisions at $\sqrt{s} = 8$ and 13 TeV”, *Phys. Lett. B* **774** (2017) 533, doi:[10.1016/j.physletb.2017.09.083](https://doi.org/10.1016/j.physletb.2017.09.083), arXiv:[1705.09171](https://arxiv.org/abs/1705.09171).
- [48] CMS Collaboration, “Search for a heavy resonance decaying into a Z boson and a vector boson in the $\nu\bar{\nu}q\bar{q}$ final state”, *JHEP* **07** (2018) 075, doi:[10.1007/JHEP07\(2018\)075](https://doi.org/10.1007/JHEP07(2018)075), arXiv:[1803.03838](https://arxiv.org/abs/1803.03838).
- [49] CMS Collaboration, “Search for heavy resonances decaying into two Higgs bosons or into a Higgs boson and a W or Z boson in proton-proton collisions at 13 TeV”, *JHEP* **01** (2019) 051, doi:[10.1007/JHEP01\(2019\)051](https://doi.org/10.1007/JHEP01(2019)051), arXiv:[1808.01365](https://arxiv.org/abs/1808.01365).
- [50] CMS Collaboration, “Search for a heavy resonance decaying into a Z boson and a Z or W boson in $2\ell 2q$ final states at $\sqrt{s} = 13 \text{ TeV}$ ”, *JHEP* **09** (2018) 101, doi:[10.1007/JHEP09\(2018\)101](https://doi.org/10.1007/JHEP09(2018)101), arXiv:[1803.10093](https://arxiv.org/abs/1803.10093).
- [51] CMS Collaboration, “Search for production of Higgs boson pairs in the four b quark final state using large-area jets in proton-proton collisions at $\sqrt{s} = 13 \text{ TeV}$ ”, *JHEP* **01** (2019) 040, doi:[10.1007/JHEP01\(2019\)040](https://doi.org/10.1007/JHEP01(2019)040), arXiv:[1808.01473](https://arxiv.org/abs/1808.01473).
- [52] CMS Collaboration, “Searches for a heavy scalar boson H decaying to a pair of 125 GeV Higgs bosons hh or for a heavy pseudoscalar boson A decaying to Zh, in the final states with $h \rightarrow \tau\tau$ ”, *Phys. Lett. B* **755** (2016) 217, doi:[10.1016/j.physletb.2016.01.056](https://doi.org/10.1016/j.physletb.2016.01.056), arXiv:[1510.01181](https://arxiv.org/abs/1510.01181).

- [53] CMS Collaboration, “Search for massive resonances decaying into WW , WZ , ZZ , qW , and qZ with dijet final states at $\sqrt{s} = 13$ TeV”, *Phys. Rev. D* **97** (2018) 072006, doi:[10.1103/PhysRevD.97.072006](https://doi.org/10.1103/PhysRevD.97.072006), arXiv:[1708.05379](https://arxiv.org/abs/1708.05379).
- [54] CMS Collaboration, “Search for heavy resonances that decay into a vector boson and a Higgs boson in hadronic final states at $\sqrt{s} = 13$ TeV”, *Eur. Phys. J. C* **77** (2017) 636, doi:[10.1140/epjc/s10052-017-5192-z](https://doi.org/10.1140/epjc/s10052-017-5192-z), arXiv:[1707.01303](https://arxiv.org/abs/1707.01303).
- [55] CMS Collaboration, “Search for heavy resonances decaying into a vector boson and a Higgs boson in final states with charged leptons, neutrinos and b quarks at $\sqrt{s} = 13$ TeV”, *JHEP* **11** (2018) 172, doi:[10.1007/JHEP11\(2018\)172](https://doi.org/10.1007/JHEP11(2018)172), arXiv:[1807.02826](https://arxiv.org/abs/1807.02826).
- [56] CMS Collaboration, “Search for resonant pair production of Higgs bosons decaying to two bottom quark-antiquark pairs in proton-proton collisions at 8 TeV”, *Phys. Lett. B* **749** (2015) 560, doi:[10.1016/j.physletb.2015.08.047](https://doi.org/10.1016/j.physletb.2015.08.047), arXiv:[1503.04114](https://arxiv.org/abs/1503.04114).
- [57] CMS Collaboration, “Search for heavy resonances decaying into a vector boson and a Higgs boson in final states with charged leptons, neutrinos, and b quarks”, *Phys. Lett. B* **768** (2017) 137, doi:[10.1016/j.physletb.2017.02.040](https://doi.org/10.1016/j.physletb.2017.02.040), arXiv:[1610.08066](https://arxiv.org/abs/1610.08066).
- [58] CMS Collaboration, “Search for a massive resonance decaying to a pair of Higgs bosons in the four b quark final state in proton-proton collisions at $\sqrt{s} = 13$ TeV”, *Phys. Lett. B* **781** (2018) 244, doi:[10.1016/j.physletb.2018.03.084](https://doi.org/10.1016/j.physletb.2018.03.084), arXiv:[1710.04960](https://arxiv.org/abs/1710.04960).
- [59] CMS Collaboration, “Search for a heavy resonance decaying to a pair of vector bosons in the lepton plus merged jet final state at $\sqrt{s} = 13$ TeV”, *JHEP* **05** (2018) 088, doi:[10.1007/JHEP05\(2018\)088](https://doi.org/10.1007/JHEP05(2018)088), arXiv:[1802.09407](https://arxiv.org/abs/1802.09407).
- [60] CMS Collaboration, “Search for massive resonances decaying into WW , WZ or ZZ bosons in proton-proton collisions at $\sqrt{s} = 13$ TeV”, *JHEP* **03** (2017) 162, doi:[10.1007/JHEP03\(2017\)162](https://doi.org/10.1007/JHEP03(2017)162), arXiv:[1612.09159](https://arxiv.org/abs/1612.09159).
- [61] CMS Collaboration, “Search for ZZ resonances in the $2\ell 2\nu$ final state in proton-proton collisions at 13 TeV”, *JHEP* **03** (2018) 003, doi:[10.1007/JHEP03\(2018\)003](https://doi.org/10.1007/JHEP03(2018)003), arXiv:[1711.04370](https://arxiv.org/abs/1711.04370).
- [62] CMS Collaboration, “Search for new resonances decaying via WZ to leptons in proton-proton collisions at $\sqrt{s} = 13$ TeV”, *Phys. Lett. B* **740** (2015) 83, doi:[10.1016/j.physletb.2014.11.026](https://doi.org/10.1016/j.physletb.2014.11.026), arXiv:[1407.3476](https://arxiv.org/abs/1407.3476).
- [63] CMS Collaboration, “Search for massive WH resonances decaying into the $\ell\nu b\bar{b}$ final state at $\sqrt{s} = 8$ TeV”, *Eur. Phys. J. C* **76** (2016) 237, doi:[10.1140/epjc/s10052-016-4067-z](https://doi.org/10.1140/epjc/s10052-016-4067-z), arXiv:[1601.06431](https://arxiv.org/abs/1601.06431).
- [64] CMS Collaboration, “Search for a massive resonance decaying into a Higgs boson and a W or Z boson in hadronic final states in proton-proton collisions at $\sqrt{s} = 8$ TeV”, *JHEP* **02** (2016) 145, doi:[10.1007/JHEP02\(2016\)145](https://doi.org/10.1007/JHEP02(2016)145), arXiv:[1506.01443](https://arxiv.org/abs/1506.01443).
- [65] CMS Collaboration, “Search for narrow high-mass resonances in proton-proton collisions at $\sqrt{s} = 8$ TeV decaying to a Z and a Higgs boson”, *Phys. Lett. B* **748** (2015) 255, doi:[10.1016/j.physletb.2015.07.011](https://doi.org/10.1016/j.physletb.2015.07.011), arXiv:[1502.04994](https://arxiv.org/abs/1502.04994).
- [66] CMS Collaboration, “Combination of CMS searches for heavy resonances decaying to pairs of bosons or leptons”, *Phys. Lett. B* **798** (2019) 134952, doi:[10.1016/j.physletb.2019.134952](https://doi.org/10.1016/j.physletb.2019.134952), arXiv:[1906.00057](https://arxiv.org/abs/1906.00057).

- [67] CMS Collaboration, “Search for a heavy vector resonance decaying to a Z boson and a Higgs boson in proton-proton collisions at $\sqrt{s} = 13 \text{ TeV}$ ”, *Eur. Phys. J. C* **81** (2021) 688, doi:10.1140/epjc/s10052-021-09348-6, arXiv:2102.08198.
- [68] CMS Collaboration, “Search for heavy resonances decaying to WW, WZ, or WH boson pairs in the lepton plus merged jet final state in proton-proton collisions at $\sqrt{s} = 13 \text{ TeV}$ ”, 2021. arXiv:2109.06055. Submitted to *Phys. Rev. D*.
- [69] CMS Collaboration, “Search for resonant Higgs boson pair production in four b quark final state using large-area jets in proton-proton collisions at $\sqrt{s} = 13 \text{ TeV}$ ”, CMS Physics Analysis Summary CMS-PAS-B2G-20-004, 2021.
- [70] CMS Collaboration, “Search for heavy resonances decaying to $Z(v\bar{v})V(q\bar{q}')$ in proton-proton collisions at $\sqrt{s} = 13 \text{ TeV}$ ”, 2021. arXiv:2109.08268. Submitted to *Phys. Rev. D*.
- [71] CMS Collaboration, “Search for heavy resonances decaying to ZZ or ZW and axion-like particles mediating nonresonant ZZ or ZH production at $\sqrt{s} = 13 \text{ TeV}$ ”, 2021. arXiv:2111.13669. Submitted to *JHEP*.
- [72] CMS Collaboration, “Search for resonances decaying to a pair of Higgs bosons in the $b\bar{b}q\bar{q}\ell\nu$ final state in proton-proton collisions at $\sqrt{s} = 13 \text{ TeV}$ ”, *JHEP* **10** (2019) 125, doi:10.1007/JHEP10(2019)125, arXiv:1904.04193.
- [73] HEPData record for this analysis, 2021. doi:10.17182/hepdata.115024.
- [74] CMS Collaboration, “The CMS experiment at the CERN LHC”, *JINST* **3** (2008) S08004, doi:10.1088/1748-0221/3/08/S08004.
- [75] CMS Collaboration, “Performance of the CMS Level-1 trigger in proton-proton collisions at $\sqrt{s} = 13 \text{ TeV}$ ”, *JINST* **15** (2020) P10017, doi:10.1088/1748-0221/15/10/P10017, arXiv:2006.10165.
- [76] CMS Collaboration, “The CMS trigger system”, *JINST* **12** (2017) P01020, doi:10.1088/1748-0221/12/01/P01020, arXiv:1609.02366.
- [77] CMS Collaboration, “Particle-flow reconstruction and global event description with the CMS detector”, *JINST* **12** (2017) P10003, doi:10.1088/1748-0221/12/10/P10003, arXiv:1706.04965.
- [78] CMS Collaboration, “Performance of missing transverse momentum reconstruction in proton-proton collisions at $\sqrt{s} = 13 \text{ TeV}$ using the CMS detector”, *JINST* **14** (2019) P07004, doi:10.1088/1748-0221/14/07/P07004, arXiv:1903.06078.
- [79] M. Cacciari, G. P. Salam, and G. Soyez, “The anti- k_T jet clustering algorithm”, *JHEP* **04** (2008) 063, doi:10.1088/1126-6708/2008/04/063, arXiv:0802.1189.
- [80] M. Cacciari, G. P. Salam, and G. Soyez, “FastJet user manual”, *Eur. Phys. J. C* **72** (2012) 1896, doi:10.1140/epjc/s10052-012-1896-2, arXiv:1111.6097.
- [81] CMS Collaboration, “Pileup mitigation at CMS in 13 TeV data”, *JINST* **15** (2020) P09018, doi:10.1088/1748-0221/15/09/p09018, arXiv:2003.00503.
- [82] D. Bertolini, P. Harris, M. Low, and N. Tran, “Pileup per particle identification”, *JHEP* **10** (2014) 059, doi:10.1007/JHEP10(2014)059, arXiv:1407.6013.

- [83] CMS Collaboration, “Jet energy scale and resolution in the CMS experiment in pp collisions at 8 TeV”, *JINST* **12** (2017) P02014,
`doi:10.1088/1748-0221/12/02/P02014`, `arXiv:1607.03663`.
- [84] J. Alwall et al., “The automated computation of tree-level and next-to-leading order differential cross sections, and their matching to parton shower simulations”, *JHEP* **07** (2014) 079, `doi:10.1007/JHEP07(2014)079`, `arXiv:1405.0301`.
- [85] J. Alwall et al., “Comparative study of various algorithms for the merging of parton showers and matrix elements in hadronic collisions”, *Eur. Phys. J. C* **53** (2008) 473,
`doi:10.1140/epjc/s10052-007-0490-5`, `arXiv:0706.2569`.
- [86] Y. Li and F. Petriello, “Combining QCD and electroweak corrections to dilepton production in FEWZ”, *Phys. Rev. D* **86** (2012) 094034,
`doi:10.1103/PhysRevD.86.094034`, `arXiv:1208.5967`.
- [87] R. Frederix and S. Frixione, “Merging meets matching in MC@NLO”, *JHEP* **12** (2012) 61, `doi:10.1007/JHEP12(2012)061`, `arXiv:1209.6215`.
- [88] P. Nason, “A new method for combining NLO QCD with shower Monte Carlo algorithms”, *JHEP* **11** (2004) 040, `doi:10.1088/1126-6708/2004/11/040`,
`arXiv:hep-ph/0409146`.
- [89] S. Frixione, P. Nason, and C. Oleari, “Matching NLO QCD computations with parton shower simulations: the POWHEG method”, *JHEP* **11** (2007) 070,
`doi:10.1088/1126-6708/2007/11/070`, `arXiv:0709.2092`.
- [90] S. Alioli, P. Nason, C. Oleari, and E. Re, “A general framework for implementing NLO calculations in shower Monte Carlo programs: the POWHEG BOX”, *JHEP* **06** (2010) 043, `doi:10.1007/JHEP06(2010)043`, `arXiv:1002.2581`.
- [91] E. Re, “Single-top Wt -channel production matched with parton showers using the POWHEG method”, *Eur. Phys. J. C* **71** (2011) 1547,
`doi:10.1140/epjc/s10052-011-1547-z`, `arXiv:1009.2450`.
- [92] T. Melia, P. Nason, R. Röntsch, and G. Zanderighi, “ W^+W^- , WZ and ZZ production in the POWHEG BOX”, *JHEP* **11** (2011) 078, `doi:10.1007/JHEP11(2011)078`,
`arXiv:1107.5051`.
- [93] P. Nason and G. Zanderighi, “ W^+W^- , WZ and ZZ production in the POWHEG-BOX-V2”, *Eur. Phys. J. C* **74** (2014) 2702,
`doi:10.1140/epjc/s10052-013-2702-5`, `arXiv:1311.1365`.
- [94] R. Frederix, E. Re, and P. Torrielli, “Single-top t -channel hadroproduction in the four-flavour scheme with POWHEG and aMC@NLO”, *JHEP* **09** (2012) 130,
`doi:10.1007/JHEP09(2012)130`, `arXiv:1207.5391`.
- [95] H. B. Hartanto, B. Jager, L. Reina, and D. Wackeroth, “Higgs boson production in association with top quarks in the POWHEG BOX”, *Phys. Rev. D* **91** (2015) 094003,
`doi:10.1103/PhysRevD.91.094003`, `arXiv:1501.04498`.
- [96] M. Czakon and A. Mitov, “Top++: A program for the calculation of the top-pair cross-section at hadron colliders”, *Comput. Phys. Commun.* **185** (2014) 2930,
`doi:10.1016/j.cpc.2014.06.021`, `arXiv:1112.5675`.

- [97] T. Sjöstrand et al., “An introduction to PYTHIA 8.2”, *Comput. Phys. Commun.* **191** (2015) 159, doi:10.1016/j.cpc.2015.01.024, arXiv:1410.3012.
- [98] CMS Collaboration, “Event generator tunes obtained from underlying event and multiparton scattering measurements”, *Eur. Phys. J. C* **76** (2016) 155, doi:10.1140/epjc/s10052-016-3988-x, arXiv:1512.00815.
- [99] CMS Collaboration, “Extraction and validation of a new set of CMS PYTHIA8 tunes from underlying-event measurements”, *Eur. Phys. J. C* **80** (2020) 4, doi:10.1140/epjc/s10052-019-7499-4, arXiv:1903.12179.
- [100] NNPDF Collaboration, “Parton distributions for the LHC Run II”, *JHEP* **04** (2015) 040, doi:10.1007/JHEP04(2015)040, arXiv:1410.8849.
- [101] NNPDF Collaboration, “Parton distributions from high-precision collider data”, *Eur. Phys. J. C* **77** (2017) doi:10.1140/epjc/s10052-017-5199-5, arXiv:1706.00428.
- [102] GEANT4 Collaboration, “GEANT4—a simulation toolkit”, *Nucl. Instrum. Meth. A* **506** (2003) 250, doi:10.1016/S0168-9002(03)01368-8.
- [103] CMS Collaboration, “Electron and photon reconstruction and identification with the CMS experiment at the CERN LHC”, *JINST* **16** (2021) P05014, doi:10.1088/1748-0221/16/05/P05014, arXiv:2012.06888.
- [104] CMS Collaboration, “Performance of the CMS muon detector and muon reconstruction with proton-proton collisions at $\sqrt{s} = 13$ TeV”, *JINST* **13** (2018) P06015, doi:10.1088/1748-0221/13/06/P06015, arXiv:1804.04528.
- [105] K. Rehermann and B. Tweedie, “Efficient identification of boosted semileptonic top quarks at the LHC”, *JHEP* **03** (2011) 059, doi:10.1007/JHEP03(2011)059, arXiv:1007.2221.
- [106] Y. L. Dokshitzer, G. D. Leder, S. Moretti, and B. R. Webber, “Better jet clustering algorithms”, *JHEP* **08** (1997) 001, doi:10.1088/1126-6708/1997/08/001, arXiv:hep-ph/9707323.
- [107] M. Wobisch and T. Wengler, “Hadronization corrections to jet cross-sections in deep inelastic scattering”, in *Proceedings of the Workshop on Monte Carlo Generators for HERA Physics, Hamburg, Germany*, p. 270. 1998. arXiv:hep-ph/9907280.
- [108] M. Dasgupta, A. Fregoso, S. Marzani, and G. P. Salam, “Towards an understanding of jet substructure”, *JHEP* **09** (2013) 029, doi:10.1007/JHEP09(2013)029, arXiv:1307.0007.
- [109] J. M. Butterworth, A. R. Davison, M. Rubin, and G. P. Salam, “Jet substructure as a new Higgs search channel at the LHC”, *Phys. Rev. Lett.* **100** (2008) 242001, doi:10.1103/PhysRevLett.100.242001, arXiv:0802.2470.
- [110] A. J. Larkoski, S. Marzani, G. Soyez, and J. Thaler, “Soft drop”, *JHEP* **05** (2014) 146, doi:10.1007/JHEP05(2014)146, arXiv:1402.2657.
- [111] CMS Collaboration, “Identification of heavy, energetic, hadronically decaying particles using machine-learning techniques”, *JINST* **15** (2020) P06005, doi:10.1088/1748-0221/15/06/P06005.

- [112] CMS Collaboration, “Identification of heavy-flavour jets with the CMS detector in pp collisions at 13 TeV”, *JINST* **13** (2018) P05011,
[doi:10.1088/1748-0221/13/05/P05011](https://doi.org/10.1088/1748-0221/13/05/P05011), arXiv:1712.07158.
- [113] E. Bols et al., “Jet flavour classification using DeepJet”, *JINST* **15** (2020) P12012,
[doi:10.1088/1748-0221/15/12/P12012](https://doi.org/10.1088/1748-0221/15/12/P12012), arXiv:2008.10519.
- [114] CMS Collaboration, “Performance of the DeepJet b tagging algorithm using 41.9/fb of data from proton-proton collisions at 13 TeV with Phase 1 CMS detector”, CMS Detector Performance Note CMS-DP-2018-058, 2018.
- [115] J. Thaler and K. Van Tilburg, “Identifying boosted objects with N-subjettiness”, *JHEP* **03** (2011) 015, doi:10.1007/JHEP03(2011)015, arXiv:1011.2268.
- [116] CMS Collaboration, “Measurement of normalized differential $t\bar{t}$ cross sections in the dilepton channel from pp collisions at $\sqrt{s} = 13$ TeV”, *JHEP* **04** (2018) 060,
[doi:10.1007/JHEP04\(2018\)060](https://doi.org/10.1007/JHEP04(2018)060), arXiv:1708.07638.
- [117] CMS Collaboration, “Measurement of differential cross sections for top quark pair production using the lepton+jets final state in proton-proton collisions at 13 TeV”, *Phys. Rev. D* **95** (2017) 092001, doi:10.1103/PhysRevD.95.092001,
arXiv:1610.04191.
- [118] M. Rosenblatt, “Remarks on some nonparametric estimates of a density function”, *Ann. Math. Statist.* **27** (1956) 832, doi:10.1214/aoms/1177728190.
- [119] B. W. Silverman, “Density estimation for statistics and data analysis”. Chapman and Hall, 1986. ISBN 0412246201.
- [120] D. W. Scott, “Multivariate density estimation: theory, practice, and visualization”. John Wiley and Sons, 1992. ISBN 0471547700.
- [121] M. J. Oreglia, “A study of the reactions $\psi' \rightarrow \gamma\gamma\psi'$ ”. PhD thesis, Stanford University, 1980. SLAC Report SLAC-R-236.
- [122] J. Gaiser, “Charmonium spectroscopy from radiative decays of the J/ψ and ψ'' ”. PhD thesis, Stanford University, 1982. SLAC Report SLAC-R-255.
- [123] CMS Collaboration, “Precision luminosity measurement in proton-proton collisions at $\sqrt{s} = 13$ TeV in 2015 and 2016 at CMS”, *Eur. Phys. J. C* **81** (2021) 800,
[doi:10.1140/epjc/s10052-021-09538-2](https://doi.org/10.1140/epjc/s10052-021-09538-2), arXiv:2104.01927.
- [124] CMS Collaboration, “CMS luminosity measurement for the 2017 data-taking period at $\sqrt{s} = 13$ TeV”, CMS Physics Analysis Summary CMS-PAS-LUM-17-004, 2018.
- [125] CMS Collaboration, “CMS luminosity measurement for the 2018 data-taking period at $\sqrt{s} = 13$ TeV”, CMS Physics Analysis Summary CMS-PAS-LUM-18-002, 2019.
- [126] M. Cacciari et al., “The $t\bar{t}$ cross-section at 1.8 TeV and 1.96 TeV: A study of the systematics due to parton densities and scale dependence”, *JHEP* **04** (2004) 068,
[doi:10.1088/1126-6708/2004/04/068](https://doi.org/10.1088/1126-6708/2004/04/068), arXiv:hep-ph/0303085.
- [127] S. Catani, D. de Florian, M. Grazzini, and P. Nason, “Soft gluon resummation for Higgs boson production at hadron colliders”, *JHEP* **07** (2003) 028,
[doi:10.1088/1126-6708/2003/07/028](https://doi.org/10.1088/1126-6708/2003/07/028), arXiv:hep-ph/0306211.

- [128] S. Baker and R. D. Cousins, “Clarification of the use of chi square and likelihood functions in fits to histograms”, *Nucl. Instrum. Meth.* **221** (1984) 437, doi:[10.1016/0167-5087\(84\)90016-4](https://doi.org/10.1016/0167-5087(84)90016-4).
- [129] G. Cowan, K. Cranmer, E. Gross, and O. Vitells, “Asymptotic formulae for likelihood-based tests of new physics”, *Eur. Phys. J. C* **71** (2011) 1554, doi:[10.1140/epjc/s10052-011-1554-0](https://doi.org/10.1140/epjc/s10052-011-1554-0), arXiv:[1007.1727](https://arxiv.org/abs/1007.1727). [Erratum: doi:[10.1140/epjc/s10052-013-2501-z](https://doi.org/10.1140/epjc/s10052-013-2501-z)].
- [130] T. Junk, “Confidence level computation for combining searches with small statistics”, *Nucl. Instrum. Meth. A* **434** (1999) 435, doi:[10.1016/S0168-9002\(99\)00498-2](https://doi.org/10.1016/S0168-9002(99)00498-2), arXiv:[hep-ex/9902006](https://arxiv.org/abs/hep-ex/9902006).
- [131] A. L. Read, “Presentation of search results: The CL_s technique”, *J. Phys. G* **28** (2002) 2693, doi:[10.1088/0954-3899/28/10/313](https://doi.org/10.1088/0954-3899/28/10/313).
- [132] A. Oliveira, “Gravity particles from Warped Extra Dimensions, predictions for LHC”, 2014. arXiv:[1404.0102](https://arxiv.org/abs/1404.0102).
- [133] M. Gouzevitch et al., “Scale-invariant resonance tagging in multijet events and new physics in Higgs pair production”, *JHEP* **07** (2013) 148, doi:[10.1007/JHEP07\(2013\)148](https://doi.org/10.1007/JHEP07(2013)148), arXiv:[1303.6636](https://arxiv.org/abs/1303.6636).

A The CMS Collaboration

Yerevan Physics Institute, Yerevan, Armenia

A. Tumasyan

Institut für Hochenergiephysik, Vienna, Austria

W. Adam , J.W. Andrejkovic, T. Bergauer , S. Chatterjee , K. Damanakis, M. Dragicevic , A. Escalante Del Valle , R. Frühwirth¹, M. Jeitler¹ , N. Krammer, L. Lechner , D. Liko, I. Mikulec, P. Paulitsch, F.M. Pitters, J. Schieck¹ , R. Schöfbeck , D. Schwarz, S. Templ , W. Waltenberger , C.-E. Wulz¹ 

Institute for Nuclear Problems, Minsk, Belarus

V. Chekhovsky, A. Litomin, V. Makarenko 

Universiteit Antwerpen, Antwerpen, Belgium

M.R. Darwish², E.A. De Wolf, T. Janssen , T. Kello³, A. Lelek , H. Rejeb Sfar, P. Van Mechelen , S. Van Putte, N. Van Remortel 

Vrije Universiteit Brussel, Brussel, Belgium

F. Blekman , E.S. Bols , J. D'Hondt , M. Delcourt, H. El Faham , S. Lowette , S. Moortgat , A. Morton , D. Müller , A.R. Sahasransu , S. Tavernier , W. Van Doninck

Université Libre de Bruxelles, Bruxelles, Belgium

D. Beghin, B. Bilin , B. Clerbaux , G. De Lentdecker, L. Favart , A.K. Kalsi , K. Lee, M. Mahdavikhorrami, I. Makarenko , L. Moureaux , L. Pétré, A. Popov , N. Postiau, E. Starling , L. Thomas , M. Vanden Bemden, C. Vander Velde , P. Vanlaer 

Ghent University, Ghent, Belgium

T. Cornelis , D. Dobur, J. Knolle , L. Lambrecht, G. Mestdach, M. Niedziela , C. Rendón, C. Roskas, A. Samalan, K. Skovpen , M. Tytgat , B. Vermassen, L. Wezenbeek

Université Catholique de Louvain, Louvain-la-Neuve, Belgium

A. Benecke, A. Bethani , G. Bruno, F. Bury , C. Caputo , P. David , C. Delaere , I.S. Donertas , A. Giammanco , K. Jaffel, Sa. Jain , V. Lemaitre, K. Mondal , J. Prisciandaro, A. Taliercio, M. Teklishyn , T.T. Tran, P. Vischia , S. Wertz 

Centro Brasileiro de Pesquisas Fisicas, Rio de Janeiro, Brazil

G.A. Alves , C. Hensel, A. Moraes , P. Rebello Teles 

Universidade do Estado do Rio de Janeiro, Rio de Janeiro, Brazil

W.L. Aldá Júnior , M. Alves Gallo Pereira , M. Barroso Ferreira Filho, H. Brandao Malbouisson, W. Carvalho , J. Chinellato⁴, E.M. Da Costa , G.G. Da Silveira⁵ , D. De Jesus Damiao , V. Dos Santos Sousa, S. Fonseca De Souza , C. Mora Herrera , K. Mota Amarilo, L. Mundim , H. Nogima, A. Santoro, S.M. Silva Do Amaral , A. Sznajder , M. Thiel, F. Torres Da Silva De Araujo⁶ , A. Vilela Pereira 

Universidade Estadual Paulista (a), Universidade Federal do ABC (b), São Paulo, Brazil

C.A. Bernardes⁵ , L. Calligaris , T.R. Fernandez Perez Tomei , E.M. Gregores , D.S. Lemos , P.G. Mercadante , S.F. Novaes , Sandra S. Padula 

Institute for Nuclear Research and Nuclear Energy, Bulgarian Academy of Sciences, Sofia, Bulgaria

A. Aleksandrov, G. Antchev , R. Hadjiiska, P. Iaydjiev, M. Misheva, M. Rodozov, M. Shopova, G. Sultanov

University of Sofia, Sofia, Bulgaria

A. Dimitrov, T. Ivanov, L. Litov , B. Pavlov, P. Petkov, A. Petrov

Beihang University, Beijing, China

T. Cheng , T. Javaid⁷, M. Mittal, L. Yuan

Department of Physics, Tsinghua University, Beijing, China

M. Ahmad , G. Bauer, C. Dozen⁸ , Z. Hu , J. Martins⁹ , Y. Wang, K. Yi^{10,11}

Institute of High Energy Physics, Beijing, China

E. Chapon , G.M. Chen⁷ , H.S. Chen⁷ , M. Chen , F. Iemmi, A. Kapoor , D. Leggat, H. Liao, Z.-A. Liu⁷ , V. Milosevic , F. Monti , R. Sharma , J. Tao , J. Thomas-Wilsker, J. Wang , H. Zhang , J. Zhao 

State Key Laboratory of Nuclear Physics and Technology, Peking University, Beijing, China

A. Agapitos, Y. An, Y. Ban, C. Chen, A. Levin , Q. Li , X. Lyu, Y. Mao, S.J. Qian, D. Wang , J. Xiao

Sun Yat-Sen University, Guangzhou, China

M. Lu, Z. You 

Institute of Modern Physics and Key Laboratory of Nuclear Physics and Ion-beam Application (MOE) - Fudan University, Shanghai, China

X. Gao³, H. Okawa , Y. Zhang 

Zhejiang University, Hangzhou, China, Zhejiang, China

Z. Lin , M. Xiao 

Universidad de Los Andes, Bogota, Colombia

C. Avila , A. Cabrera , C. Florez , J. Fraga

Universidad de Antioquia, Medellin, Colombia

J. Mejia Guisao, F. Ramirez, J.D. Ruiz Alvarez , C.A. Salazar Gonzalez 

University of Split, Faculty of Electrical Engineering, Mechanical Engineering and Naval Architecture, Split, Croatia

D. Giljanovic, N. Godinovic , D. Lelas , I. Puljak 

University of Split, Faculty of Science, Split, Croatia

Z. Antunovic, M. Kovac, T. Sculac 

Institute Rudjer Boskovic, Zagreb, Croatia

V. Brigljevic , D. Ferencek , D. Majumder , M. Roguljic, A. Starodumov¹² , T. Susa 

University of Cyprus, Nicosia, Cyprus

A. Attikis , K. Christoforou, A. Ioannou, G. Kole , M. Kolosova, S. Konstantinou, J. Mousa , C. Nicolaou, F. Ptochos , P.A. Razis, H. Rykaczewski, H. Saka 

Charles University, Prague, Czech Republic

M. Finger¹³, M. Finger Jr.¹³ , A. Kveton

Escuela Politecnica Nacional, Quito, Ecuador

E. Ayala

Universidad San Francisco de Quito, Quito, Ecuador

E. Carrera Jarrin 

Academy of Scientific Research and Technology of the Arab Republic of Egypt, Egyptian Network of High Energy Physics, Cairo, Egypt

S. Elgammal¹⁴, A. Ellithi Kamel¹⁵

Center for High Energy Physics (CHEP-FU), Fayoum University, El-Fayoum, Egypt

M.A. Mahmoud , Y. Mohammed 

National Institute of Chemical Physics and Biophysics, Tallinn, Estonia

S. Bhowmik , R.K. Dewanjee , K. Ehataht, M. Kadastik, S. Nandan, C. Nielsen, J. Pata, M. Raidal , L. Tani, C. Veelken

Department of Physics, University of Helsinki, Helsinki, Finland

P. Eerola , H. Kirschenmann , K. Osterberg , M. Voutilainen 

Helsinki Institute of Physics, Helsinki, Finland

S. Bharthuar, E. Brücken , F. Garcia , J. Havukainen , M.S. Kim , R. Kinnunen, T. Lampén, K. Lassila-Perini , S. Lehti , T. Lindén, M. Lotti, L. Martikainen, M. Myllymäki, J. Ott , H. Siikonen, E. Tuominen , J. Tuominiemi

Lappeenranta University of Technology, Lappeenranta, Finland

P. Luukka , H. Petrow, T. Tuuva

IRFU, CEA, Université Paris-Saclay, Gif-sur-Yvette, France

C. Amendola , M. Besancon, F. Couderc , M. Dejardin, D. Denegri, J.L. Faure, F. Ferri , S. Ganjour, P. Gras, G. Hamel de Monchenault , P. Jarry, B. Lenzi , E. Locci, J. Malcles, J. Rander, A. Rosowsky , M.Ö. Sahin , A. Savoy-Navarro¹⁶, M. Titov , G.B. Yu 

Laboratoire Leprince-Ringuet, CNRS/IN2P3, Ecole Polytechnique, Institut Polytechnique de Paris, Palaiseau, France

S. Ahuja , F. Beaudette , M. Bonanomi , A. Buchot Perraguin, P. Busson, A. Cappati, C. Charlot, O. Davignon, B. Diab, G. Falmagne , S. Ghosh, R. Granier de Cassagnac , A. Hakimi, I. Kucher , J. Motta, M. Nguyen , C. Ochando , P. Paganini , J. Rembser, R. Salerno , U. Sarkar , J.B. Sauvan , Y. Sirois , A. Tarabini, A. Zabi, A. Zghiche 

Université de Strasbourg, CNRS, IPHC UMR 7178, Strasbourg, France

J.-L. Agram¹⁷ , J. Andrea, D. Apparu, D. Bloch , G. Bourgatte, J.-M. Brom, E.C. Chabert, C. Collard , D. Darej, J.-C. Fontaine¹⁷, U. Goerlach, C. Grimault, A.-C. Le Bihan, E. Nibigira , P. Van Hove 

Institut de Physique des 2 Infinis de Lyon (IP2I), Villeurbanne, France

E. Asilar , S. Beauceron , C. Bernet , G. Boudoul, C. Camen, A. Carle, N. Chanon , D. Contardo, P. Depasse , H. El Mamouni, J. Fay, S. Gascon , M. Gouzevitch , B. Ille, I.B. Laktineh, H. Lattaud , A. Lesauvage , M. Lethuillier , L. Mirabito, S. Perries, K. Shchablo, V. Sordini , L. Torterot , G. Touquet, M. Vander Donckt, S. Viret

Georgian Technical University, Tbilisi, Georgia

I. Bagaturia¹⁸, I. Lomidze, Z. Tsamalaidze¹³

RWTH Aachen University, I. Physikalisches Institut, Aachen, Germany

V. Botta, L. Feld , K. Klein, M. Lipinski, D. Meuser, A. Pauls, N. Röwert, J. Schulz, M. Teroerde 

RWTH Aachen University, III. Physikalisches Institut A, Aachen, Germany

A. Dodonova, D. Eliseev, M. Erdmann , P. Fackeldey , B. Fischer, S. Ghosh , T. Hebbeker , K. Hoepfner, F. Ivone, L. Mastrolorenzo, M. Merschmeyer , A. Meyer , G. Mocellin, S. Mondal, S. Mukherjee , D. Noll , A. Novak, T. Pook , A. Pozdnyakov , Y. Rath, H. Reithler, J. Roemer, A. Schmidt , S.C. Schuler, A. Sharma , L. Vigilante,

S. Wiedenbeck, S. Zaleski

RWTH Aachen University, III. Physikalisches Institut B, Aachen, Germany

C. Dziwok, G. Flügge, W. Haj Ahmad¹⁹ , O. Hlushchenko, T. Kress, A. Nowack , O. Pooth, D. Roy , A. Stahl²⁰ , T. Ziemons , A. Zotz

Deutsches Elektronen-Synchrotron, Hamburg, Germany

H. Aarup Petersen, M. Aldaya Martin, P. Asmuss, S. Baxter, M. Bayatmakou, O. Behnke, A. Bermúdez Martínez, S. Bhattacharya, A.A. Bin Anuar , K. Borras²¹, D. Brunner, A. Campbell , A. Cardini , C. Cheng, F. Colombina, S. Consuegra Rodríguez , G. Correia Silva, V. Danilov, M. De Silva, L. Didukh, G. Eckerlin, D. Eckstein, L.I. Estevez Banos , O. Filatov , E. Gallo²², A. Geiser, A. Giraldi, A. Grohsjean , M. Guthoff, A. Jafari²³ , N.Z. Jomhari , H. Jung , A. Kasem²¹ , M. Kasemann , H. Kaveh , C. Kleinwort , R. Kogler , D. Krücker , W. Lange, J. Lidrych , K. Lipka, W. Lohmann²⁴, R. Mankel, I.-A. Melzer-Pellmann , M. Mendizabal Morentin, J. Metwally, A.B. Meyer , M. Meyer , J. Mnich , A. Mussgiller, Y. Otarid, D. Pérez Adán , D. Pitzl, A. Raspereza, B. Ribeiro Lopes, J. Rübenach, A. Saggio , A. Saibel , M. Savitskyi , M. Scham²⁵, V. Scheurer, S. Schnake, P. Schütze, C. Schwanenberger²² , M. Shchedrolosiev, R.E. Sosa Ricardo , D. Stafford, N. Tonon , M. Van De Klundert , R. Walsh , D. Walter, Q. Wang , Y. Wen , K. Wichmann, L. Wiens, C. Wissing, S. Wuchterl 

University of Hamburg, Hamburg, Germany

R. Aggleton, S. Albrecht , S. Bein , L. Benato , P. Connor , K. De Leo , M. Eich, F. Feindt, A. Fröhlich, C. Garbers , E. Garutti , P. Gunnellini, M. Hajheidari, J. Haller , A. Hinzmann , G. Kasieczka, R. Klanner , T. Kramer, V. Kutzner, J. Lange , T. Lange , A. Lobanov , A. Malara , A. Nigamova, K.J. Pena Rodriguez, M. Rieger , O. Rieger, P. Schleper, M. Schröder , J. Schwandt , J. Sonneveld , H. Stadie, G. Steinbrück, A. Tews, I. Zoi 

Karlsruher Institut fuer Technologie, Karlsruhe, Germany

J. Bechtel , S. Brommer, M. Burkart, E. Butz , R. Caspart , T. Chwalek, W. De Boer[†], A. Dierlamm, A. Droll, K. El Morabit, N. Faltermann , M. Giffels, J.O. Gosewisch, A. Gottmann, F. Hartmann²⁰ , C. Heidecker, U. Husemann , P. Keicher, R. Koppenhöfer, S. Maier, M. Metzler, S. Mitra , Th. Müller, M. Neukum, A. Nürnberg, G. Quast , K. Rabbertz , J. Rauser, D. Savoiu , M. Schnepf, D. Seith, I. Shvetsov, H.J. Simonis, R. Ulrich , J. Van Der Linden, R.F. Von Cube, M. Wassmer, M. Weber , S. Wieland, R. Wolf , S. Wozniewski, S. Wunsch

Institute of Nuclear and Particle Physics (INPP), NCSR Demokritos, Aghia Paraskevi, Greece

G. Anagnostou, G. Daskalakis, T. Geralis , A. Kyriakis, D. Loukas, A. Stakia 

National and Kapodistrian University of Athens, Athens, Greece

M. Diamantopoulou, D. Karasavvas, P. Kontaxakis , C.K. Koraka, A. Manousakis-Katsikakis, A. Panagiotou, I. Papavergou, N. Saoulidou , K. Theofilatos , E. Tziaferi , K. Vellidis, E. Vourliotis

National Technical University of Athens, Athens, Greece

G. Bakas, K. Kousouris , I. Papakrivopoulos, G. Tsipolitis, A. Zacharopoulou

University of Ioánnina, Ioánnina, Greece

K. Adamidis, I. Bestintzanos, I. Evangelou , C. Foudas, P. Gianneios, P. Katsoulis, P. Kokkas, N. Manthos, I. Papadopoulos , J. Strologas 

MTA-ELTE Lendület CMS Particle and Nuclear Physics Group, Eötvös Loránd University, Budapest, Hungary

M. Csanad , K. Farkas, M.M.A. Gadallah²⁶ , S. Lököс²⁷ , P. Major, K. Mandal , A. Mehta , G. Pasztor , A.J. Rádl, O. Surányi, G.I. Veres 

Wigner Research Centre for Physics, Budapest, Hungary

M. Bartók²⁸ , G. Bencze, C. Hajdu , D. Horvath^{29,30} , F. Sikler , V. Veszpremi 

Institute of Nuclear Research ATOMKI, Debrecen, Hungary

S. Czellar, D. Fasanella , F. Fienga , J. Karancsi²⁸ , J. Molnar, Z. Szillasi, D. Teyssier

Institute of Physics, University of Debrecen, Debrecen, Hungary

P. Raics, Z.L. Trocsanyi³¹ , B. Ujvari

Karoly Robert Campus, MATE Institute of Technology, Gyongyos, Hungary

T. Csorgo³² , F. Nemes³², T. Novak

Indian Institute of Science (IISc), Bangalore, India

S. Choudhury, J.R. Komaragiri , D. Kumar, L. Panwar , P.C. Tiwari 

National Institute of Science Education and Research, HBNI, Bhubaneswar, India

S. Bahinipati³³ , C. Kar , P. Mal, T. Mishra , V.K. Muraleedharan Nair Bindhu³⁴, A. Nayak³⁴ , P. Saha, N. Sur , S.K. Swain, D. Vats³⁴

Panjab University, Chandigarh, India

S. Bansal , S.B. Beri, V. Bhatnagar , G. Chaudhary , S. Chauhan , N. Dhingra³⁵ , R. Gupta, A. Kaur, M. Kaur , P. Kumari , M. Meena, K. Sandeep , J.B. Singh , A.K. Virdi 

University of Delhi, Delhi, India

A. Ahmed, A. Bhardwaj , B.C. Choudhary , M. Gola, S. Keshri , A. Kumar , M. Naimuddin , P. Priyanka , K. Ranjan, A. Shah 

Saha Institute of Nuclear Physics, HBNI, Kolkata, India

M. Bharti³⁶, R. Bhattacharya, S. Bhattacharya , D. Bhowmik, S. Dutta, S. Dutta, B. Gomber³⁷ , M. Maity³⁸, P. Palit , P.K. Rout , G. Saha, B. Sahu , S. Sarkar, M. Sharan, S. Thakur³⁶

Indian Institute of Technology Madras, Madras, India

P.K. Behera , S.C. Behera, P. Kalbhor , A. Muhammad, R. Pradhan, P.R. Pujahari, A. Sharma , A.K. Sikdar

Bhabha Atomic Research Centre, Mumbai, India

D. Dutta , V. Jha, V. Kumar , D.K. Mishra, K. Naskar³⁹, P.K. Netrakanti, L.M. Pant, P. Shukla 

Tata Institute of Fundamental Research-A, Mumbai, India

T. Aziz, S. Dugad, M. Kumar

Tata Institute of Fundamental Research-B, Mumbai, India

S. Banerjee , R. Chudasama, M. Guchait, S. Karmakar, S. Kumar, G. Majumder, K. Mazumdar, S. Mukherjee 

Indian Institute of Science Education and Research (IISER), Pune, India

A. Alpana, S. Dube , B. Kansal, A. Laha, S. Pandey , A. Rastogi , S. Sharma 

Isfahan University of Technology, Isfahan, Iran

A. Gholami⁴⁰, E. Khazaie⁴¹, M. Zeinali⁴²

Institute for Research in Fundamental Sciences (IPM), Tehran, Iran

S. Chenarani⁴³, S.M. Etesami , M. Khakzad , M. Mohammadi Najafabadi 

University College Dublin, Dublin, Ireland

M. Grunewald 

INFN Sezione di Bari ^a, Bari, Italy, Università di Bari ^b, Bari, Italy, Politecnico di Bari ^c, Bari, Italy

M. Abbrescia^{a,b} , R. Aly^{a,b,44} , C. Aruta^{a,b}, A. Colaleo^a , D. Creanza^{a,c} , N. De Filippis^{a,c} , M. De Palma^{a,b} , A. Di Florio^{a,b}, A. Di Pilato^{a,b} , W. Elmetenawee^{a,b} , L. Fiore^a , A. Gelmi^{a,b} , M. Gul^a , G. Iaselli^{a,c} , M. Ince^{a,b} , S. Lezki^{a,b} , G. Maggi^{a,c} , M. Maggi^a , I. Margjeka^{a,b}, V. Mastrapasqua^{a,b} , S. My^{a,b} , S. Nuzzo^{a,b} , A. Pellecchia^{a,b}, A. Pompili^{a,b} , G. Pugliese^{a,c} , D. Ramos^a, A. Ranieri^a , G. Selvaggi^{a,b} , L. Silvestris^a , F.M. Simone^{a,b} , Ü. Sözbilir^a, R. Venditti^a , P. Verwilligen^a 

INFN Sezione di Bologna ^a, Bologna, Italy, Università di Bologna ^b, Bologna, Italy

G. Abbiendi^a , C. Battilana^{a,b} , D. Bonacorsi^{a,b} , L. Borgonovi^a, R. Campanini^{a,b} , P. Capiluppi^{a,b} , A. Castro^{a,b} , F.R. Cavallo^a , C. Ciocca^a , M. Cuffiani^{a,b} , G.M. Dallavalle^a , T. Diotalevi^{a,b} , F. Fabbri^a , A. Fanfani^{a,b} , P. Giacomelli^a , L. Giommi^{a,b} , C. Grandi^a , L. Guiducci^{a,b}, S. Lo Meo^{a,45}, L. Lunerti^{a,b}, S. Marcellini^a , G. Masetti^a , F.L. Navarreria^{a,b} , A. Perrotta^a , F. Primavera^{a,b} , A.M. Rossi^{a,b} , T. Rovelli^{a,b} , G.P. Siroli^{a,b} 

INFN Sezione di Catania ^a, Catania, Italy, Università di Catania ^b, Catania, Italy

S. Albergo^{a,b,46} , S. Costa^{a,b,46} , A. Di Mattia^a , R. Potenza^{a,b}, A. Tricomi^{a,b,46} , C. Tuve^{a,b} 

INFN Sezione di Firenze ^a, Firenze, Italy, Università di Firenze ^b, Firenze, Italy

G. Barbagli^a , A. Cassese^a , R. Ceccarelli^{a,b}, V. Ciulli^{a,b} , C. Civinini^a , R. D'Alessandro^{a,b} , E. Focardia^{a,b} , G. Latino^{a,b} , P. Lenzi^{a,b} , M. Lizzo^{a,b}, M. Meschini^a , S. Paoletti^a , R. Seidita^{a,b}, G. Sguazzoni^a , L. Viliani^a 

INFN Laboratori Nazionali di Frascati, Frascati, Italy

L. Benussi , S. Bianco , D. Piccolo 

INFN Sezione di Genova ^a, Genova, Italy, Università di Genova ^b, Genova, Italy

M. Bozzo^{a,b} , F. Ferro^a , R. Mulargia^{a,b}, E. Robutti^a , S. Tosi^{a,b} 

INFN Sezione di Milano-Bicocca ^a, Milano, Italy, Università di Milano-Bicocca ^b, Milano, Italy

A. Benaglia^a , G. Boldrini , F. Brivio^{a,b}, F. Cetorelli^{a,b}, F. De Guio^{a,b} , M.E. Dinardo^{a,b} , P. Dini^a , S. Gennai^a , A. Ghezzi^{a,b} , P. Govoni^{a,b} , L. Guzzi^{a,b} , M.T. Lucchini^{a,b} , M. Malberti^a, S. Malvezzi , A. Massironi^a , D. Menasce^a , L. Moroni^a , M. Paganoni^{a,b} , D. Pedrini^a , B.S. Pinolini, S. Ragazzi^{a,b} , N. Redaelli^a , T. Tabarelli de Fatis^{a,b} , D. Valsecchi^{a,b,20}, D. Zuolo^{a,b} 

INFN Sezione di Napoli ^a, Napoli, Italy, Università di Napoli 'Federico II' ^b, Napoli, Italy, Università della Basilicata ^c, Potenza, Italy, Università G. Marconi ^d, Roma, Italy

S. Buontempo^a , F. Carnevali^{a,b}, N. Cavallo^{a,c} , A. De Iorio^{a,b} , F. Fabozzi^{a,c} , A.O.M. Iorio^{a,b} , L. Lista^{a,b,47} , S. Meola^{a,d,20} , P. Paolucci^{a,20} , B. Rossi^a , C. Sciacca^{a,b} 

INFN Sezione di Padova ^a, Padova, Italy, Università di Padova ^b, Padova, Italy, Università

di Trento ^c, Trento, Italy

P. Azzi^a , N. Bacchetta^a , D. Bisello^{a,b} , P. Bortignon^a , A. Bragagnolo^{a,b} , R. Carlin^{a,b} , P. Checchia^a , T. Dorigo^a , U. Dosselli^a , F. Gasparini^{a,b} , U. Gasparini^{a,b} , G. Grossi, S.Y. Hoh^{a,b} , L. Layer^{a,48}, E. Lusiani , M. Margoni^{a,b} , A.T. Meneguzzo^{a,b} , J. Pazzini^{a,b} , P. Ronchese^{a,b} , R. Rossin^{a,b} , F. Simonetto^{a,b} , G. Strong^a , M. Tosi^{a,b} , H. Yarar^{a,b} , M. Zanetti^{a,b} , P. Zotto^{a,b} , A. Zucchetta^{a,b} , G. Zumerle^{a,b}

INFN Sezione di Pavia ^a, Pavia, Italy, Università di Pavia ^b, Pavia, Italy

C. Aimè^{a,b}, A. Braghieri^a , S. Calzaferri^{a,b} , D. Fiorina^{a,b} , P. Montagna^{a,b} , S.P. Ratti^{a,b}, V. Re^a , C. Riccardi^{a,b} , P. Salvini^a , I. Vai^a , P. Vitulò^{a,b}

INFN Sezione di Perugia ^a, Perugia, Italy, Università di Perugia ^b, Perugia, Italy

P. Asenov^{a,49} , G.M. Bilei^a , D. Ciangottini^{a,b} , L. Fanò^{a,b} , M. Magherini^b, G. Mantovani^{a,b} , V. Mariani^{a,b} , M. Menichelli^a , F. Moscatelli^{a,49} , A. Piccinelli^{a,b} , M. Presilla^{a,b} , A. Rossi^{a,b} , A. Santocchia^{a,b} , D. Spiga^a , T. Tedeschi^{a,b}

INFN Sezione di Pisa ^a, Pisa, Italy, Università di Pisa ^b, Pisa, Italy, Scuola Normale Superiore di Pisa ^c, Pisa, Italy, Università di Siena ^d, Siena, Italy

P. Azzurri^a , G. Bagliesi^a , V. Bertacchi^{a,c} , L. Bianchini^a , T. Boccali^a , E. Bossini^{a,b} , R. Castaldi^a , M.A. Ciocci^{a,b} , V. D'Amante^{a,d} , R. Dell'Orso^a , M.R. Di Domenico^{a,d} , S. Donato^a , A. Giassi^a , F. Ligabue^{a,c} , E. Manca^{a,c} , G. Mandorli^{a,c} , D. Matos Figueiredo, A. Messineo^{a,b} , F. Palla^a , S. Parolia^{a,b} , G. Ramirez-Sánchez^{a,c} , A. Rizzi^{a,b} , G. Rolandi^{a,c} , S. Roy Chowdhury^{a,c} , A. Scribano^a, N. Shafiei^{a,b} , P. Spagnolo^a , R. Tenchini^a , G. Tonelli^{a,b} , N. Turini^{a,d} , A. Venturi^a , P.G. Verdini^a

INFN Sezione di Roma ^a, Rome, Italy, Sapienza Università di Roma ^b, Rome, Italy

P. Barria^a , M. Campana^{a,b} , F. Cavallari^a , D. Del Re^{a,b} , E. Di Marco^a , M. Diemoz^a , E. Longo^{a,b} , P. Meridiani^a , G. Organtini^{a,b} , F. Pandolfi^a, R. Paramatti^{a,b} , C. Quaranta^{a,b} , S. Rahatlou^{a,b} , C. Rovelli^a , F. Santanastasio^{a,b} , L. Soffi^a , R. Tramontano^{a,b}

INFN Sezione di Torino ^a, Torino, Italy, Università di Torino ^b, Torino, Italy, Università del Piemonte Orientale ^c, Novara, Italy

N. Amapane^{a,b} , R. Arcidiacono^{a,c} , S. Argiro^{a,b} , M. Arneodo^{a,c} , N. Bartosik^a , R. Bellan^{a,b} , A. Bellora^{a,b} , J. Berenguer Antequera^{a,b} , C. Biino^a , N. Cartiglia^a , M. Costa^{a,b} , R. Covarelli^{a,b} , N. Demaria^a , B. Kiani^{a,b} , F. Legger^a , C. Mariotti^a , S. Maselli^a , E. Migliore^{a,b} , E. Monteil^{a,b} , M. Monteno^a , M.M. Obertino^{a,b} , G. Ortona^a , L. Pacher^{a,b} , N. Pastrone^a , M. Pelliccioni^a , M. Ruspa^{a,c} , K. Shchelina^a , F. Siviero^{a,b} , V. Sola^a , A. Solano^{a,b} , D. Soldi^{a,b} , A. Staiano^a , M. Tornago^{a,b} , D. Trocino^a , A. Vagnerini^{a,b}

INFN Sezione di Trieste ^a, Trieste, Italy, Università di Trieste ^b, Trieste, Italy

S. Belforte^a , V. Candelise^{a,b} , M. Casarsa^a , F. Cossutti^a , A. Da Rold^{a,b} , G. Della Ricca^{a,b} , G. Sorrentino^{a,b} , F. Vazzoler^{a,b}

Kyungpook National University, Daegu, Korea

S. Dogra , C. Huh , B. Kim, D.H. Kim , G.N. Kim , J. Kim, J. Lee, S.W. Lee , C.S. Moon , Y.D. Oh , S.I. Pak, S. Sekmen , Y.C. Yang

Chonnam National University, Institute for Universe and Elementary Particles, Kwangju, Korea

H. Kim , D.H. Moon 

Hanyang University, Seoul, Korea

B. Francois , T.J. Kim , J. Park 

Korea University, Seoul, Korea

S. Cho, S. Choi , B. Hong , K. Lee, K.S. Lee , J. Lim, J. Park, S.K. Park, J. Yoo

Kyung Hee University, Department of Physics, Seoul, Republic of Korea, Seoul, Korea

J. Goh , A. Gurtu

Sejong University, Seoul, Korea

H.S. Kim , Y. Kim

Seoul National University, Seoul, Korea

J. Almond, J.H. Bhyun, J. Choi, S. Jeon, J. Kim, J.S. Kim, S. Ko, H. Kwon, H. Lee , S. Lee, B.H. Oh, M. Oh , S.B. Oh, H. Seo , U.K. Yang, I. Yoon 

University of Seoul, Seoul, Korea

W. Jang, D.Y. Kang, Y. Kang, S. Kim, B. Ko, J.S.H. Lee , Y. Lee, J.A. Merlin, I.C. Park, Y. Roh, M.S. Ryu, D. Song, I.J. Watson , S. Yang

Yonsei University, Department of Physics, Seoul, Korea

S. Ha, H.D. Yoo

Sungkyunkwan University, Suwon, Korea

M. Choi, H. Lee, Y. Lee, I. Yu 

College of Engineering and Technology, American University of the Middle East (AUM), Egaila, Kuwait, Dasman, Kuwait

T. Beyrouthy, Y. Maghrbi

Riga Technical University, Riga, Latvia

K. Dreimanis , V. Veckalns⁵⁰ 

Vilnius University, Vilnius, Lithuania

M. Ambrozas, A. Carvalho Antunes De Oliveira , A. Juodagalvis , A. Rinkevicius , G. Tamulaitis 

National Centre for Particle Physics, Universiti Malaya, Kuala Lumpur, Malaysia

N. Bin Norjoharuddeen , W.A.T. Wan Abdullah, M.N. Yusli, Z. Zolkapli

Universidad de Sonora (UNISON), Hermosillo, Mexico

J.F. Benitez , A. Castaneda Hernandez , M. León Coello, J.A. Murillo Quijada , A. Sehrawat, L. Valencia Palomo 

Centro de Investigacion y de Estudios Avanzados del IPN, Mexico City, Mexico

G. Ayala, H. Castilla-Valdez, E. De La Cruz-Burelo , I. Heredia-De La Cruz⁵¹ , R. Lopez-Fernandez, C.A. Mondragon Herrera, D.A. Perez Navarro, A. Sánchez Hernández 

Universidad Iberoamericana, Mexico City, Mexico

S. Carrillo Moreno, C. Oropeza Barrera , F. Vazquez Valencia

Benemerita Universidad Autonoma de Puebla, Puebla, Mexico

I. Pedraza, H.A. Salazar Ibarguen, C. Uribe Estrada

University of Montenegro, Podgorica, Montenegro

J. Mijuskovic⁵², N. Raicevic

University of Auckland, Auckland, New Zealand

D. Kofcheck 

University of Canterbury, Christchurch, New Zealand

P.H. Butler 

National Centre for Physics, Quaid-I-Azam University, Islamabad, Pakistan

A. Ahmad, M.I. Asghar, A. Awais, M.I.M. Awan, H.R. Hoorani, W.A. Khan, M.A. Shah, M. Shoaib , M. Waqas 

AGH University of Science and Technology Faculty of Computer Science, Electronics and Telecommunications, Krakow, Poland

V. Avati, L. Grzanka, M. Malawski

National Centre for Nuclear Research, Swierk, Poland

H. Bialkowska, M. Bluj , B. Boimska , M. Górska, M. Kazana, M. Szleper , P. Zalewski

Institute of Experimental Physics, Faculty of Physics, University of Warsaw, Warsaw, Poland

K. Bunkowski, K. Doroba, A. Kalinowski , M. Konecki , J. Krolikowski 

Laboratório de Instrumentação e Física Experimental de Partículas, Lisboa, Portugal

M. Araujo, P. Bargassa , D. Bastos, A. Boletti , P. Faccioli , M. Gallinaro , J. Hollar , N. Leonardo , T. Niknejad, M. Pisano, J. Seixas , O. Toldaiev , J. Varela 

Joint Institute for Nuclear Research, Dubna, Russia

S. Afanasiev, D. Budkouski, I. Golutvin, I. Gorbunov , V. Karjavine, V. Korenkov , A. Lanev, A. Malakhov, V. Matveev^{53,54}, V. Palichik, V. Perelygin, M. Savina, D. Seitova, V. Shalaev, S. Shmatov, S. Shulha, V. Smirnov, O. Teryaev, N. Voitishin, B.S. Yuldashev⁵⁵, A. Zarubin, I. Zhizhin

Petersburg Nuclear Physics Institute, Gatchina (St. Petersburg), Russia

G. Gavrilov , V. Golovtcov, Y. Ivanov, V. Kim⁵⁶ , E. Kuznetsova⁵⁷ , V. Murzin, V. Oreshkin, I. Smirnov, D. Sosnov , V. Sulimov, L. Uvarov, S. Volkov, A. Vorobyev

Institute for Nuclear Research, Moscow, Russia

Yu. Andreev , A. Dermenev, S. Glinenko , N. Golubev, A. Karneyeu , D. Kirpichnikov , M. Kirsanov, N. Krasnikov, A. Pashenkov, G. Pivovarov , A. Toropin

Institute for Theoretical and Experimental Physics named by A.I. Alikhanov of NRC 'Kurchatov Institute', Moscow, Russia

V. Epshteyn, V. Gavrilov, N. Lychkovskaya, A. Nikitenko⁵⁸, V. Popov, A. Stepennov, M. Toms, E. Vlasov , A. Zhokin

Moscow Institute of Physics and Technology, Moscow, Russia

T. Aushev

National Research Nuclear University 'Moscow Engineering Physics Institute' (MEPhI), Moscow, Russia

O. Bychkova, R. Chistov⁵⁹ , M. Danilov⁵⁹ , A. Oskin, P. Parygin, S. Polikarpov⁵⁹ 

P.N. Lebedev Physical Institute, Moscow, Russia

V. Andreev, M. Azarkin, I. Dremin , M. Kirakosyan, A. Terkulov

Skobeltsyn Institute of Nuclear Physics, Lomonosov Moscow State University, Moscow, Russia

A. Belyaev, E. Boos , V. Bunichev, M. Dubinin⁶⁰ , L. Dudko , A. Gribushin, V. Klyukhin , O. Kodolova , I. Lokhtin , S. Obraztsov, M. Perfilov, S. Petrushanko, V. Savrin

Novosibirsk State University (NSU), Novosibirsk, Russia

V. Blinov⁶¹, T. Dimova⁶¹, L. Kardapoltsev⁶¹, A. Kozyrev⁶¹, I. Ovtin⁶¹, O. Radchenko⁶¹, Y. Skovpen⁶¹ 

Institute for High Energy Physics of National Research Centre 'Kurchatov Institute', Protvino, Russia

I. Azhgirey , I. Bayshev, D. Elumakhov, V. Kachanov, D. Konstantinov , P. Mandrik , V. Petrov, R. Ryutin, S. Slabospitskii , A. Sobol, S. Troshin , N. Tyurin, A. Uzunian, A. Volkov

National Research Tomsk Polytechnic University, Tomsk, Russia

A. Babaev, V. Okhotnikov

Tomsk State University, Tomsk, Russia

V. Borshch, V. Ivanchenko , E. Tcherniaev 

University of Belgrade: Faculty of Physics and VINCA Institute of Nuclear Sciences, Belgrade, Serbia

P. Adzic⁶² , M. Dordevic , P. Milenovic , J. Milosevic 

Centro de Investigaciones Energéticas Medioambientales y Tecnológicas (CIEMAT), Madrid, Spain

M. Aguilar-Benitez, J. Alcaraz Maestre , A. Álvarez Fernández, I. Bachiller, M. Barrio Luna, Cristina F. Bedoya , C.A. Carrillo Montoya , M. Cepeda , M. Cerrada, N. Colino , B. De La Cruz, A. Delgado Peris , J.P. Fernández Ramos , J. Flix , M.C. Fouz , O. Gonzalez Lopez , S. Goy Lopez , J.M. Hernandez , M.I. Josa , J. León Holgado , D. Moran, Á. Navarro Tobar , C. Perez Dengra, A. Pérez-Calero Yzquierdo , J. Puerta Pelayo , I. Redondo , L. Romero, S. Sánchez Navas, L. Urda Gómez , C. Willmott

Universidad Autónoma de Madrid, Madrid, Spain

J.F. de Trocóniz, R. Reyes-Almanza 

Universidad de Oviedo, Instituto Universitario de Ciencias y Tecnologías Espaciales de Asturias (ICTEA), Oviedo, Spain

B. Alvarez Gonzalez , J. Cuevas , C. Erice , J. Fernandez Menendez , S. Folgueras , I. Gonzalez Caballero , J.R. González Fernández, E. Palencia Cortezon , C. Ramón Álvarez, V. Rodríguez Bouza , A. Soto Rodríguez, A. Trapote, N. Trevisani , C. Vico Villalba

Instituto de Física de Cantabria (IFCA), CSIC-Universidad de Cantabria, Santander, Spain

J.A. Brochero Cifuentes , I.J. Cabrillo, A. Calderon , J. Duarte Campderros , M. Fernández , C. Fernandez Madrazo , P.J. Fernández Manteca , A. García Alonso, G. Gomez, C. Martinez Rivero, P. Martinez Ruiz del Arbol , F. Matorras , P. Matorras Cuevas , J. Piedra Gomez , C. Prieels, A. Ruiz-Jimeno , L. Scodellaro , I. Vila, J.M. Vizan Garcia 

University of Colombo, Colombo, Sri Lanka

M.K. Jayananda, B. Kailasapathy⁶³, D.U.J. Sonnadara, D.D.C. Wickramarathna

University of Ruhuna, Department of Physics, Matara, Sri Lanka

W.G.D. Dharmaratna , K. Liyanage, N. Perera, N. Wickramage

CERN, European Organization for Nuclear Research, Geneva, Switzerland

T.K. Arrestad , D. Abbaneo, J. Alimena , E. Auffray, G. Auzinger, J. Baechler, P. Baillon[†], D. Barney , J. Bendavid, M. Bianco , A. Bocci , C. Caillol, T. Camporesi, M. Capeans Garrido , G. Cerminara, N. Chernyavskaya , S.S. Chhibra , M. Cipriani , L. Cristella , D. d'Enterria , A. Dabrowski , A. David , A. De Roeck , M.M. Defranchis , M. Deile , M. Dobson, M. Dünser , N. Dupont, A. Elliott-Peisert, N. Emriskova, F. Fallavollita⁶⁴,

A. Florent , L. Forthomme , G. Franzoni , W. Funk, S. Giani, D. Gigi, K. Gill, F. Glege, L. Gouskos , M. Haranko , J. Hegeman , V. Innocente , T. James, P. Janot , J. Kaspar , J. Kieseler , M. Komm , N. Kratochwil, C. Lange , S. Laurila, P. Lecoq , A. Lintuluoto, K. Long , C. Lourenço , B. Maier, L. Malgeri , S. Mallios, M. Mannelli, A.C. Marini , F. Meijers, S. Mersi , E. Meschi , F. Moortgat , M. Mulders , S. Orfanelli, L. Orsini, F. Pantaleo , E. Perez, M. Peruzzi , A. Petrilli, G. Petrucciani , A. Pfeiffer , M. Pierini , D. Piparo, M. Pitt , H. Qu , T. Quast, D. Rabady , A. Racz, G. Reales Gutiérrez, M. Rovere, H. Sakulin, J. Salfeld-Nebgen , S. Scarfi, C. Schäfer, C. Schwick, M. Selvaggi , A. Sharma, P. Silva , W. Snoeys , P. Sphicas⁶⁵ , S. Summers , K. Tatar , V.R. Tavolaro , D. Treille, P. Tropea, A. Tsirou, G.P. Van Onsem , J. Wanczyk⁶⁶, K.A. Wozniak, W.D. Zeuner

Paul Scherrer Institut, Villigen, Switzerland

L. Caminada⁶⁷ , A. Ebrahimi , W. Erdmann, R. Horisberger, Q. Ingram, H.C. Kaestli, D. Kotlinski, U. Langenegger, M. Missiroli⁶⁷ , L. Noehte⁶⁷, T. Rohe

ETH Zurich - Institute for Particle Physics and Astrophysics (IPA), Zurich, Switzerland

K. Androsov⁶⁶ , M. Backhaus , P. Berger, A. Calandri , A. De Cosa, G. Dissertori , M. Dittmar, M. Donegà, C. Dorfer , F. Eble, K. Gedia, F. Glessgen, T.A. Gómez Espinosa , C. Grab , D. Hits, W. Lustermann, A.-M. Lyon, R.A. Manzoni , L. Marchese , C. Martin Perez, M.T. Meinhard, F. Nessi-Tedaldi, J. Niedziela , F. Pauss, V. Perovic, S. Pigazzini , M.G. Ratti , M. Reichmann, C. Reissel, T. Reitenspiess, B. Ristic , D. Ruini, D.A. Sanz Becerra , V. Stampf, J. Steggemann⁶⁶ , R. Wallny , D.H. Zhu

Universität Zürich, Zurich, Switzerland

C. Amsler⁶⁸ , P. Bärtschi, C. Botta , D. Brzhechko, M.F. Canelli , K. Cormier, A. De Wit , R. Del Burgo, J.K. Heikkilä , M. Huwiler, W. Jin, A. Jofrehei , B. Kilminster , S. Leontsinis , S.P. Liechti, A. Macchiolo , P. Meiring, V.M. Mikuni , U. Molinatti, I. Neutelings, A. Reimers, P. Robmann, S. Sanchez Cruz , K. Schweiger , M. Senger, Y. Takahashi 

National Central University, Chung-Li, Taiwan

C. Adloff⁶⁹, C.M. Kuo, W. Lin, A. Roy , T. Sarkar³⁸ , S.S. Yu

National Taiwan University (NTU), Taipei, Taiwan

L. Ceard, Y. Chao, K.F. Chen , P.H. Chen , P.s. Chen, H. Cheng , W.-S. Hou , Y.y. Li, R.-S. Lu, E. Paganis , A. Psallidas, A. Steen, H.y. Wu, E. Yazgan , P.r. Yu

Chulalongkorn University, Faculty of Science, Department of Physics, Bangkok, Thailand

B. Asavapibhop , C. Asawatangtrakuldee , N. Srimanobhas 

Çukurova University, Physics Department, Science and Art Faculty, Adana, Turkey

F. Boran , S. Damarseckin⁷⁰, Z.S. Demiroglu , F. Dolek , I. Dumanoglu⁷¹ , E. Eskut, Y. Guler⁷² , E. Gurpinar Guler⁷² , C. Isik, O. Kara, A. Kayis Topaksu, U. Kiminsu , G. Onengut, K. Ozdemir⁷³, A. Polatoz, A.E. Simsek , B. Tali⁷⁴, U.G. Tok , S. Turkcapar, I.S. Zorbakir 

Middle East Technical University, Physics Department, Ankara, Turkey

G. Karapinar, K. Ocalan⁷⁵ , M. Yalvac⁷⁶ 

Bogazici University, Istanbul, Turkey

B. Akgun, I.O. Atakisi , E. Gülmез , M. Kaya⁷⁷ , O. Kaya⁷⁸, Ö. Özçelik, S. Tekten⁷⁹, E.A. Yetkin⁸⁰ 

Istanbul Technical University, Istanbul, Turkey

A. Cakir , K. Cankocak⁷¹ , Y. Komurcu, S. Sen⁸¹ 

Istanbul University, Istanbul, Turkey

S. Cerci⁷⁴, I. Hos⁸², B. Isildak⁸³, B. Kaynak, S. Ozkorucuklu, H. Sert , D. Sunar Cerci⁷⁴ , C. Zorbilmez

Institute for Scintillation Materials of National Academy of Science of Ukraine, Kharkov, Ukraine

B. Grynyov

National Scientific Center, Kharkov Institute of Physics and Technology, Kharkov, Ukraine

L. Levchuk 

University of Bristol, Bristol, United Kingdom

D. Anthony, E. Bhal , S. Bologna, J.J. Brooke , A. Bundock , E. Clement , D. Cussans , H. Flacher , J. Goldstein , G.P. Heath, H.F. Heath , L. Kreczko , B. Krikler , S. Paramesvaran, S. Seif El Nasr-Storey, V.J. Smith, N. Stylianou⁸⁴ , K. Walkingshaw Pass, R. White

Rutherford Appleton Laboratory, Didcot, United Kingdom

K.W. Bell, A. Belyaev⁸⁵ , C. Brew , R.M. Brown, D.J.A. Cockerill, C. Cooke, K.V. Ellis, K. Harder, S. Harper, M.-L. Holmberg⁸⁶, J. Linacre , K. Manolopoulos, D.M. Newbold , E. Olaiya, D. Petyt, T. Reis , T. Schuh, C.H. Shepherd-Themistocleous, I.R. Tomalin, T. Williams 

Imperial College, London, United Kingdom

R. Bainbridge , P. Bloch , S. Bonomally, J. Borg , S. Breeze, O. Buchmuller, V. Cepaitis , G.S. Chahal⁸⁷ , D. Colling, P. Dauncey , G. Davies , M. Della Negra , S. Fayer, G. Fedi , G. Hall , M.H. Hassanshahi, G. Iles, J. Langford, L. Lyons, A.-M. Magnan, S. Malik, A. Martelli , D.G. Monk, J. Nash⁸⁸ , M. Pesaresi, B.C. Radburn-Smith, D.M. Raymond, A. Richards, A. Rose, E. Scott , C. Seez, A. Shtipliyski, A. Tapper , K. Uchida, T. Virdee²⁰ , M. Vojinovic , N. Wardle , S.N. Webb , D. Winterbottom

Brunel University, Uxbridge, United Kingdom

K. Coldham, J.E. Cole , A. Khan, P. Kyberd , I.D. Reid , L. Teodorescu, S. Zahid 

Baylor University, Waco, Texas, USA

S. Abdullin , A. Brinkerhoff , B. Caraway , J. Dittmann , K. Hatakeyama , A.R. Kanuganti, B. McMaster , N. Pastika, M. Saunders , S. Sawant, C. Sutantawibul, J. Wilson 

Catholic University of America, Washington, DC, USA

R. Bartek , A. Dominguez , R. Uniyal , A.M. Vargas Hernandez

The University of Alabama, Tuscaloosa, Alabama, USA

A. Buccilli , S.I. Cooper , D. Di Croce , S.V. Gleyzer , C. Henderson , C.U. Perez , P. Rumerio⁸⁹ , C. West 

Boston University, Boston, Massachusetts, USA

A. Akpinar , A. Albert , D. Arcaro , C. Cosby , Z. Demiragli , E. Fontanesi, D. Gastler, S. May , J. Rohlf , K. Salyer , D. Sperka, D. Spitzbart , I. Suarez , A. Tsatsos, S. Yuan, D. Zou

Brown University, Providence, Rhode Island, USA

G. Benelli , B. Burkle , X. Coubez²¹, D. Cutts , M. Hadley , U. Heintz , J.M. Hogan⁹⁰ 

T. KWON, G. Landsberg , K.T. Lau , D. Li, M. Lukasik, J. Luo , M. Narain, N. Pervan, S. Sagir⁹¹ , F. Simpson, E. Usai , W.Y. Wong, X. Yan , D. Yu , W. Zhang

University of California, Davis, Davis, California, USA

J. Bonilla , C. Brainerd , R. Breedon, M. Calderon De La Barca Sanchez, M. Chertok , J. Conway , P.T. Cox, R. Erbacher, G. Haza, F. Jensen , O. Kukral, R. Lander, M. Mulhearn , D. Pellett, B. Regnery , D. Taylor , Y. Yao , F. Zhang 

University of California, Los Angeles, California, USA

M. Bachtis , R. Cousins , A. Datta , D. Hamilton, J. Hauser , M. Ignatenko, M.A. Iqbal, T. Lam, N. Mccoll , W.A. Nash, S. Regnard , D. Saltzberg , B. Stone, V. Valuev 

University of California, Riverside, Riverside, California, USA

K. Burt, Y. Chen, R. Clare , J.W. Gary , M. Gordon, G. Hanson , G. Karapostoli , O.R. Long , N. Manganelli, M. Olmedo Negrete, W. Si , S. Wimpenny, Y. Zhang

University of California, San Diego, La Jolla, California, USA

J.G. Branson, P. Chang , S. Cittolin, S. Cooperstein , N. Deelen , D. Diaz , J. Duarte , R. Gerosa , L. Giannini , J. Guiang, R. Kansal , V. Krutelyov , R. Lee, J. Letts , M. Masciovecchio , F. Mokhtar, M. Pieri , B.V. Sathia Narayanan , V. Sharma , M. Tadel, F. Würthwein , Y. Xiang , A. Yagil 

University of California, Santa Barbara - Department of Physics, Santa Barbara, California, USA

N. Amin, C. Campagnari , M. Citron , A. Dorsett, V. Dutta , J. Incandela , M. Kilpatrick , J. Kim , B. Marsh, H. Mei, M. Oshiro, M. Quinnan , J. Richman, U. Sarica , F. Setti, J. Sheplock, P. Siddireddy, D. Stuart, S. Wang 

California Institute of Technology, Pasadena, California, USA

A. Bornheim , O. Cerri, I. Dutta , J.M. Lawhorn , N. Lu , J. Mao, H.B. Newman , T.Q. Nguyen , M. Spiropulu , J.R. Vlimant , C. Wang , S. Xie , Z. Zhang , R.Y. Zhu 

Carnegie Mellon University, Pittsburgh, Pennsylvania, USA

J. Alison , S. An , M.B. Andrews, P. Bryant , T. Ferguson , A. Harilal, C. Liu, T. Mudholkar , M. Paulini , A. Sanchez, W. Terrill

University of Colorado Boulder, Boulder, Colorado, USA

J.P. Cumalat , W.T. Ford , A. Hassani, G. Karathanasis, E. MacDonald, R. Patel, A. Perloff , C. Savard, K. Stenson , K.A. Ulmer , S.R. Wagner 

Cornell University, Ithaca, New York, USA

J. Alexander , S. Bright-Thonney , X. Chen , Y. Cheng , D.J. Cranshaw , S. Hogan, J. Monroy , J.R. Patterson , D. Quach , J. Reichert , M. Reid , A. Ryd, W. Sun , J. Thom , P. Wittich , R. Zou 

Fermi National Accelerator Laboratory, Batavia, Illinois, USA

M. Albrow , M. Alyari , G. Apolinari, A. Apresyan , A. Apyan , L.A.T. Bauerick , D. Berry , J. Berryhill , P.C. Bhat, K. Burkett , J.N. Butler, A. Canepa, G.B. Cerati , H.W.K. Cheung , F. Chlebana, K.F. Di Petrillo , V.D. Elvira , Y. Feng, J. Freeman, Z. Gecse, L. Gray, D. Green, S. Grünendahl , O. Gutsche , R.M. Harris , R. Heller, T.C. Herwig , J. Hirschauer , B. Jayatilaka , S. Jindariani, M. Johnson, U. Joshi, T. Klijnsma , B. Klima , K.H.M. Kwok, S. Lammel , D. Lincoln , R. Lipton, T. Liu, C. Madrid, K. Maeshima, C. Mantilla , D. Mason, P. McBride , P. Merkel, S. Mrenna , S. Nahn , J. Ngadiuba , V. O'Dell, V. Papadimitriou, K. Pedro , C. Pena⁶⁰ , O. Prokofyev,

F. Ravera [ID](#), A. Reinsvold Hall⁹² [ID](#), L. Ristori [ID](#), E. Sexton-Kennedy [ID](#), N. Smith [ID](#), A. Soha [ID](#), L. Spiegel, S. Stoynev [ID](#), J. Strait [ID](#), L. Taylor [ID](#), S. Tkaczyk, N.V. Tran [ID](#), L. Uplegger [ID](#), E.W. Vaandering [ID](#), H.A. Weber [ID](#)

University of Florida, Gainesville, Florida, USA

D. Acosta [ID](#), P. Avery, D. Bourilkov [ID](#), L. Cadamuro [ID](#), V. Cherepanov, F. Errico [ID](#), R.D. Field, D. Guerrero, B.M. Joshi [ID](#), M. Kim, E. Koenig, J. Konigsberg [ID](#), A. Korytov, K.H. Lo, K. Matchev [ID](#), N. Menendez [ID](#), G. Mitselmakher [ID](#), A. Muthirakalayil Madhu, N. Rawal, D. Rosenzweig, S. Rosenzweig, J. Rotter, K. Shi [ID](#), J. Wang [ID](#), E. Yigitbasi [ID](#), X. Zuo

Florida State University, Tallahassee, Florida, USA

T. Adams [ID](#), A. Askew [ID](#), R. Habibullah [ID](#), V. Hagopian, K.F. Johnson, R. Khurana, T. Kolberg [ID](#), G. Martinez, H. Prosper [ID](#), C. Schiber, O. Viazlo [ID](#), R. Yohay [ID](#), J. Zhang

Florida Institute of Technology, Melbourne, Florida, USA

M.M. Baarmann [ID](#), S. Butalla, T. Elkafrawy⁹³ [ID](#), M. Hohlmann [ID](#), R. Kumar Verma [ID](#), D. Noonan [ID](#), M. Rahmani, F. Yumiceva [ID](#)

University of Illinois at Chicago (UIC), Chicago, Illinois, USA

M.R. Adams, H. Becerril Gonzalez [ID](#), R. Cavanaugh [ID](#), S. Dittmer, O. Evdokimov [ID](#), C.E. Gerber [ID](#), D.A. Hangal [ID](#), D.J. Hofman [ID](#), A.H. Merrit, C. Mills [ID](#), G. Oh [ID](#), T. Roy, S. Rudrabhatla, M.B. Tonjes [ID](#), N. Varelas [ID](#), J. Viinikainen [ID](#), X. Wang, Z. Wu [ID](#), Z. Ye [ID](#)

The University of Iowa, Iowa City, Iowa, USA

M. Alhusseini [ID](#), K. Dilsiz⁹⁴ [ID](#), L. Emediato, R.P. Gandrajula [ID](#), O.K. Köseyan [ID](#), J.-P. Merlo, A. Mestvirishvili⁹⁵, J. Nachtman, H. Ogul⁹⁶ [ID](#), Y. Onel [ID](#), A. Penzo, C. Snyder, E. Tiras⁹⁷ [ID](#)

Johns Hopkins University, Baltimore, Maryland, USA

O. Amram [ID](#), B. Blumenfeld [ID](#), L. Corcodilos [ID](#), J. Davis, M. Eminizer [ID](#), A.V. Gritsan [ID](#), S. Kyriacou, P. Maksimovic [ID](#), J. Roskes [ID](#), M. Swartz, T.Á. Vámi [ID](#)

The University of Kansas, Lawrence, Kansas, USA

A. Abreu, J. Anguiano, C. Baldenegro Barrera [ID](#), P. Baringer [ID](#), A. Bean [ID](#), A. Bylinkin [ID](#), Z. Flowers, T. Isidori, S. Khalil [ID](#), J. King, G. Krintiras [ID](#), A. Kropivnitskaya [ID](#), M. Lazarovits, C. Le Mahieu, C. Lindsey, J. Marquez, N. Minafra [ID](#), M. Murray [ID](#), M. Nickel, C. Rogan [ID](#), C. Royon, R. Salvatico [ID](#), S. Sanders, E. Schmitz, C. Smith [ID](#), J.D. Tapia Takaki [ID](#), Q. Wang [ID](#), Z. Warner, J. Williams [ID](#), G. Wilson [ID](#)

Kansas State University, Manhattan, Kansas, USA

S. Duric, A. Ivanov [ID](#), K. Kaadze [ID](#), D. Kim, Y. Maravin [ID](#), T. Mitchell, A. Modak, K. Nam

Lawrence Livermore National Laboratory, Livermore, California, USA

F. Rebassoo, D. Wright

University of Maryland, College Park, Maryland, USA

E. Adams, A. Baden, O. Baron, A. Belloni [ID](#), S.C. Eno [ID](#), N.J. Hadley [ID](#), S. Jabeen [ID](#), R.G. Kellogg, T. Koeth, Y. Lai, S. Lascio, A.C. Mignerey, S. Nabili, C. Palmer [ID](#), M. Seidel [ID](#), A. Skuja [ID](#), L. Wang, K. Wong [ID](#)

Massachusetts Institute of Technology, Cambridge, Massachusetts, USA

D. Abercrombie, G. Andreassi, R. Bi, W. Busza [ID](#), I.A. Cali, Y. Chen [ID](#), M. D'Alfonso [ID](#), J. Eysermans, C. Freer [ID](#), G. Gomez Ceballos, M. Goncharov, P. Harris, M. Hu, M. Klute [ID](#), D. Kovalevskyi [ID](#), J. Krupa, Y.-J. Lee [ID](#), C. Mironov [ID](#), C. Paus [ID](#), D. Rankin [ID](#), C. Roland [ID](#), G. Roland, Z. Shi [ID](#), G.S.F. Stephans [ID](#), J. Wang, Z. Wang [ID](#), B. Wyslouch [ID](#)

University of Minnesota, Minneapolis, Minnesota, USA

R.M. Chatterjee, A. Evans , J. Hiltbrand, Sh. Jain , M. Krohn, Y. Kubota, J. Mans , M. Revering, R. Rusack , R. Saradhy, N. Schroeder , N. Strobbe , M.A. Wadud

University of Nebraska-Lincoln, Lincoln, Nebraska, USA

K. Bloom , M. Bryson, S. Chauhan , D.R. Claes, C. Fangmeier, L. Finco , F. Golf , C. Joo, I. Kravchenko , M. Musich, I. Reed, J.E. Siado, G.R. Snow[†], W. Tabb, A. Wightman, F. Yan, A.G. Zecchinelli

State University of New York at Buffalo, Buffalo, New York, USA

G. Agarwal , H. Bandyopadhyay , L. Hay , I. Iashvili , A. Kharchilava, C. McLean , D. Nguyen, J. Pekkanen , S. Rappoccio , A. Williams 

Northeastern University, Boston, Massachusetts, USA

G. Alverson , E. Barberis, Y. Haddad , Y. Han, A. Hortiangtham, A. Krishna, J. Li , G. Madigan, B. Marzocchi , D.M. Morse , V. Nguyen, T. Orimoto , A. Parker, L. Skinnari , A. Tishelman-Charny, T. Wamorkar, B. Wang , A. Wisecarver, D. Wood 

Northwestern University, Evanston, Illinois, USA

S. Bhattacharya , J. Bueghly, Z. Chen , A. Gilbert , T. Gunter , K.A. Hahn, Y. Liu, N. Odell, M.H. Schmitt , M. Velasco

University of Notre Dame, Notre Dame, Indiana, USA

R. Band , R. Bucci, M. Cremonesi, A. Das , N. Dev , R. Goldouzian , M. Hildreth, K. Hurtado Anampa , C. Jessop , K. Lannon , J. Lawrence, N. Loukas , D. Lutton, J. Mariano, N. Marinelli, I. Mcalister, T. McCauley , C. McGrady, K. Mohrman, C. Moore, Y. Musienko⁵³, R. Ruchti, A. Townsend, M. Wayne, M. Zarucki , L. Zygalas

The Ohio State University, Columbus, Ohio, USA

B. Bylsma, L.S. Durkin , B. Francis , C. Hill , M. Nunez Ornelas , K. Wei, B.L. Winer, B.R. Yates 

Princeton University, Princeton, New Jersey, USA

F.M. Addesa , B. Bonham , P. Das , G. Dezoort, P. Elmer , A. Frankenthal , B. Greenberg , N. Haubrich, S. Higginbotham, A. Kalogeropoulos , G. Kopp, S. Kwan , D. Lange, D. Marlow , K. Mei , I. Ojalvo, J. Olsen , D. Stickland , C. Tully 

University of Puerto Rico, Mayaguez, Puerto Rico, USA

S. Malik , S. Norberg

Purdue University, West Lafayette, Indiana, USA

A.S. Bakshi, V.E. Barnes , R. Chawla , S. Das , L. Gutay, M. Jones , A.W. Jung , D. Kondratyev , A.M. Koshy, M. Liu, G. Negro, N. Neumeister , G. Paspalaki, S. Piperov , A. Purohit, J.F. Schulte , M. Stojanovic¹⁶, J. Thieman , F. Wang , R. Xiao , W. Xie 

Purdue University Northwest, Hammond, Indiana, USA

J. Dolen , N. Parashar

Rice University, Houston, Texas, USA

A. Baty , T. Carnahan, M. Decaro, S. Dildick , K.M. Ecklund , S. Freed, P. Gardner, F.J.M. Geurts , A. Kumar , W. Li, B.P. Padley , R. Redjimi, W. Shi , A.G. Stahl Leiton , S. Yang , L. Zhang⁹⁸, Y. Zhang 

University of Rochester, Rochester, New York, USA

A. Bodek , P. de Barbaro, R. Demina , J.L. Dulemba , C. Fallon, T. Ferbel , M. Galanti,

A. Garcia-Bellido , O. Hindrichs , A. Khukhunaishvili, E. Ranken, R. Taus

Rutgers, The State University of New Jersey, Piscataway, New Jersey, USA

B. Chiarito, J.P. Chou , A. Gandrakota , Y. Gershtein , E. Halkiadakis , A. Hart, M. Heindl , O. Karacheban²⁴ , I. Laflotte, A. Lath , R. Montalvo, K. Nash, M. Osherson, S. Salur , S. Schnetzer, S. Somalwar , R. Stone, S.A. Thayil , S. Thomas, H. Wang 

University of Tennessee, Knoxville, Tennessee, USA

H. Acharya, A.G. Delannoy , S. Fiorendi , S. Spanier 

Texas A&M University, College Station, Texas, USA

O. Bouhali⁹⁹ , M. Dalchenko , A. Delgado , R. Eusebi, J. Gilmore, T. Huang, T. Kamon¹⁰⁰, H. Kim , S. Luo , S. Malhotra, R. Mueller, D. Overton, D. Rathjens , A. Safonov 

Texas Tech University, Lubbock, Texas, USA

N. Akchurin, J. Damgov, V. Hegde, S. Kunori, K. Lamichhane, S.W. Lee , T. Mengke, S. Muthumuni , T. Peltola , I. Volobouev, Z. Wang, A. Whitbeck

Vanderbilt University, Nashville, Tennessee, USA

E. Appelt , S. Greene, A. Gurrola , W. Johns, A. Melo, H. Ni, K. Padeken , F. Romeo , P. Sheldon , S. Tuo, J. Velkovska 

University of Virginia, Charlottesville, Virginia, USA

M.W. Arenton , B. Cardwell, B. Cox , G. Cummings , J. Hakala , R. Hirosky , M. Joyce , A. Ledovskoy , A. Li, C. Neu , C.E. Perez Lara , B. Tannenwald , S. White 

Wayne State University, Detroit, Michigan, USA

N. Poudyal 

University of Wisconsin - Madison, Madison, WI, Wisconsin, USA

S. Banerjee, K. Black , T. Bose , S. Dasu , I. De Bruyn , P. Everaerts , C. Galloni, H. He, M. Herndon , A. Hervé, U. Hussain, A. Lanaro, A. Loeliger, R. Loveless, J. Madhusudanan Sreekala , A. Mallampalli, A. Mohammadi, D. Pinna, A. Savin, V. Shang, V. Sharma , W.H. Smith , D. Teague, S. Trembath-Reichert, W. Vetens 

†: Deceased

1: Also at TU Wien, Wien, Austria

2: Also at Institute of Basic and Applied Sciences, Faculty of Engineering, Arab Academy for Science, Technology and Maritime Transport, Alexandria, Egypt

3: Also at Université Libre de Bruxelles, Bruxelles, Belgium

4: Also at Universidade Estadual de Campinas, Campinas, Brazil

5: Also at Federal University of Rio Grande do Sul, Porto Alegre, Brazil

6: Also at The University of the State of Amazonas, Manaus, Brazil

7: Also at University of Chinese Academy of Sciences, Beijing, China

8: Also at Department of Physics, Tsinghua University, Beijing, China

9: Also at UFMS, Nova Andradina, Brazil

10: Also at Nanjing Normal University Department of Physics, Nanjing, China

11: Now at The University of Iowa, Iowa City, Iowa, USA

12: Also at Institute for Theoretical and Experimental Physics named by A.I. Alikhanov of NRC ‘Kurchatov Institute’, Moscow, Russia

13: Also at Joint Institute for Nuclear Research, Dubna, Russia

14: Now at British University in Egypt, Cairo, Egypt

15: Now at Cairo University, Cairo, Egypt

16: Also at Purdue University, West Lafayette, Indiana, USA

-
- 17: Also at Université de Haute Alsace, Mulhouse, France
 - 18: Also at Ilia State University, Tbilisi, Georgia
 - 19: Also at Erzincan Binali Yildirim University, Erzincan, Turkey
 - 20: Also at CERN, European Organization for Nuclear Research, Geneva, Switzerland
 - 21: Also at RWTH Aachen University, III. Physikalisches Institut A, Aachen, Germany
 - 22: Also at University of Hamburg, Hamburg, Germany
 - 23: Also at Isfahan University of Technology, Isfahan, Iran
 - 24: Also at Brandenburg University of Technology, Cottbus, Germany
 - 25: Also at Forschungszentrum Jülich, Juelich, Germany
 - 26: Also at Physics Department, Faculty of Science, Assiut University, Assiut, Egypt
 - 27: Also at Karoly Robert Campus, MATE Institute of Technology, Gyongyos, Hungary
 - 28: Also at Institute of Physics, University of Debrecen, Debrecen, Hungary
 - 29: Also at Institute of Nuclear Research ATOMKI, Debrecen, Hungary
 - 30: Now at Universitatea Babes-Bolyai - Facultatea de Fizica, Cluj-Napoca, Romania
 - 31: Also at MTA-ELTE Lendület CMS Particle and Nuclear Physics Group, Eötvös Loránd University, Budapest, Hungary
 - 32: Also at Wigner Research Centre for Physics, Budapest, Hungary
 - 33: Also at IIT Bhubaneswar, Bhubaneswar, India
 - 34: Also at Institute of Physics, Bhubaneswar, India
 - 35: Also at Punjab Agricultural University, Ludhiana, India
 - 36: Also at Shoolini University, Solan, India
 - 37: Also at University of Hyderabad, Hyderabad, India
 - 38: Also at University of Visva-Bharati, Santiniketan, India
 - 39: Also at Indian Institute of Technology (IIT), Mumbai, India
 - 40: Also at Department of Electrical and Computer Engineering, Isfahan University of Technology, Isfahan, Iran
 - 41: Also at Department of Physics, Isfahan University of Technology, Isfahan, Iran
 - 42: Also at Sharif University of Technology, Tehran, Iran
 - 43: Also at Department of Physics, University of Science and Technology of Mazandaran, Behshahr, Iran
 - 44: Now at INFN Sezione di Bari, Università di Bari, Politecnico di Bari, Bari, Italy
 - 45: Also at Italian National Agency for New Technologies, Energy and Sustainable Economic Development, Bologna, Italy
 - 46: Also at Centro Siciliano di Fisica Nucleare e di Struttura Della Materia, Catania, Italy
 - 47: Also at Scuola Superiore Meridionale, Università di Napoli Federico II, Napoli, Italy
 - 48: Also at Università di Napoli 'Federico II', Napoli, Italy
 - 49: Also at Consiglio Nazionale delle Ricerche - Istituto Officina dei Materiali, Perugia, Italy
 - 50: Also at Riga Technical University, Riga, Latvia
 - 51: Also at Consejo Nacional de Ciencia y Tecnología, Mexico City, Mexico
 - 52: Also at IRFU, CEA, Université Paris-Saclay, Gif-sur-Yvette, France
 - 53: Also at Institute for Nuclear Research, Moscow, Russia
 - 54: Now at National Research Nuclear University 'Moscow Engineering Physics Institute' (MEPhI), Moscow, Russia
 - 55: Also at Institute of Nuclear Physics of the Uzbekistan Academy of Sciences, Tashkent, Uzbekistan
 - 56: Also at St. Petersburg Polytechnic University, St. Petersburg, Russia
 - 57: Also at University of Florida, Gainesville, Florida, USA
 - 58: Also at Imperial College, London, United Kingdom
 - 59: Also at P.N. Lebedev Physical Institute, Moscow, Russia

- 60: Also at California Institute of Technology, Pasadena, California, USA
61: Also at Budker Institute of Nuclear Physics, Novosibirsk, Russia
62: Also at Faculty of Physics, University of Belgrade, Belgrade, Serbia
63: Also at Trincomalee Campus, Eastern University, Sri Lanka, Nilaveli, Sri Lanka
64: Also at INFN Sezione di Pavia, Università di Pavia, Pavia, Italy
65: Also at National and Kapodistrian University of Athens, Athens, Greece
66: Also at Ecole Polytechnique Fédérale Lausanne, Lausanne, Switzerland
67: Also at Universität Zürich, Zurich, Switzerland
68: Also at Stefan Meyer Institute for Subatomic Physics, Vienna, Austria
69: Also at Laboratoire d'Annecy-le-Vieux de Physique des Particules, IN2P3-CNRS, Annecy-le-Vieux, France
70: Also at Şırnak University, Sirnak, Turkey
71: Also at Near East University, Research Center of Experimental Health Science, Nicosia, Turkey
72: Also at Konya Technical University, Konya, Turkey
73: Also at Piri Reis University, Istanbul, Turkey
74: Also at Adiyaman University, Adiyaman, Turkey
75: Also at Necmettin Erbakan University, Konya, Turkey
76: Also at Bozok Üniversitesi Rektörlüğü, Yozgat, Turkey
77: Also at Marmara University, Istanbul, Turkey
78: Also at Milli Savunma University, Istanbul, Turkey
79: Also at Kafkas University, Kars, Turkey
80: Also at Istanbul Bilgi University, Istanbul, Turkey
81: Also at Hacettepe University, Ankara, Turkey
82: Also at Istanbul University - Cerrahpasa, Faculty of Engineering, Istanbul, Turkey
83: Also at Ozyegin University, Istanbul, Turkey
84: Also at Vrije Universiteit Brussel, Brussel, Belgium
85: Also at School of Physics and Astronomy, University of Southampton, Southampton, United Kingdom
86: Also at Rutherford Appleton Laboratory, Didcot, United Kingdom
87: Also at IPPP Durham University, Durham, United Kingdom
88: Also at Monash University, Faculty of Science, Clayton, Australia
89: Also at Università di Torino, Torino, Italy
90: Also at Bethel University, St. Paul, Minneapolis, USA
91: Also at Karamanoğlu Mehmetbey University, Karaman, Turkey
92: Also at United States Naval Academy, Annapolis, N/A, USA
93: Also at Ain Shams University, Cairo, Egypt
94: Also at Bingol University, Bingol, Turkey
95: Also at Georgian Technical University, Tbilisi, Georgia
96: Also at Sinop University, Sinop, Turkey
97: Also at Erciyes University, Kayseri, Turkey
98: Also at Institute of Modern Physics and Key Laboratory of Nuclear Physics and Ion-beam Application (MOE) - Fudan University, Shanghai, China
99: Also at Texas A&M University at Qatar, Doha, Qatar
100: Also at Kyungpook National University, Daegu, Korea